Prediction of Homeland Happiness Index by Applying Deep Learning Techniques on Satellite Imagery

A

thesis

submitted for the Award

of the Degree of

DOCTOR OF PHILOSOPHY

in

Computer Applications

By

Yasir Afaq

11816025

Supervised By

Dr. Ankush Manocha

LOVELY PROFESSIONAL UNIVERSITY

Punjab

April-2022

Declaration of Authorship

I, Yasir Afaq, declare that this thesis titled, "Prediction of Homeland Happiness Index by Applying Deep Learning Techniques on Satellite Imagery" and the work presented in it are my own. I confirm that:

- This work was done wholly or mainly while in candidature for a research degree at this University.
- Where any part of this thesis has previously been submitted for a degree or any other qualification at this University or any other institution, this has been clearly stated.
- Where I have consulted the published work of others, this is always clearly attributed.
- Where I have quoted from the work of others, the source is always given. With the exception of such quotations, this thesis is entirely my own work.
- I have acknowledged all main sources of help.
- Where the thesis is based on work done by myself jointly with others, I have made clear exactly what was done by others and what I have contributed myself.

Signed:

Date:

Certification

This is to certify that the thesis entitled "Prediction of Homeland Happiness Index by Applying Deep Learning Techniques on Satellite Imagery", which is being submitted by Mr. Yasir Afaq for the award of the degree of Doctor of Philosophy in Computer Applications from the Faculty of Technology and Sciences, Lovely Professional University, Punjab, India, is entirely based on the work carried out by him under my supervision and guidance. The work reported, embodies the original work of the candidate and has not been submitted to any other university or institution for the award of any degree or diploma, according to the best of my knowledge.

Dr. Ankush Manocha
Assistant Professor
School of Computer Application
Lovely Professional University
Phagwara, Punjab-144411, India
Date:

Abstract

Remote Sensing data is widely used in many applications such as object detection, classification, segmentation, urban development monitoring, water extraction, and natural disaster assessment. According to the survey conducted by Geospatial World, there are a total number of 906 satellites present in the atmosphere that is used to monitor the condition of the earth. Each satellite is following a different clock pattern for capturing earth images with multiple resolutions. Over the last few years, a constant improvement has been observed in both spatial and spectral resolution that offering an opportunity to observe the condition of resources on earth. As per the United Nations Sustainable Development goals, monitoring the development of nations through satellite images is considered one of the most important goals among its seventeen goals. Monitoring the quality of infrastructure by following the traditional approaches is extremely expensive and makes it difficult to track the progress toward these goals. Moreover, several factors such as lack of transportation, illiteracy, and many others in the underdeveloped countries make it difficult to conduct the survey and that can be a cause less accuracy.

To overcome these challenges, remote sensing can be used to monitor the infrastructural status effectively by using advanced data processing techniques such as machine learning and deep learning. Deep Learning is considered an emerging field of data processing that is having potential to be used in the domain of remote sensing for earth observation. In previous studies, deep learning is primarily focused on urban mapping, classification, and object detection by utilizing high spatial resolution of satellite images. However, limited solutions have been introduced in the domain of remote sensing. To overcome these challenges, several different deep learning algorithms have been introduced to extract the features from the satellite images to predict environmental conservation, sustainability, and socioeconomic development. In this thesis, different deep learning-assisted data processing

approaches are proposed to process the combination of multispectral false-color based Sentinel-2 satellite images to evaluate the degree of the Happiness Index of farmers by analyzing the availability of water.

Water is considered one of the imperative factors of living for a human being. The primary objective of the thesis is to extract spatial and spectral features from the satellite images to determine the availability of natural resources such as water, forest, and agriculture that can help the Government and other NGOs in real-time monitoring of urbanization. The availability of resource of water is taken to evaluate the degree of the Happiness Index among the farmers of Punjab from the satellite images and the survey data. In this manner, three different frameworks have been proposed to evaluate the degree of happiness with respect to different regions of Punjab such as Malwa, Doaba, and Majha. The degree of the happiness index is evaluated and justified by calculating the correlation between the outcomes related to satellite images and the survey data. The higher availability of water defines the higher index of happiness. The predicted outcomes are revealing that the farmers of Punjab belong to the Malwa and Majha regions are containing a large number of manmade water resources as compared to the Doaba region. Therefore, a higher degree of happiness is calculated in the farmers of the Majha and Malwa regions as compared to the doaba region. The outcome of the thesis defines the future scope of urbanization.

Acknowledgements

First of all, I would like to express my gratitude to my supervisor, Dr. Ankush Manocha, for his supervision, advice, and guidance from the very first day of this research as well as giving me extraordinary experiences throughout the work. I am truly very fortunate to have the opportunity to work with him. I found this guidance to be extremely valuable.

I am grateful to the friends especially Nafiaah Naqash, Parminder Kaur, Bharat Yadav, Shaikh Vaseem Akram, Dr. Sumaiya Farooq, Simranjeet Kaur, Himani Malhotra, Nagraju, and Dr. Majid Sadeeq for their constructive criticism and suggestions.

I would like to show my gratitude to the entire family of Lovely Professional University for providing me a suitable research atmosphere to carry out my work in proper time. I would like to thank the Division of Research and Development and School of Computer Applications for all the support encouragement throughout the research work.

I am also very much grateful to my Father, Mr. Mohd Rafi, my brothers and sisters for their moral support and care that they shown me during the period of this work.

Last but not least, I thank God for sailing me through all the rough and tough times during this research work.

Yasir Afaq **Date.....**

Contents

List of Figures

[1] **Source: https://earthexplorer.usgs.gov/**.

List of Tables

List of Abbreviations

Abbreviations	Description
LULC	Land Use Land Cover
RS	Remote Sensing
CD	Change Detection
AE	Auto Encoder
VHR	Very High Resolution
CNN	Convolutional Neural Network
LSTM	Long Short-Term Memory
RNN	Recurrent Neural Network
3D	3 Dimensional
2D	2 Dimensional
GRU	Gated Recurrent Unit
GIS	Graphical Information System
ReLU	Rectified Linear Unit
DL	Deep Learning
ML	Machine Learning
AI	Artificical Intelligence
HR	High Rsolution
RF	Random Forest
DCNN	Deep Convolution Neural Network
MDIT	Multi-scaler Integration Technique
DSA	Deep Sparse Auto-encoder
SVM	Support Vector Machine
NIR	Near Infrared
VNIR	Very Near Infrared
SLIC	Simple Linear Iterative Clustering

SGD	Stochastic Gradiant ALgorithm
RGB	Red Green Blue
GPU	Graphical Processing Unit
DCRM	Deep Convo-restrictive Model
SAR	Synthetic-aperture Radar
HSI	Hyper spectral Images
MSI	Multi spectral Images
HI	Hapiness Index
MR-DNN	Multi-resolution Deep Neural Network
MDIT	Multi-data Integration Technique

I would like to dedicate my thesis to my entire family and especially my Father, Mr. Mohd Rafi Khawaja

Chapter 1

Introduction

Remote Sensing (RS) is a real-time process of capturing data in the form of images of objects at a distance without making a physical appearance. Remote sensing images are one type of image that is used in the field of remote sensing for solving earth observation problems. The sensors that produce electromagnetic radiation or acoustic energy acquire distant sensing images. Even though the electromagnetic spectrum is vast, not all wavelengths are equally useful in remote sensing. The radiation in the electromagnetic spectrum is used to target specific objects, depending on the properties of the materials. The human eye, which is the true remote sensor, detects objects using the visible spectrum. The ultraviolet and infrared wavelengths are used to acquire the majority of remote sensing images. Sensors are devices that record the motion of objects based on the electromagnetic spectrum including cameras and scanners. Moreover, a vehicle is used to transport the sensors from one place to another place. Ground-level platforms, aerial platforms, and space-borne platforms are all types of carriers. Furthermore, multiple sensors are used to capture satellite images. For both natural and anthropogenic operations, RS images provide extensive global observation and insights into ecosystem health and sustainability. As of 2021, there were about 906 satellites with the primary use of "earth observation"[1]. The constant improvement in both spatial and temporal resolutions of satellite images has provided greater chances of resolving small features on the Earth. The Worldview-2 satellite has an average revisiting period of 1.1 days on

[1] **source: https://www.geospatialworld.net/blogs/how-many-satellites-are-orbiting-the-earth-in-2021/**.

the Earth's surface and can gather up to 1 million square kilometers of 8-band images per day with a panchromatic resolution of 0.46 meters and a multispectral resolution of 1.84 meters (Xiong et al., 2021). Every day, the Sentinel-2 spacecraft collects 6 TB of data, and every five days, a complete picture of the Earth is acquired (Phiri et al., 2020). Multispectral images (MSI) are satellite images that have more than 3 bands. Since the 1970s, MSIs have been widely and routinely utilized in the field of remote sensing. Meanwhile, spectrometry is also known as hyperspectral imaging (HSI) which are gaining popularity in various application of remote sensing. In comparison to multispectral images, HSI typically comprises hundreds or thousands of bands with a significantly smaller spectral bandwidth (10-20 nm). Every pixel in a hyperspectral image may be considered a high-dimensional vector that represents the spectral reflectance of hundreds of continuous narrow spectral channels across a given wavelength range. Not only can modern HSI collection systems provide great spectral resolution, but they can also provide high spatial resolution. Data from MSIs and HSIs may express extremely sophisticated features as well as more spectral and geographical information. For advanced image processing for different earth observation applications such as target identification, anomalous materials, and object recognition, HSIs are the most effective and accurate solution for solving such problems (Lu, 2020; Pawar et al., 2021; Shi et al., 2020c; Qu et al., 2020; Yang et al., 2020). Over the last several years, researchers have developed several algorithms for the detection of objects in RS images. The main purpose of remote sensing is to solve the collection of household census data through satellite imagery which is previously held by field surveys.

The collection of census data is a crucial task in India as well as other countries in terms of giving information to decision-makers. Census data collection requires a lot of resources and time to collect important information. This is particularly happening in those places that are having inadequate communication and transportation services. To solve such problems, remote sensing has taken place in the last few years. Remote sensing technology has been utilized in various domains such as classification, change detection, climate change, drought detection, etc. However, satellite images need

some preprocessing procedures for classification and change detection. In this manner, the remote sensing community is always working to improve remote sensing algorithms for features including change detection, preprocessing, segmentation, and classification. Remote sensing data is mostly utilized to monitor environmental changes using physical models (Liang, 2005). Life has become more modest as the Remote Sensing (RS) imaging framework has improved by the accessibility of Very High Resolution (VHR) satellite images. It assists researchers in classifying things for remote sensing applications that were previously handled through field surveys. One of the key features of real-time remote sensing satellite imagery is that the development changes can be analyzed accurately by using high-resolution satellite imagery. The importance of recognizing change contributes to a better understanding of human interactions with the environment, which may aid with growth decision-making in a given region. The application for which the change detection is employed determines the change decision entirely. Detecting changes in real-time applications is difficult because it necessitates several processing stages, including identifying a problem with change detection, preprocessing the image, and assessing the application-specific technique. In this manner, several data-driven machine learning (ML) approaches have traditionally been useful for monitoring the environmental condition in the domain of remote sensing. With the growing availability of "earth big data" and fast developments in machine learning, new approaches for earth monitoring are becoming more viable.

1.1 Homeland Happiness Index

The main Agenda of the Sustainable Development Goals and Millennium Development Goals of the United Nation is to eradicate poverty by 2030. However, due to the lack of updated data on the happiness index based on Socioeconomic, Infrastructure data, Development, Education, and Health, many more developing countries become the key challenge for policymakers. Conventionally, the survey data was used to calculate the development of a specific region. However, surveying a specific location is a laborious

process and expensive. As region-based development measurement is an important aspect for policymakers to evaluate the livelihood programs by government and non-governmental organizations. Monitoring the status of the development and deployment of new schemes or products from private sectors or government sectors makes people happy. Therefore, deep learning and satellite images are combined to predict the development status of a particular region. Based on the evaluated results a degree of happiness can easily be calculated by combining the satellite imagery and survey data of a specific region.

1.2 Role of Deep Learning in Remote Sensing

Over the last decade, deep learning has become one of the most important approaches in artificial intelligence for the extraction of important information from satellite images. Moreover, deep learning comes up with several techniques such as Neural networks, supervised approaches, and unsupervised approaches for feature extraction. The role of deep learning in remote sensing gained a significant role in the extraction of hierarchical features in an automatic manner. Understanding multispectral images that are captured by remote sensing sensors such as Sentinel-2, Landsat-8, Quickbird, BirdEye, and many more is a very important task in the domain of remote sensing. Deep learning (DL), which has received a lot of attention in recent years, is a potentially useful method for the extraction of large-scale information from satellite imagery. Due to the multi-layer learning process (LeCun, Bengio, and Hinton, 2015; Bengio, Courville, and Vincent, 2013), the DL model can effectively estimate the complicated nonlinear relationship between environmental parameters, which helps capture the potential association among environmental factors such as retrieval of information, fusion, downscaling, and many more. Furthermore, DL has reported great superiorities in multi-resolution and multilevel learning in remote sensing applications. DL is highly contributed to image processing and classification problems (Zhang, Zhang, and Du, 2016). Deep learning (DL) techniques are based on neural networks, which have been utilized in the remote sensing

field for the last few years. However, before the development of DL, the remote sensing community was utilizing support vector machines (SVM) and ensemble classifiers, such as random forest (RF), for image classification and other tasks (e.g. change detection). Out of all classifiers SVM gain the attention in the field of remote sensing due to its ability to handle the high dimensionality data and performed better on training (Mountrakis, Im, and Ogole, 2011), on the other hand, RF is popular due to its ease of use for classification and high precision (Belgiu and Drăguţ, 2016a). Since 2014, the remote sensing community has focused on deep learning (DL), and DL algorithms have shown promising solutions in a variety of image processing tasks, including LULC classification, scene classification, and object recognition (Yu et al., 2017b; Kussul et al., 2017; Sharma et al., 2017; Vetrivel et al., 2018). The main focus of the study is on Remote Sensing Image Analysis which will help decision-makers with urban planning and development. The following are some examples of remote sensing images.

1. **Multi Spectral Images (MSI):** MSI is a type of satellite image which is the combination of 3 to 15 multispectral bands. The scene is captured from MSI by using these bands. However, in general colored image is made up of three bands such as (Blue, Green, and Red), but in remote sensing applications, multispectral images are utilized to solve the remote sensing problems.

2. **Hyper Spectral Images (HSI):** HSI is another type of satellite image which is a combination of 100 to 1000 spectral bands. The type of image is better than multispectral images because the information inside the image is visible. These types of images are mostly used to solve change detection problems.

3. **Panchromatic Images:** A panchromatic image is a high-resolution single-band grayscale image that "combines" information from the visible R, G, and B bands. It results in a single integrated band with no wavelength data. The word pan-sharpening refers to the simultaneous acquisition of a panchromatic and a multispectral image over the same

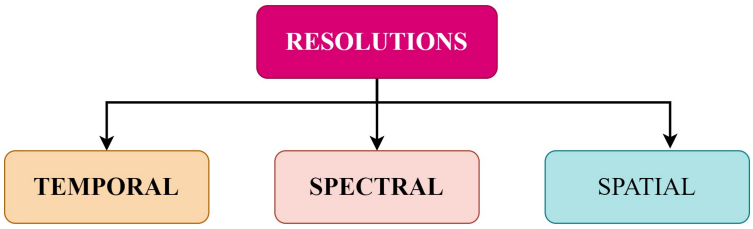

FIGURE 1.1: Different resolutions of satellite images

region. This might be thought of as a specific data fusion issue. Satellites with a spatial resolution of 15 meters, DigitalGlobe's satellites, and the Satellite for Earth Observation produce such images.

1.3 Resolutions and It's approaching

Satellite image resolution refers to the number of pixels /inch known in an image is known resolution. The quality and detail of images depend upon the number of pixels per inch. In general, images resolution is also known as low resolution, medium resolution, and high resolution The details of the smallest feature of an image are found in high-resolution images, while the details of the largest feature of an image are found in low and medium-resolution images. The resolution of remote sensing data is divided into three categories: Spatial resolution, Spectral resolution, and Temporal resolution as presented in Figure 1.1. These resolutions are used to solve the different problems of remote sensing.

Remote Sensing data is widely used in many applications such as change detection, classification, climate change, and Land Use Land Cover classification. However, in addition to classification and change detection, remote-sensing image processing requires a few preprocessing steps, and it is highly dependent on the method used that are selected to perform such specific tasks in the field of remote sensing. Some of the common applications of remote sensing are listed below and shown in Figure 1.2.

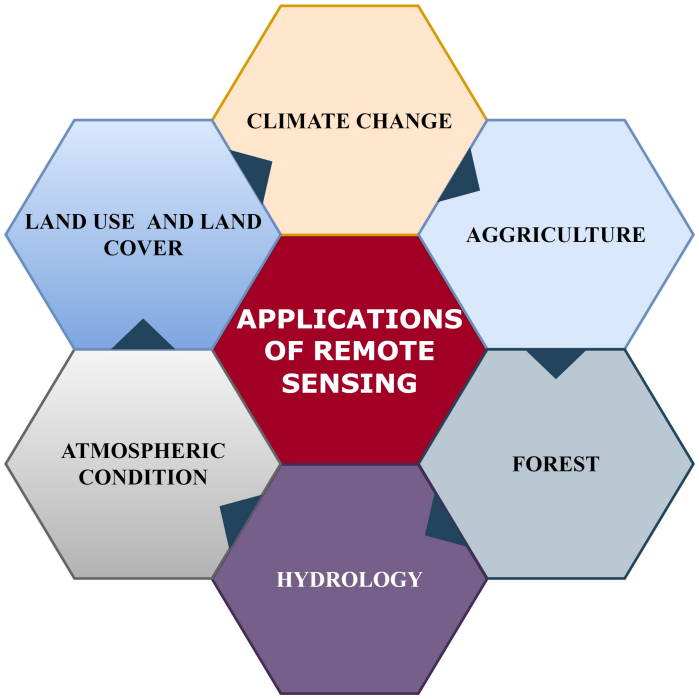

FIGURE 1.2: Different applications of Remote Sensing

Agriculture

In the agriculture domain, RS data is mainly used to extract the crop field, crop monitoring, and crop disease detection. By utilizing the RS data the type of the crop and condition, crop yield production, and crop status can be monitored by applying some advanced data processing approaches such as Deep learning, CNN, RNN, Segmentation, Fusion many more.

Forest

RS data are widely used on forest data to manage the forest or detect fire right from the high-resolution satellite imagery. The RS data in the forest domain can provide information about deforestation, monitoring of biophysical, biodiversity monitoring, watershed protection, forest fire detection, and many more.

Hydrology

To address the problem of water shortage, the identification of water resources has received a lot of attention in the field of remote sensing (Afaq and Manocha, 2021b). The Remote Sensing data is used to extract the location of water for the production of rice. Moreover, by utilizing advanced algorithms on RS data small rivers, lakes, man-made wetlands, reservoirs and other sources of water can be extracted automatically directly from satellite images.

Atmoshpheric Condition

In order to comprehend the weather and climate, remote sensing is also utilized to monitor and examine the atmosphere. The RS data is utilized for a variety of things, including weather forecasting, air pollution monitoring, climate change, and much more (Feng et al., 2015).

Land-Use Land-Cover

Recent advances in remote sensing and high-resolution image capture by satellites have aided in the collection of datasets for research and development. There have been considerable advancements in remote sensing and high-resolution image processing, as well as the development of a range of Land Use and Land Cover (LULC) classification algorithms in recent years. One problem with LULC classification is that there is a lot of variability in the data at high resolutions. The original datasets for classification are not enough to generalize the instances collected at various times and locations. Recently Deep learning has shown better performance for the extraction of valuable information from satellite images. In RS data deep learning is utilized for various tasks to accomplish such as Image processing, change detection, Accuracy assessment, and Classification. Furthermore, the utilization of deep learning in the various domain are prested in Figure 1.3.

1.4 Remote Sensing Image Classification

The classification approach is an effective solution in the domain of remote sensing for urban planning, weather forecasting, mineral monitoring, and environment monitoring. The classification is accomplished by assigning a semantic label to every pixel based on previously learned class information. The classification is performed by turning the colors, size, shape, and texture characteristics of an object into a class object. The classification can be performed in two different ways in remote sensing:

- Pixel-based Classification.
- Object-based Classification.
- **Pixel-based Classification**: Pixel-based classification is a conventional classification method in which each pixel is used to indicate a training sample for the method. It simply considers single-pixel spectral data. In pixel-based classification, the adjacent pixel value, which aids incorrectly classifying the pixel, is not employed, which may result in an undesirable error during the process. Because of these drawbacks, pixel-based classification is not recommended for RS data classification, particularly for high-resolution RS images.
- **Object-based Classification:** The object-based classification is an alternative to pixel-based classification, in which a group of pixels is properly considered depending on their spatial and spectral qualities. Objects are a collection of pixels with similar significant values. The objects are subsequently categorized using the classification methods as training samples. Furthermore, the entire images are divided into small groups and segmented with the use of spectral and spatial features. The segmented objects are then classified using the appropriate classification algorithm based on the features and criteria applied by the user, which may include color, texture, shape, size, and many more. In this thesis, object-based classification with high-resolution images is utilized for RS application.

Furthermore, the classification approaches are broadly classified into two different classification types: i) Supervised and ii) Unsupervised classification.

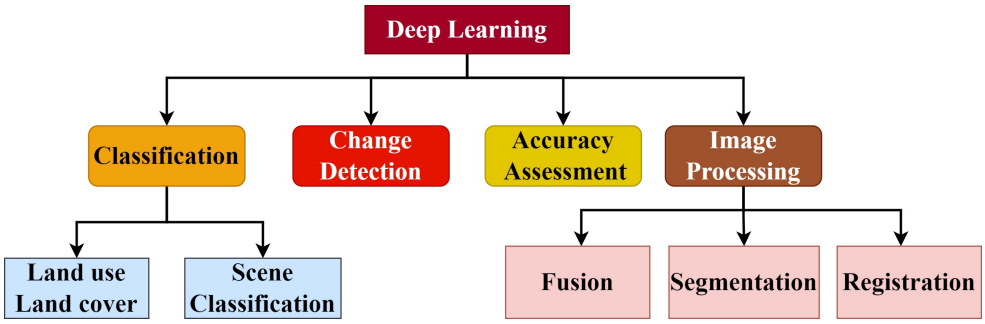

FIGURE 1.3: Use of Deep Learning in various application of remote sesing

1. Supervised: The method of categorizing image pixels to the given training set is known as supervised classification. The training set is produced by sampling the image with homogenous characteristics across several locations. The initial step is to determine the training set's information categories. The second stage is to use the trained set to identify the input image, with each image pixel being labeled according to the algorithm parameters. As a result, semi-automated classification is also termed supervised classification. The result of supervised classification is far more accurate than that of unsupervised classification. Moreover, if the training set is produced from extensive knowledge, the accuracy will be high. Although this classification yields a very accurate result, it requires significantly more effort and money than unsupervised classification.

2. Unsupervised: Unsupervised classification is a fully automated classification in which the input image is used to create the clusters. Without any prior knowledge, the images are categorized. The first stage is to group items together based on their characteristics. The next step is to assign classes to the clusters that have been established. When there

is no prior knowledge of the data in the remote sensing image, such classification is beneficial. Unsupervised classification is faster than supervised classification, however, selecting an efficient classification technique is a challenging task. There is a high chance of misclassification of pixels due to a lack of prior knowledge.

1.5 Problem Statement

To analyze the scale of infrastructural, Socio-economical, and industrial development, the conduction of a survey is considered one of the most common and traditional techniques followed by most Government and Non-government agencies around the globe. In India, the development with respect to social and economical factors is evaluated by surveying after every ten years. However, the management of the collected data by following traditional approaches is more challenging in terms of cost, manpower, and resources. Moreover, the lack of participation in the survey is also considered one of the most challenging aspects for the determination of socio-economic development. These types of limitations are most common in the areas with respect to a number of the factors such as lack of communication, limited availability of transportation, less manpower, and many others. To overcome the above-discussed limitations, several different organizations are an opting technique of remote sensing for monitoring and analyzing the quality of resources. Moreover, the data processing capability of ML and DL is continuously growing for the prediction of targeted objects from satellite images. A number of ML techniques such as Random forests (Belgiu and Drăguţ, 2016a; Otukei and Blaschke, 2010), support vector machines (Gualtieri and Cromp, 1999; Heumann, 2011; Maulik and Chakraborty, 2017; Oommen et al., 2008; Wang et al., 2017), and decision trees (Wang et al., 2017) were often employed for the classification of the objects from multispectral or hyperspectral satellite images. The process of image processing related to machine learning approaches is completely dependent upon handcrafted features. However, due to high dimensionality, it is difficult for traditional image processing approaches to extract features with optimum accuracy. To

overcome the data processing limitation of machine learning approaches, deep learning-based solutions have been widely utilized in the domain of remote sensing. As compared to ML approaches, DL methods are more efficient to extract the considerable features from the images (Garcia-Garcia et al., 2017; Guo et al., 2016; Ioannidou et al., 2017). Moreover, several supervised and semi-supervised machine learning approaches have been proposed for patch-based, pixel-based, object-based, rule-based classification to improve the prediction efficiency from the images belonging to the domain of remote sensing (Kaur and Garg, 2011; Soille and Pesaresi, 2002; Garcia-Garcia et al., 2017; Guo et al., 2016). In this manner, several deep learning-based object detection solutions have been proposed to address the above-mentioned challenges.

1.6 Contribution of the Thesis

The ultimate goal of this research is to propose a model for the prediction of the Homeland Happiness Index from satellite imagery. In order to achieve the desired result, this study is divided into the following four objectives.

1. Identification of deep learning techniques suitable for prediction of Environmental conservation, sustainable Socio-economic Development, and Citizen Safety and security from satellite imagery.

2. To conduct a survey for prediction of Good Governance, cultural preservation, and citizen safety and security.

3. To propose a novel method for Homeland Happiness Index (H2I) and modeling using satellite imagery and Survey data.

4. To apply and validate the developed model in different districts of Punjab.

1.7 Thesis Outline

The thesis is organized into six chapters. A brief outline of the chapters is given below.

In Chapter 2, we present the background studies on remote sensing for classification change detection, segmentation, and many more. This chapter aims to explore the state-of-the-art literature for the selection of appropriate techniques for the proposed study.

In Chapter 3, we propose a deep learning-based framework for the evaluation of the happiness index by using satellite images and survey data. The motivation of the study is to predict the degree of happiness index of the farmers of Punjab country India by correlating the sources of water and the survey data.

In Chapter 4, some limitations from chapter-3 such as shadows identification, extracting data from multi-resolution images, and small water bodies have been overcome by introducing a Fog-inspired Deep Learning-based Multi-resolution Data Integration technique for the water resources identification from urban areas by applying multi-resolution satellite images. The fundamental goal of the proposed study is to provide an automatic prediction of water resources from satellite imagery that helps farmers to get sufficient water for their cultivation land. The performance of the proposed solution is also analyzed in the chapter.

In Chapter 5, we present an advanced multi-stream deep learning approach to map rice fields through satellite images in a precise manner. The proposed model has the capability to access multispectral information from satellite images. The outcomes of the proposed solution are properly analyzed in the chapter.

In chapter 6, the outcomes of the thesis are concluded and also notify the scope of future work in the domain of remote sensing.

Chapter 2

Related Work

In the resolution of 2011, the United Nations declared a higher degree of happiness as a fundamental goal of a nation. The Quality of living with respect to socio-economic, industrial, and infrastructural development is one of the important aspects of our life (Dixit, Chaudhary, and Sahni, 2020). To determine the quality of living, a higher degree of happiness is performing an imperative role. Several different aspects such as conceptual data, social media, job, philosophy, psychology, sociology, economics, and many more need to be considered for the prediction of the happiness index (Jannani, Sael, and Benabbou, 2021). As happiness is a fundamental right of every citizen, the happiness index belonging to a particular individual is evaluated by calculating from the above-discussed factors (Pérez-Benito et al., 2019). Huang, Wu, and Deng, 2016 calculated the happiness index of urban China by evaluating two factors such as household income and the quality of assets. Peng et al., 2020b calculated the happiness index of 57 countries by utilizing World Values Survey Wave 6 (WV6) dataset and big data techniques. (You, 2021) employed machine learning techniques to predict the degree of happiness index based on the survey collected from the individuals belonging to different regions of China. However, a number of drawbacks have been observed while calculating the degree of happiness Index due to the calculated results being entirely based on the survey data collected for each individual. As the traditional approaches are time-consuming and costly, it is difficult to implement to process the data in real-time. To overcome the limitation of traditional approaches of data collection and processing, remote sensing and deep learning have shown promising outcomes in the last few years to

analyze the development of a particular region. Satellite imagery has been effectively implementing in classification, change detection, feature extraction, and many other applications. However, concerning change detection and classification, remote sensing imagery processing includes a few preprocessing processes. Besides, it is majorly dependent on the techniques that have been applied (Mountrakis, Im, and Ogole, 2011). Lately, deep learning techniques have been successful not only in classical issues like voice recognition, detection, recognition, and text segmentation but also in much other real-world application (Huang et al., 2013; Bengio, LeCun, et al., 2007; Simonyan and Zisserman, 2014; Hu et al., 2015). The deep learning techniques are influenced by the structure of the brain which is considered as a profound architecture of human visual systems and the perceptron's are expressing several absorption phases (Li, Chen, and Rao, 2018).
Satellite image classification and Change detection is characterizing as the mechanism by which a feature or phenomenon is identified by analyzing it at its distinctive period. Due to natural or human-made occurrences, detection of a change is a process of detecting geospatial changes from Geographical Information system (GIS) data (Manakos and Lavender, 2014).Change detection is of great significance to detect satellite mapping changes, observing environmental changes, and Land use and Land cover (Lu-Lc). Remote sensing satellite collects satellite images at different resolutions and uses them to detect changes (Asokan and Anitha, 2019). The remote sensing techniques are utilized to monitor and analyze environmental issues at the global, national, and regional level. The purpose of change detection is to analyze the variability in the images related to a specific area that is captured over a distinct period of times. Multi feature-based fusion techniques are utilized for the detection of changes in Landsat images with three bands that are Red, Green, and Blue (RGB) (Cai et al., 2018). The method of change detection is commonly used for tracking environmental conditions such as the impact of natural disasters and urban expansion, finding changes in vegetation, evaluating desertification, and detecting specific urban or natural variations in the environment (Jianya et al., 2008). Change identification due to repeated coverage at short intervals and reliable image quality is one of the primary

features of remotely sensed data collected from Earth-orbiting satellites (Anderson et al., 1977; Ingram, Knapp, and Robinson, 1981; Nelson, 1983; Singh, 1984). Techniques for change detection executing in different ways, like LuLc (Liu et al., 2017b; Liu et al., 2018; Liu et al., 2017c; Liu et al., 2016a; Amici et al., 2017), Deforestation, settlement in urban areas, and natural disaster change (Vickers, 2017; Hölbling, Friedl, and Eisank, 2015; Kleynhans, Salmon, and Olivier, 2015). Remote Sensing (RS) technology has proved to be the essential data source for continuous observation and evaluation over time. Table 2.1 provides a brief survey on classification and change detection in remote sensing using Landsat data with different resolutions.

Although the change detection techniques are applied in several different fields, only a few methods are followed by the researchers. The purpose of these approaches is to determine the substantial changes with respect to a specific area from the satellite images. Figure. 1 illustrates the flow for the detection of changes from satellite imagery. It has been realized that the presence of noise and artifacts in original images influencing the detection accuracy. Moreover, the selection of a Change detection (CD) and classification techniques also affects the performance of the detection. This chapter includes the literatures survey on remote sensing satellite imagery, classification, change detection, and deep learning approaches.

2.1 Preprocesing and process of detecting changes and classifying satellite images for remote sensing

Remote sensing data is commonly used to detect the scale of change that include a significant change in two different images with respect to a distinct period. The differences are identified to constitute a change map. 2.1 explains the complete process of detecting the changes within two images. The process of change detection method starts with data collection, where a series of images are taken from the same location at different periods. It has

TABLE 2.1: Different studies on classifications and change detection applications

Authors	Dataset	Location	No. of images	Resolution	bands
(Zanchetta, Bitelli, and Karnieli, 2016)	LANDSAT	AZRAQ OASIS	42,992	2634 × 3126	7 bands
(Singh and Singh, 2017b)	LANDSAT	JAMMU & KASHMIR	256	–	7 bands
(Johnson et al., 2017)	LANDSAT	PHILIPPINES	108	4500 × 4500	3 bands
(Pandey and Khare, 2017)	LANDSAT	UPPER NARMADA BASIN (UNB)		931 × 644	4 bands
(Luo and Zhang, 2016)	LANDSAT	–	5000	1024 × 614	3 bands
(Luo et al., 2018)	-	HANYANG	-	3000 × 3000	–
(Suresh and Lal, 2017)	-	LANDSAT	–	1464 × 1163	-
(Hagag, Fan, and Abd El-Samie, 2017)	LANDSAT	–	4000	677 × 512	3 bands
(Vickers, 2017)	LANDSAT	BANGLADESH	–	938 × 528	4 bands
(Vickers, 2017)	LANDSAT	NIGERIA	-	938 × 528	4 bands
(Wang et al., 2018a)	LANDSAT	ANHUI PROVINCE, CHINA	853	1669 × 1368	3 bands
(Wang et al., 2018b)	LANDSAT	NORTH XINJIANG, CHINA	853	1426 × 1426	3 bands
(Pradhan et al., 2017)	LANDSAT	-	48,828	256 × 256	-

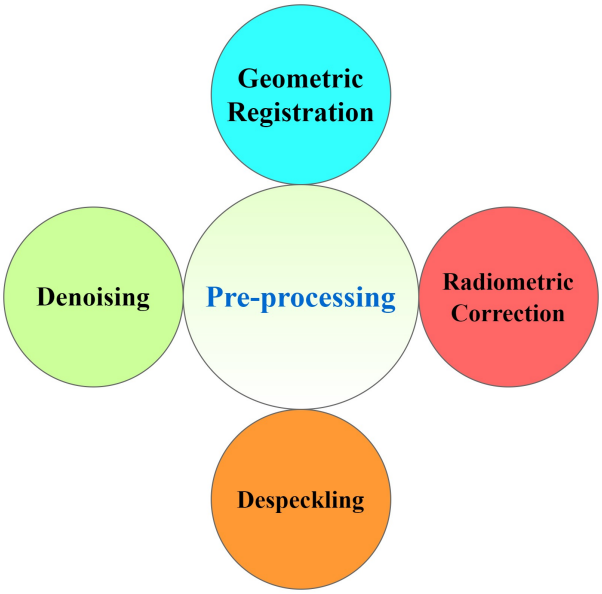

FIGURE 2.1: Different Image pre-processig techniques

been realized that it is imperative to apply the process of preprocessing on targeted images to check the atmospheric effect and noise. After completing the task of preprocessing, the change detection algorithms need to apply to detect the scale of variability.

Image Preprocessing

To address the problem of atmospheric effects such as unwanted noise or objects, researchers have developed different image processing methods. It is hard to distinguish among various ground artifacts with human vision due to the spatial resolution of satellite images. False-color variation helps to classify the ground artifacts and helps to detect the efficacy of the change map (Ma et al., 2017). Figure 2.1 shows the different methods of satellite image preprocessing for change detection.

- Geometric registration: Geometric registration is a solution that helps to detect unavoidable parts of satellite images to analyze change (Wu et al., 2014; Zhang et al., 2016). This approach is primarily employed to detect the changes in images that are captured in multiple dimensions

that can be a reason for the misclassification of the pixels. To operate geometric registration, Rational Polynomial Coefficient (RPC), Digital Terrain Model (DTM), Scale-Invariant Feature Transform (SIFT), Particle Swarm Optimization Sample Consensus (PSOSAC), Continuous Ant Colony Optimization (CACO), and Random Sample Consensus (RANSAC) are proposed (Fytsilis et al., 2016; Wu et al., 2017; Wu et al., 2019b; Cao, Zhou, and Li, 2016). Apart from these methods, one more registration approach named as Harris Laplace is employed for change detection (Cao et al., 2016). In this method, the identified points are clustered and balanced using SIFT to improve the accuracy of point detection.

- Radiometric correction: To normalize the multi-temporary data obtained over different periods, relative radiometric correction can be applied. While comparing several data sets, it has been analyzed that the process of image enhancement and correction is performing a significant role (Franklin and Giles, 1995). Here, the radiometric correction method enhances the interpretability and consistency of remotely sensed data. Radiometric correction is a series of methods designed to transform the digital values of the sensors such as radiance, specular reflection, and surface temperature (Pons and Arcalís, 2013). For stabilizing the brightness and contrast in the satellite images, the intensity normalization method is performed. It can be evaluated by changing a satellite image histogram as per requirement (Wan et al., 2018). Radiometric corrections are also utilized in the Digital Elevation Model (DEM) to improve the incidentangel oriented surface area (Ajadi, Meyer, and Webley, 2016). Sensors that causes adjustments in scene illumination and geometric corrections are removed by radiometric corrections that eliminate geometric distortions.

- Despeckling: Despeckling is mostly used to minimize noise as well as retain the information of the image. The pixel intensities are typically influenced by additive gaussian noise in optical images. Rather

than utilizing Landsat 8 images, Synthetic Aperture Radar (SAR) images are commonly used in change detection. SAR images contain less amount of atmospheric effects or clouds. However, the speckle noise may influence the image's pixels in the SAR image. Researchers have developed different methods to increase the efficacy of the techniques to detect changes in SAR images (Zhang et al., 2020). To eliminate multiplicative noise in SAR images, spatiotemporal speckle filtering is used (Wang, Zhao, and Chen, 2017). Another filter such as Lee sigma filter used on SAR images for despeckling (Iino et al., 2018). In the process of despeckling, Lee sigma filter showed a better result, among other filters. On the other hand, the Gaussian noise model was developed that was widely used to eliminate Gaussian noise (Golilarz, Gao, and Demirel, 2019; Masse et al., 2018). The pixel values are determined by analyzing the complete image instead of considering the neighborhood pixels of an image. In (Feng and Chen, 2017), nonlinear diffusion filtering is proposed to deal with the speckle noise in SAR images. Moreover, to denoise SAR images, a non-local mean filter is presented (Devapal, Kumar, and Jojy, 2017). In (Reich, Wörgötter, and Dellen, 2018), a real-time image dimensionality reduction filter is proposed that uses a thresholding-based approach to identify the edges of the images. Adaptive Cuckoo Search is another method based on optimal bilateral filtering to accelerate the convergence of the bilateral filter control parameter (Asokan and Anitha, 2020).

2.2 Different Classification and Change Detection Techniques for Remote Sensing Application

To analyze the scale of urban growth, the primary objective of change detection methods has to analyze the condition of a specific location to identify variations from the images captured at different periods. Through satellite-based remote sensing, high spatial and spectral resolution-oriented images

are captured that are used to analyze the scale of change. Based on its implementation, different methods for the identification of changes have been introduced in Figure 2.2.

2.2.1 Algebra Based approaches for remote sensing

To identify the scale of change, algebraic expressions are utilized to evaluate each pixel of an image in algebra-based change detection techniques. Image differencing (Ke et al., 2018), Image rationing (Liu et al., 2015), Change Vector Analysis (CVA) (Ferraris et al., 2017), and Image regression (Ridd and Liu, 1998) is the most common algebra detection methods. The selection of a threshold value is considered the most imperative process in standard algebraic change detection techniques that helps to detect the targeted region of an image to analyze the scale of change. These solutions are easy to implement, however, it is difficult to select an acceptable value of the threshold that can cause poor determination of the scale of change. The major drawback of these approaches is the classification of the areas from the images that contain a high ratio of noise. An unsupervised change detection approach is introduced to determine change vectors and statistical parameters by utilizing the Expectation-Maximization (EM) algorithm (He et al., 2014). The change vectors help to identify the image variance and the EM algorithm is used to compute its statistical parameters. In (Qi et al., 2015), three mechanisms such as object-oriented image analysis, Post Classification comparison (PCC), and Principal Component Analysis (PCA) are utilized to analyze the change that significantly minimized the rate of false alarms. Image differentiation is a procedure that is used to analyze the greyscaled images to access spatial information from the images. In the process of image processing, a variation in two images can be analyzed adequately by accessing the intensity of pixels in grey color (Vickers, 2017). Change vector analysis is another change detection technique that describes the evolutionary nature of multispectral images. In this manner, it has been analyzed that the algebraic change identification methods are easy to implement and simpler to apply on images to detect the scale of change. (See Table 2.2)

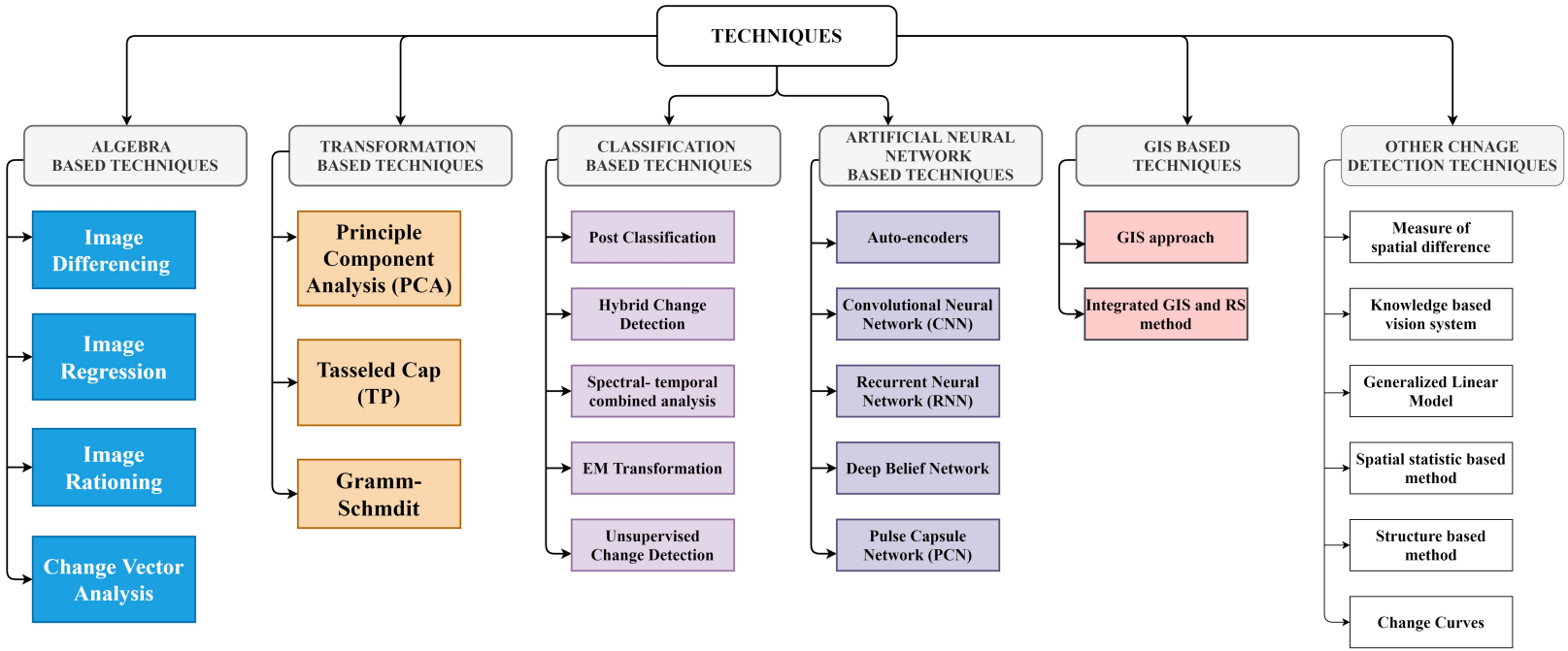

FIGURE 2.2: Classification and change detection approach

TABLE 2.2: Different studies on algebra-based approaches

Authors	Approaches	Images	Area	Accuracy
(Ke et al., 2018)	Image Differencing	Multispectral Images	China	0.9451
(Luppino et al., 2019)	Image regression	Heterogeneous Images	-	-
(Liu et al., 2015)	CVA (changevector analysis and Image Rationing)	Multi-temporal HS Images	California	0.99
(Ferraris et al., 2017)	Fusion Based approach	Multispectral and hyperspectral (HRand LR) LANDSAT 8	USA	0.97
(Xiong, Chen, and Kuang, 2012)	Image Rationing	SAR Images	China	–
(Barber, 2015)	Generalized Likelihood ratio test (GLTR)	SAR Images	–	–
(Ridd and Liu, 1998)	Dynamic thresholding	Multispectral images	Alaska	0.94
(Qi et al., 2015)	CVA	PolSAR	Panyu China	0.99

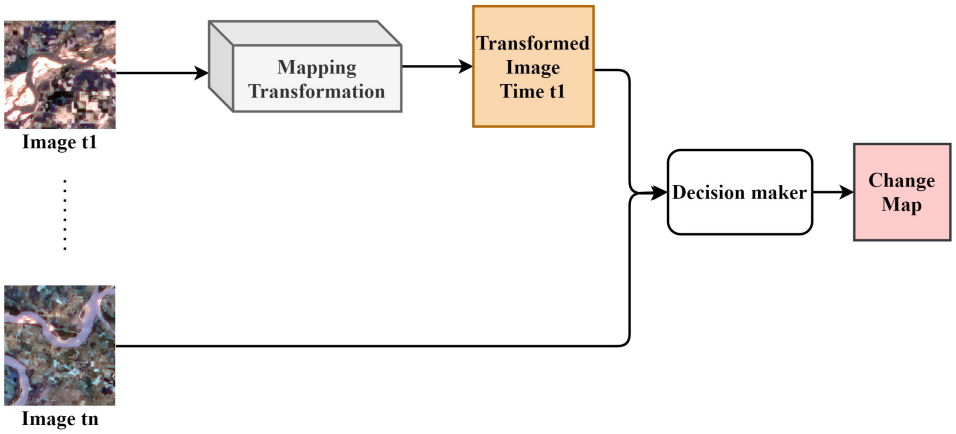

FIGURE 2.3: Transformation based process for detection of changes from satellite imagery in remote sensing application

2.2.2 Transformation based approaches for remote sensing

The change detection also includes the use of pixel transformation to detect the scale of change in the images by utilizing transformation techniques such as Principal Component Analysis (PCA) (Abdi and Williams, 2010), Tasseled Cap Transformation, and Chi-Square Transformation (CST) that are illustrated in Figures 2.3 and 2.4 for better understanding. While implementing a transform-based change identification process, the redundant bands are reduced by decomposing the objects and the change is observed through transformation. In the case of fast detection of changes for reference images, the Homogenous Pixel Transformation (HPT) technique is proposed (Liu et al., 2017b; Liu et al., 2018; Liu et al., 2017c; Liu et al., 2016b; Liu et al., 2016c). The main disadvantage of this approach is, it is difficult for labeling the changing area in the image. (See Table 2.3)

2.2.3 Classfication based approaches

The classification approach is completely dependent on the selection of data for change analysis. As the change detection accuracy is not affected by external factors such as atmospheric disturbance, this is considered as one of

TABLE 2.3: Different studies on transformation-based approaches

Authors	Approaches	Images	Area	Accuracy
(Sadeghi, Ahmadi, and Ebadi, 2016)	PCA	Landsat-TM4	Islami Island (Urmia Lake, Iran)	0.96
(Massarelli, 2018)	Tasseled Cap Transformation	Landsat	Brindisi	0.91
(Thakkar et al., 2016)	Tasseled Cap Transformation	IRS 1C LISS-III, Landsat 5 –TM, Landsat 8-OLI SR	India	0.84
(Vázquez-Jiménez et al., 2017)	Chi-square	Quickbird, WorldView, GeoEye	Guerrero Mexico	–
(Solano-Correa, Bovolo, and Bruzzone, 2018)	Tasseled Cap Transformation	Heterogeneous	Trentino Italy	–
(Liu et al., 2016b)	Discrete Wavelet Transform	Quickbird	UK	0.96
(Zhang et al., 2016)	Discrete Wavelet Transform	USACE, NOVA 2.1 small UASS	Yanzhou, China	–
(Liu et al., 2016b)	Discrete Wavelet Transform	SAR	Ranch, Florida	0.87

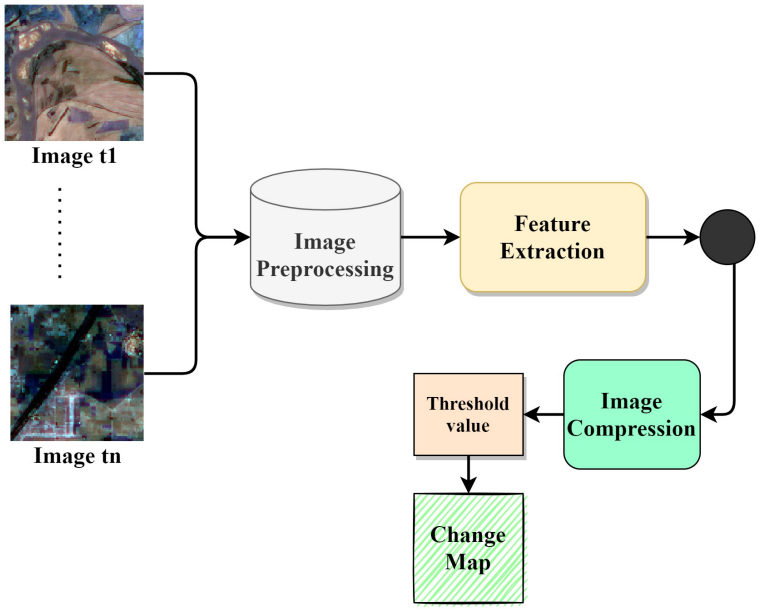

FIGURE 2.4: Principle component analysis

the most influential advantages of this approach. By utilizing the classification-based change detection technique, the better outcomes related to the change recognition can be achieved, however, the proposed solutions are suffering from the limitation of the training data. The scale of change is determined by following the concept of multi-dimensional distribution and the variables are determined by implementing the Expectation-Maximization (EM) algorithm (Prendes et al., 2014). To determine the area of land, an unsupervised classification approach is proposed named as for Ensemble Minimizing Learning Algorithm (EML) that categorize the multiple images into clusters (Vignesh et al., 2016). However, as the size of the samples is limited, the value of the predictive outcome is unsatisfactory. For multitemporal satellite images, Principle Component Analysis (PCA) is combined with an available classification if urban levels change in the river delta, can be efficiently monitored (Li and Yeh, 1998; Li et al., 2010). (See Figure 2.5)

TABLE 2.4: Survey on classification-based aproaches

Authors	Approach	Images	Area	Accuracy
(Raja et al., 2013)	Wavelet-Based Post Classification	IRS-1B and IRSP6	Madura city south India	0.82
(Gong et al., 2015)	Deep learning	SAR	Ottawa	0.98
(Vickers, 2017)	Bayesian network classifier	Cloud images	–	0.97
(Singh and Singh, 2017a)	Genetic algorithm trained radial basis function neural network	SAR	Ottawa	0.85
(**65**)	Deep neural network	Heterogeneous optical and Radar	China Mexico	0.98
(Jin et al., 2019)	Deep Convolutional Neural Network	NGS	China	0.96
(Zhang and Shi, 2020)	Convolutional Neural Network	VHR World View 3	–	0.92
(Ren et al., 2020)	Generative Adversal Network	VHR	–	–
(Saha, Bovolo, and Bruzzone, 2019)	Deep Change Vector Analysis	VHR World View 2, Pleiades, and Quickbird	-	0.96
(Touati, Mignotte, and Dahmane, 2020)	Deep Sparse Residual	VHR WorldView2,Quick Bird2	–	0.96
(Kalinicheva et al., 2020)	Unsupervised approach	HR	–	–

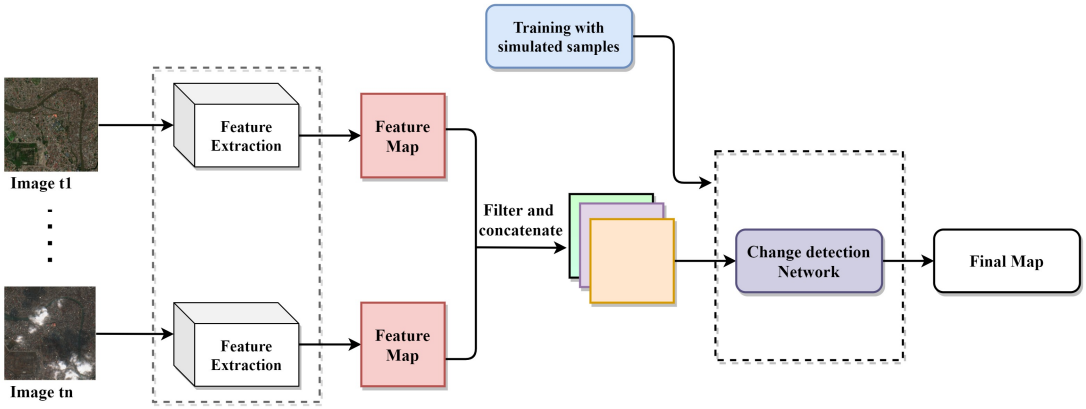

FIGURE 2.5: Complete process of classification based approaches for change detection

2.2.4 Advanced deep learning approaches in remote sensing for classificaton and change detection

The advanced method of identification of changes consists of various reflection and spectral mixing models. In these approaches, the image value is transformed into a substantial variable by following the concept of linear pattern analysis. (Wang et al., 2014) has introduced a Hopfield Neural Network (HNN) model (Li et al., 2014) to analyze the condition of the land. Another change detection method named a temporal unmixing method is proposed by (Xu et al., 2017) that analyzes the landscape images to identify the change in the coverage area. A hybrid spectral change-based change detection approach is explored by (Yan et al., 2018a). This approach defines the differences between the spectral values and shapes, and it requires only spectral features to defines the modifications which are not readily detectable. This method is also suffering from the problem of over-clustering that defines the limitation in the prediction of change with respect to the predefined classes. In this manner, developing a model for the conversion of reflectance value is considered as a big challenge in advanced models. (See Table 2.5)

TABLE 2.5: Survey on advance methods for change detection and classification

Authors	Approaches	Images	Area	Accuracy
(Xu et al., 2017)	Empirical orthogonal function (EOF)	Landsat	Jiangsu, china	89.25
(Wang et al., 2014)	Resolution lan cover change detection (RLCCD)	Landsat 7	Liaoning, china	-
(Marinelli, Bovolo, and Bruzzone, 2017)	Spectral change vectors (SCVs)	Multitemporal HS	Washington, USA	-
(Yan et al., 2018a)	Hybrid Spectral Difference (HSD)	WorldView 2 VHR Landsat 7	EMTM China	–
(Ma et al., 2019a)	Image Mapping	Homogeneous dataset (SAR) Ottawa dataset	China	0.97

2.3 Artificial Intelligence and Fuzzy-based Approaches in Remote Sensing

Several new methods have incorporated in Artificial Intelligence (AI)techniques that enhanced the scale of precision for change detection. A wide variety of Remote Sensing (RS) research has suggested the superiority of AI-based change detection approaches over the conventional approach for extracting the features from the images (Zhang and Lu, 2019; Fang et al., 2020). The neural network-based approach consists of assessing the area of change by using a combination of different neural network approaches, blurred method, and remote sensing techniques. By following the proficiency of AI techniques for feature extraction and learning, the evaluation of real-world geographical features has become possible with significant accuracy. Figure 2.6 illustrates different AIassisted frameworks that are specifically designed to analyze the change from the extracted feature maps. Based on the process

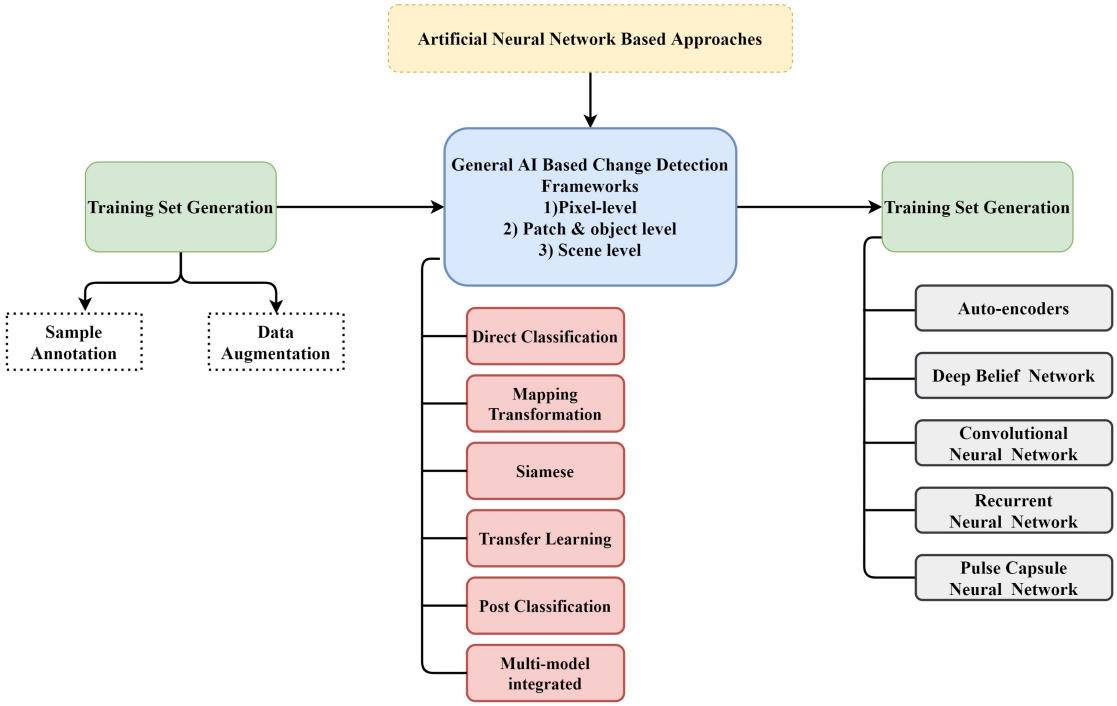

FIGURE 2.6: Artificial intelligence-based classification and change detection approaches in remote sensing

of in-depth feature extraction and training, the AI-based change detection frameworks can be categorized into three types: Single-stream framework, Double-stream framework, and Multi-modal integrated structure.

2.3.1 Single stream framework

In single-stream frameworks, only one primary AI method has to embed in the predictive solution to identify the change. The categorization of the single-stream frameworks can be done in two categories such as direct classification structure and transformation-based mapping structure as represented in Figure 2.7. It is imperative to mention that several studies have updated the solutions for fulfilling the objective of change detection with respect to the need for application and domain (Shi et al., 2020b; Shi et al., 2020a).

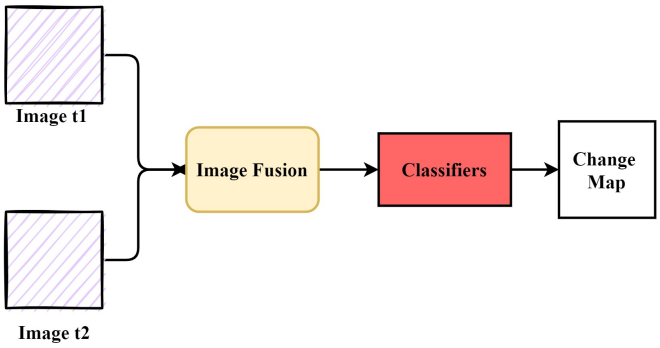

FIGURE 2.7: Direct classification structure

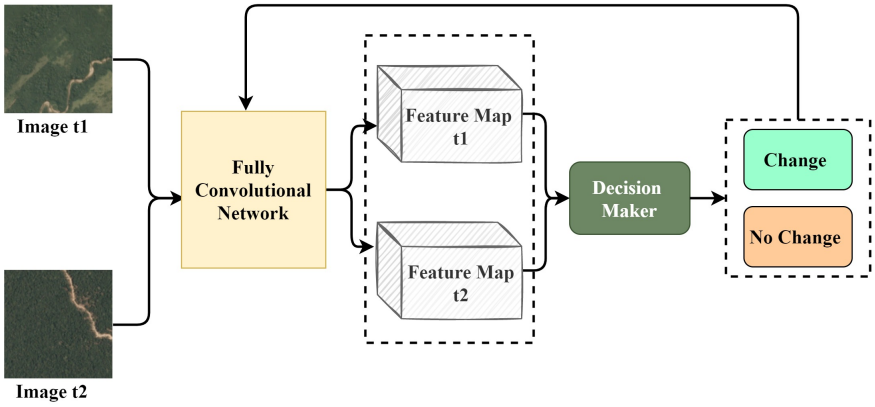

FIGURE 2.8: Siamese framework for change detection

2.3.2 Double stream framework

The double-stream structures are always been preferred to recognize the change by analyzing the images which are captured at two different time-stamps. Moreover, these methods can broadly categorize into three categories such as Siamese structure (Arabi, Karoui, and Djerriri, 2018; Jiang et al., 2020; Varghese et al., 2018; Zhan et al., 2017), transformation-based structure, and post-classification form (Bruzzone and Cossu, 2002; Abuelgasim et al., 1999; Lyu et al., 2018; Cao, Dragićević, and Li, 2019) as illustrated in Figure 2.9.

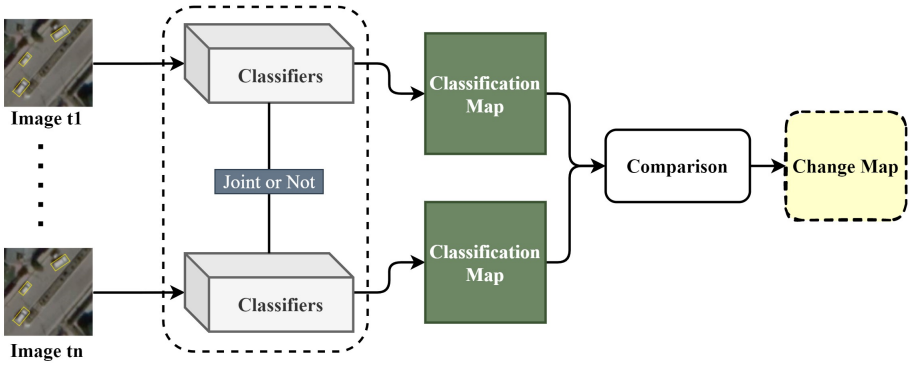

FIGURE 2.9: Post classification structure

2.3.3 Multi-model integrated structure

The multi-model integrated framework is a hybrid structure similar to a double-stream design. Change detection is the spatiotemporal analysis that can be achieved by acquiring the spatial and temporal features from the sequence of frames. In multi-model structures, both spatial and temporal features are utilized to analyze the scale of change. The spatial features are utilized to analyze the change patterns and temporal features are utilized to analyze the dependency of change over spatial features captured on different time-stamps (Vickers, 2017; Chen et al., 2019; Song et al., 2018; Shendryk et al., 2018; Liu et al., 2019b). Several different architectures such as Auto-Encoders (AEs), Deep Belief Networks (DBNs), Convolutional Neural Network (CNN), Recurrent Neural Networks (RNNs), and Pulse Capsule Neural Network (PCNNs) are also used for change detection (Gong, Yang, and Zhang, 2017; Han et al., 2019).

2.3.4 Auto-encoder (AE)

Auto-encoder can be used to reduce the dimensionality of a component. It is widely used in for feature extractor, as, it has the robust feature learning capability of neural network. The commonly used AE models are stacked auto-encoders (Ma et al., 2019a; De et al., 2017; Planinšič and Gleich, 2018), stacked denoising auto-encoders (Zhang et al., 2016; Su et al., 2016; Su et al.,

2017), stacked fisher autoencoders (Liu et al., 2019a; Liu et al., 2019b), Sparse auto-encoders (Fan, Lin, and Han, 2019), and denoising auto-encoders (Li, Chen, and Rao, 2018). These autoencoders maintain spatial information by extending pixel neighborhood values into vectors. In contrast, convolutional auto-encoders are implemented directly by convolution kernels (Kerner et al., 2019). Depending on its features, auto-encoders can detect changes in an unsupervised manner and work effectively.

2.3.5 Deep belief network (DBN)

A deep belief network is a generative statistical approach that learns to rebuild its inputs empirically. The deep belief network consists of several hidden layers that are responsible to make interactions between the layers. However, the units within the same layer are not connected and each hidden layer serves as a transparent layer for the next layer. It can be greedily trained, i.e., one layer at a time, and appears in many unsupervised image processing techniques (Ozdarici-Ok, 2015; Chu, Cao, and Hayat, 2016; Samadi, Akbarizadeh, and Kaabi, 2019). A DBNassisted framework is proposed for the classification of numerous changes from an image (Su et al., 2017). The proposed solution incorporated a greedy layer-wise training approach that dramatically eliminates the problem of overfitting.

2.3.6 Convolutional Neural Network (CNN)

CNN techniques are effectively utilized in a wide range of remote sensing applications such as land use Land cover, object detection, feature extraction, and change detection (Gong et al., 2015; Liu et al., 2016c; Lyu et al., 2018; Puig, Hyman, and Bolaños, 2002). It is used to improve the other change detection techniques and to learn the non-linear mapping between modified and unchanged image pairS. Due to the strong capability of feature learning from images, CNN becomes the best choice for researchers when training samples are sufficient (Chatfield et al., 2015; Peng and Guan, 2019). The procedure of extracting information from images is illustrated in Figure 2.10.

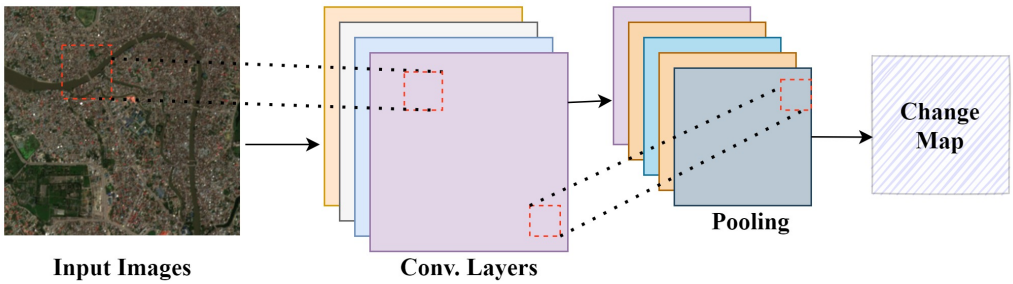

FIGURE 2.10: Working process of Convolutional Neural Network

CNN architecture incorporates the convolutional layers with subsampling operations that decrease design complexity and improves the capability of generalization with less trainable parameters (Krizhevsky, Sutskever, and Hinton, 2017; Gong et al., 2015; Liu et al., 2016c; Lyu et al., 2018). By considering the ability to learn the extracted features from an image, CNN has obtained a considerable performance in various image analysis tasks. Many classical CNNs and their extensions such as VGGNet (Peng and Guan, 2019; Nemoto et al., 2017; Sakurada and Okatani, 2015), CaffeNet (El Amin, Liu, and Wang, 2016), SegNet (Zhu et al., 2018), UNet (Peng, Zhang, and Guan, 2019), InceptionNet (Pomente, Picchiani, and Del Frate, 2018), and ResNet (Venugopal, 2020) are used as a classifier. A multiscale convolutional neural network (CNN) model is proposed by (Zhang et al., 2020) that trained the model on non-normalized images for securing the more details of an image. Moreover, to learn deep features for the detection of change, spatially registered images are required for CNN (Guo et al., 2018). To detect the complex features from high-resolution satellite imagery, a Deep Difference Convolutional Neural Network (DDCNN) is proposed by (Zhang and Shi, 2020). While training the CNN model, a huge amount of labelled data is required for the detection of change that is addressed in SemiCDNet model which is developed by (Peng et al., 2020a). Hence, the use of CNN has changed the process of image analysis, there is still no systematic way to design and train the network which would be considered a long-standing issue in the remote sensing community.

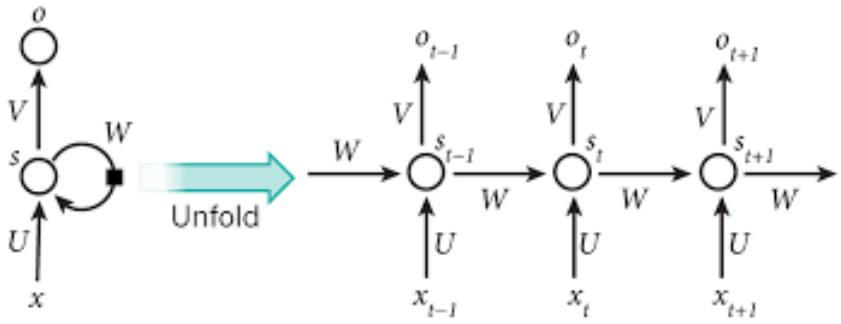

FIGURE 2.11: Recurrent Neural Network

2.3.7 Recurrent Neural Network (RNN)

As the task of change detection involves data with respect to multiple periods, the input can be converted in the form of a process that obtains the information related to change from the data sets (Shi et al., 2020b; Shi et al., 2020a). RNN techniques have received considerable attention to solving many complex issues involving sequential time series data, in particular Long Short-Term Memory (LSTM) models (Ordóñez and Roggen, 2016). To detect the changes from satellite images, it is necessary to provide a stable framework for the expression of data extraction for change detection. In this manner, RNN represents the feasible methods for learning imperative information for the detection of change from sequential time-series remote sensing data (Lyu, Lu, and Mou, 2016; Chen et al., 2019). However, due to vanishing gradient problem in RNN, the enhanced version of RNN named as Long Short-Term Memory (LSTM) network alleviates gradient disappearance and gradient explosion from the sequential data (Lyu, Lu, and Mou, 2016; Song et al., 2018; Liu et al., 2019a; Liu et al., 2019b). The researchers have utilized LSTM networks to obtain changes from the multi-temporal RS data (Lyu, Lu, and Mou, 2016). The trained model could be transferred to other data domains with an adequate generalization capacity. Figure 2.11 shows the core directive part in the form of a directed graph that can be unfolded to a chain of series-connected units (i.e., RNN cells).

2.3.8 Pulse capsule neural network

The pulse capsule neural network (PCNN) is a bionic neural network focused on the primate's visual cortex (Dewan, Kashyap, and Kushwaha, 2019). Unlike conventional neural networks, the learning and training phase does not require the extraction of successful information from very complex backgrounds in PCNN. The pulse neural network (PCNN) takes two-dimensional image data and each neuron correlates to a single pixel of an image. The pixel value acts as an external stimulation for each neuron that interconnects the adjacent neurons and supply regional stimuli to the next connected neurons. External and regional stimuli are mixed in a modulation field with a pulse generator to generate the output. As the duration of training increases, the PCNN produces a pulse sequence that can be used for the segmentation and extraction of the features from the images (Dewan, Kashyap, and Kushwaha, 2019) and, similarly, for the detection of change (Benedetti, Picchiani, and Del Frate, 2018; Huang, Yu, and Feng, 2019; Ma et al., 2019a; Ma et al., 2019b).

2.3.9 Fuzzy-based change detection approaches

The detection of change from a Synthetic Aperture Radar (SAR) by utilizing a fuzzy clustering approach from an image is introduced in (Li et al., 2016). The primary benefit of these approaches is, it has the ability to handle the noise in an effective manner. Different studies investigate the detection of changes by utilizing deep learning approaches (Huang et al., 2018a; Huang et al., 2018b; Huang, Yu, and Feng, 2019). To enhance the ability of change detection, a combination of fuzzy and Markov random fields is proposed (Subudhi et al., 2014). Table 2.6 provides an in-depth analysis of the all the above-dicussed ANN and fuzzy-based approaches with their respective areas.

TABLE 2.6: Suevey on neural network and fuzzy-based approaches

Authors	Approaches	Images	Area	Accuracy
(Subudhi et al., 2014)	Gibbs Markov Random Field (GMRF)	Landsat	Italy	–
(Li et al., 2016)	Multi-objective Fuzzy Clustering	Ottawa	Bern, Switzerland	0.95
(Su et al., 2016)	Deep learning and Mapping (DLM)	Chanba	Farmland	0.96
(Tian and Gong, 2018)	Edge-weighted fuzzy clustering	SAR Ottawa dataset	Bern	0.78
(Huang et al., 2018b)	Semi-transfer deep convolutional network (STDCNN)	WorldView 3, Worldview 2	Hong Kong Shenzhen	0.91
(Huang et al., 2018a)	Object-oriented change detection	IKONOS	Tang Jiao	0.92
(Jing, Gong, and Guan, 2020)	SLIC-CNN and CAE Features	Google Earth	Beijing, Wuhan	0.95
(Zhang and Shi, 2020)	Essemble CNN	WorldView-3 UAV	–	0.92
(Kalinicheva et al., 2020)	Deep learning with Graph-based approach	Sentinel-2 and SPOT-5	–	–
(Karim and Zyl, 2020)	Deep Learning and Transfer Learning	Sentinel-1 and Sentinel-2	–	0.85
(Wang et al., 2020b)	Deep Siamese Network	ZY-3 and GF-2	Dalong Lake and China	0.97
(Song et al., 2018)	Fully Convolutional Network and Transfer learning	KOMSAT-3A	Korea	0.97
(Seydi, Hasanlou, and Amani, 2020)	Convolutional Neural Network	Polar SAR	Abudhabi, (UAE)	0.98
(Shi et al., 2020a)	Deep Neural Network	OSM	Hong Kong	-

2.3.10 GIS-based approaches

A Geographical Information System (GIS) incorporates various sources of information in the detection of change. The main benefit of using GIS is to identify a change in the area that is being examined in a regular manner. It has been analyzed that multiple sources of data affect the performance of the model. However, the GIS method is more effective for handling and visualizing the multidimensional data in the field of remote sensing. GIS incorporates quantitative data sources and makes it much easier to obtain and analyze information on the detection of changes. Detection of vegetation cover changes using remote sensing and utilized the Normalized Difference Vegetation Index (NDVI) to categorize the vegetations (Gandhi et al., 2015). GIS-inspired Land cover change detection with remote sensing is introduced by (Rawat and Kumar, 2015). The proposed solution makes it easier to detect improvements with better accuracy and lower cost.

2.3.11 Other clasification and change detection approaches

Besides the popular categories of change detection, some other approaches are also used to detect changes in multi-temporal remote sensing images (Mohamed, Mobarak, et al., 2016; Pasanen and Holmström, 2015; Lv et al., 2016). In (Feng et al., 2018), objects are identified accurately and neighborhood similarity is measured by utilizing an object-based change detection approach. The biggest challenge of this approach is to deal with scattered and distributed samples. In (Yang et al., 2017a), the authors described a vegetation cover change study by following Multivariate Adaptive Regression Splines (MARS) model and the Back-Propagation Neural Networks (BPNNs) modelassisted a hybrid approach. Another change detection approach for remote sensing data is proposed in (He et al., 2015), which utilized an advanced Markov model to deal with the local ambiguity. Therefore, the need for high computation resources is considered as one of the major disadvantages (Gu, Lv, and Hao, 2017). (Han and Zhou, 2017) introduced the Adaptive Unimodal Subclass Decomposition (AUSD) learning system to analyze change with respect to the land. For estimating change from heterogeneous

images, a fusion-based FastMap approach is followed is proposed by (Touati, Mignotte, and Dahmane, 2020).

2.4 Discussion and Conclusion

A change detection classification approach becomes considerably acceptable if it provides details about change areas, accurately identifying the change forms, and better understanding the detection of change outcomes. The scale of accuracy is completely dependent upon the quality of the dataset, data complexity, domain of study, and the method opted to perform the task of change detection. This study discusses an overview of different techniques and stages that are essential for the detection of changes. The limitations of each method for the detection of change are highlighted and presented in Table 2.7.

TABLE 2.7: Classification and change detection approach with their limitations

Sr. No.	Approaches	Advantages	Limitations
	Algebra-based approaches		
1	Image Differencing	Execution is simple and basic	This approach does not give a point by point matrix, and also it requires an acceptable range
2	Image Regression	Diminish the effect of atmospherical and environmental variations between reference images	Requires precision regression function for developing this approach
3	Change vector analysis	Capacity to handle more bands of spectrum	Complexity in recognizing the land cover change (LC)

	Transformation based techniques		
1	Principal Component Analysis (PCA)	The repetition of information diminishes	It can't give a total matrix to change data and require an edge to recognize the progressions that happened in the territory.
2	Tasseled Cap (TC)	Reduce the amount of data between bands	It is inconvenient to interpret and probably won't offer an entire matrix of changes.
	Classification based approach		
1	Post Classification	Comparison Reduce the impact of atmospheric	This classification requires more time to produce output. The image quality relies upon a definitive precision.
2	Unsupervised Change Detection	An unsupervised technique utilizes a clustering approach.	The change path is hard to recognize and label.
	Advanced models for change detection		
1	Spectral Mixture Model	The outcome is steady and precise	Implementation compared to other methods is complicated
	Visual based change detection approach		
1	Visual Interpretation	During analysis, human expertise and information are useful.	Incapable of giving a point by point data that has been changing but consumes more and more time to update the result.

		Gis based approach	
1	GIS approach	It allows mapping the changes in the image of the present and past data	Performance of results varying in mathematical and classification process.
2	Integrated GIS and RS method	It empowers the elucidation and investigation of information to be accessed	Detailed data from various sources change the identification.

The data related to remote sensing is always dependent upon the need of the application. The accessibility of satellite information additionally plays a vital role in the detection of change. After reviewing the different research works, it has been concluded that the post classification approach delivers considerable accuracy as compared to the algebraic approaches. There are numerous techniques for detecting changes; however, it is difficult for selecting an optimum and definite method. As detection of change is considered as one of the challenging areas, data analysts are implementing different techniques by applying their skills to detect change. However, processing the heterogeneous data is considered as one of the most common challenges in change detection and classification. Due to advancements in technology, satellite image processing is considered as an appropriate technology for remote sensing applications. In the traditional image processing methods, the collection of the satellite images, computational approach, and the impact of disturbance on the satellite images were considered as the most common issues. Advanced data analysis methods are developed for overcoming the limitations of the traditional image processing approaches. In the past few years, deep learning techniques have increased the efficiency of data processing provided considerable prediction outcomes. In this manner, it has been concluded that the development of deep learning-assisted hybrid approaches can help to obtain promising outcomes with respect to the domain of change detection.

Chapter 3

Satellite Images and Survey Data to Predict Happiness Index

3.1 Introduction

The utilization of satellite images to map natural resources such as forests and water bodies has become increasingly popular in recent years. Forest and water resources are heavily used, therefore, regular monitoring is essential for the long-term management of these resources. The industrial revolution brought the large need for water that causes the problem of global warming and climate change. This development generates the need to identify the sources water bodies in a persistent way to estimate the quantity and quality of water resources (Feng et al., 2015; Famiglietti and Rodell, 2013). Moreover, the continuous growth of industries also causes the change of urbanization that claim the improper control of water conservation (Du, Ottens, and Sliuzas, 2010; Xie et al., 2018; Shuster et al., 2005). In this manner, an actual and accurate view of urban sources of water is critical for the development of sustainability.

3.1.1 Problem Idendification and Motivation

Recognition of water bodies in a precise manner from satellite images is considered one of the important applications in the domain of environment monitoring. Different water prediction techniques have been developed in

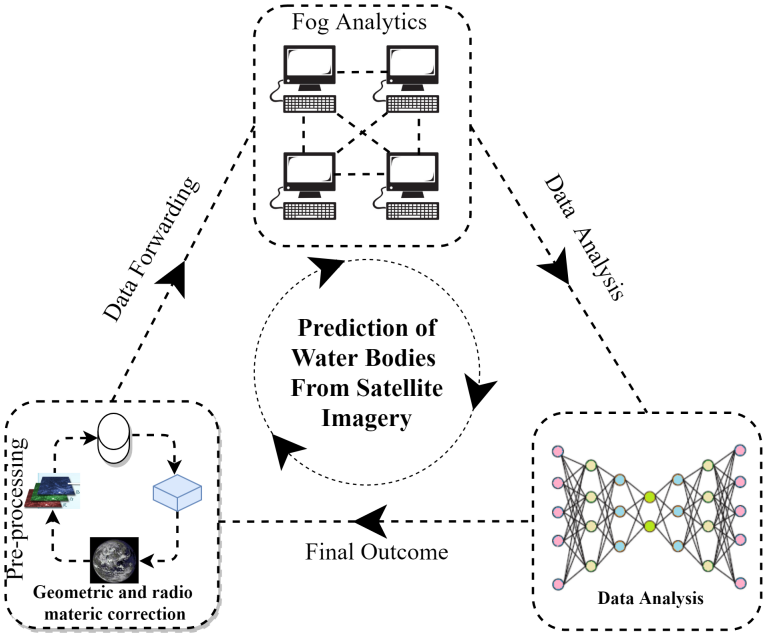

FIGURE 3.1: Conceptual Framework for Water bodies identification from satellite imagery.

previous studies for resolving the issue of water index misclassification. However, accurately assessing the dynamics of water spectral features from a series of images is challenging due to the complex properties of water spectral reflectance (Fisher, Flood, and Danaher, 2016). In this manner, water index methods have been misclassified by the majority of the traditional approaches. Therefore, several limitations have been identified in terms of water bodies recognization.

3.1.2 Contribution

Water extraction methods employ standard procedures to acquire data about water availability using remote sensing images (Du et al., 2016; Wu et al., 2019a; Zhou et al., 2014; Afaq and Manocha, 2021a). By following the need of analyzing the water resource, the proposed solution has utilized RS images as illustrated in Figure.3.1. Moreover, it has been analyzed that forwarding

the data to the cloud is increasing the transmission cost with latency. However, fog computing is considered one of the most effective solutions to deal with these two parameters. In this manner, the fog layer helps to achieve the distributed computing environment by processing the data near to the user. To fulfill the objective of the study, the contributions of the proposed study are listed as:

1. To develop Deep Convo-Restrictive Model for covering the large targeted area by analyzing the structural relationships among the smaller area.

2. To add Conditional Random Field (CRF) layer in the proposed MDFN to enhance the process of inferencing.

3. To improve spatial inferences by utilizing the Spatial-Inferred-Features (SIF) to calculate the information of the targeted region for a significant representation.

4. To transfer features to the Deep-Sparse-Auto-encoder (DSA) module and calculate non-linear connection from local and global data.

3.1.3 Chapter Organization

The remaining chapter is structured into different sections and subsections. Section 3.2 is devoted to a survey of the major literature on conventional and advanced techniques for water identification. In Section 3.3, every potential element of the suggested architecture is examined. The experimental outcomes are presented in Section 3.4. Lastly, in Section 3.5, the conclusion of the proposed solution and future perspective of the proposed study is discussed.

3.2 Literature Review

Several solutions have been introduced to evaluate water bodies using remote sensing data by utilizing sub-pixels (Li et al., 2015; Yan et al., 2018b).

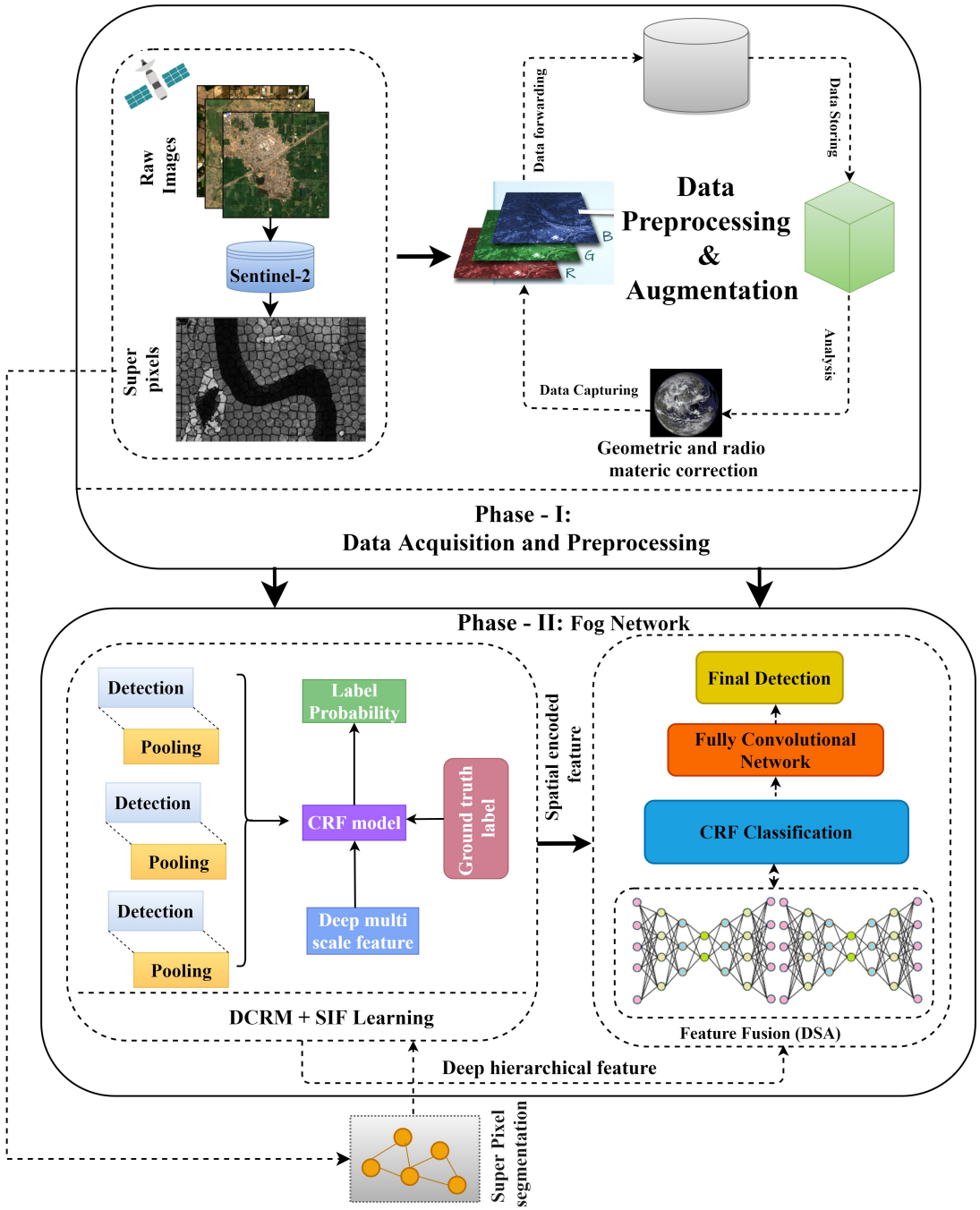

FIGURE 3.2: Complete process of proposed MDFN.

The previously developed solutions are divided into two following categories: (i) Conventional approaches and (ii) Advanced approaches.

3.2.1 Conventional approaches

Researchers have suggested several ML approaches such as SVM, k-means clustering, and many others to evaluate RS images with different resolutions(Kang et al., 2016; Katz, 2016) and the selection of important features is critical in these proposed techniques from RS images. The hand-crafting process for the collection of spatial features by using such methods is laborious and time-consuming (Kang et al., 2016). (McFeeters, 1996) proposed an NDWI approach for analyzing the target objects. This model has a limitation in terms of gap analysis among shadows and water sources. To improvise the performance of the NDWI model, author (Xu, 2006) recommended an infrared band instead of the green band to easily differentiate the shadows and water from satellite images. The method yielded the best results for urban water bodies identification.

TABLE 3.1: Comparison of multiple parameters

Studies	Fining	RS Data	Data Type	Fog Platform	Cloud Platform
(Feyisa et al., 2014)	An automatic water extraction index is proposed to enhance the water extraction accuracy while taking into consideration of various types of environmental noise	✓	NIR	×	×

(McFeeters, 1996)	The NDWI approach is proposed to extract the aource of water from satellite images	✓	NIR	×	×
(Huang et al., 2015)	Empirical evaluation is conducted on VIIR data for surface water detection	✓	SWIR	×	×
(Xu, 2006)	The modified NDWI called MNDWI is proposed to enhance the open water features	✓	NIR	×	×
(Kang et al., 2016)	Multireservoir is identifies by developing Hybrid approach	✓	-	×	×
(Katz, 2016)	In this study these issues are discussed 1) Remote sensing classification, 2) Change detection, 3) Fusion of diverse images	✓	SAR	×	×
(Fang et al., 2019)	The CNN-based framework is developed for the detection of reservoir	✓	Multi spectral Bands	×	×
(Chen et al., 2018b)	The identification water resources from satellite images are evaluated by developing deep learning approach	✓	False-color composite	×	×

(Yu et al., 2017a)	To extract water from landsat 8 data, a hybrid technique based on deep learning is presented	✓	Spectral bands	×	×
(Isikdogan, Bovik, and Passalacqua, 2017)	Fully convolutional neural network is designed that specifically used to segment the water from landsat-8 images	✓	All reflective bands	×	×
Proposed Solution	A new Multi-scale Data Fusion Network (MDFN) is presented in this proposed study to segment the water resources from a desired area	✓	False-Color Composite	✓	✓

3.2.2 Advanced Methods

In RS applications, deep learning has overcome the limitation of previously developed image processing techniques (Huang et al., 2017; Badrinarayanan, Kendall, and Cipolla, 2017; Zhu et al., 2017; Afaq and Manocha, 2021a). The Convolutional Neural Network (CNN) is widely used for obtaining spatial characteristics. CNN has a potential to extract multi-level characteristics. The potential of the extraction of multi-level characteristics is the major asset of the CNN approach. Weinstein and Ebert proposed MFCN which was upgraded by adding Fully Convolutional Network (FCN) (Han et al., 2020) to extract multiscale features for water extraction (Fang et al., 2019; Chen et al., 2018b; Yu et al., 2017a; Isikdogan, Bovik, and Passalacqua, 2017). CNN has been utilized by certain researchers to monitor the source of water from multi-resolution satellite images. In this manner, the findings show

that CNN has the capability to differentiate water area and ground shadows (Weinstein and Ebert, 1971; Geng et al., 2020; Wang et al., 2020a) proposed a novel DeepUNet model based on Convolution Neural Network to segment pixels of an image to differentiate sea water. Furthermore, the semantic segmentation with extended DeepLabv3+ was utilized on cityscapes dataset with different parameters. Lately, a novel DeepWaterMapV2 was proposed to map the surface water at a lower cost with improved precision and recall value.
As significant research towards this path has been observed, researchers have tried to incorporate advanced approaches for the effective prediction of natural resources from satellite images. However, several militations have been observed. To overcome those limitations and gaps, this research is aiming to develop a robust solution for the prediction of water from RS data.

3.3 Proposed Methodology

The proposed study aims to segment different water resources by utilizing data processing and handling principles of deep learning and fog analytics. Every possible aspect of the proposed MDFN is explained by dividing it into three phases as Data Acquisition and Image pre-processing, Water resource determination, and Degree of happiness index determination as illustrated in Figure. 3.2.

3.3.1 Data Acquisition and Pre-processing

As Punjab is considered as an essential food production state in India (Kumar and Singh, 2020), the availability of water bodies resources facilitates the farmer to cultivate the variety of crops for their livelihood that implies the happiness index of farmers. Three wetlands such as Harike, Roper, and Kanjli have been included to evaluate the status of water as demonstrated in Figure. 3.3. In the proposed study, satellite images of 12 distinct natural wetlands (839 km^2 area) and 9 man-made wetlands (14739 km^2 area) (Ladhar, 2002) are considered to identify the sources of water. The largest area of the

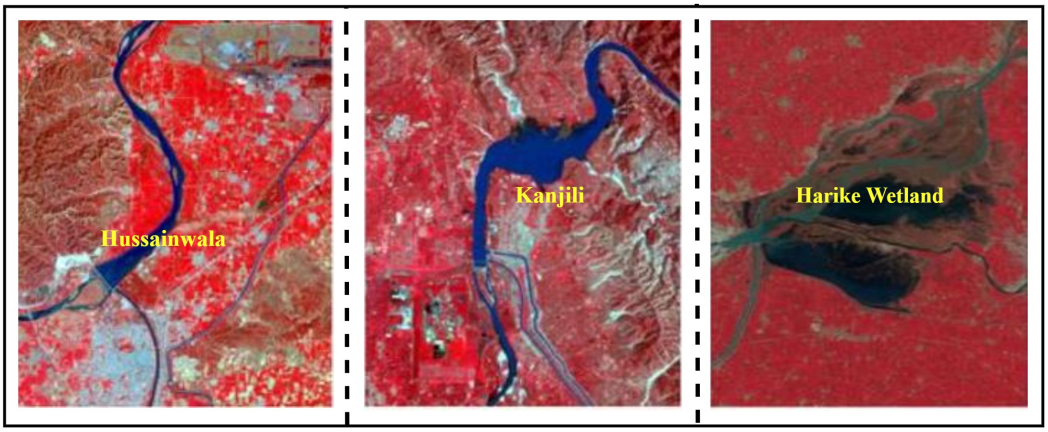

FIGURE 3.3: Different wetlands sleclected for the proposed study[2]

TABLE 3.2: Description of dataset used in the proposed study

Dataset	Color Composition	Image description	Original Images	Agumented Images
Sentinel-2 Images	False-color bands	Pixel Density: 256×256, Resolution: 10m/pixel, Bands: False-color composite	5600	11090

wetland with a percentage of 69%, 14%, and 17% belong to rivers, reservoirs, and ponds/tanks, respectively. The images of the targeted areas are captured from Copernicus Open Access Hub [1]. Moreover, the detailed description of the dataset is provided in Table 3.2 and Table 3.3 for easy understanding of the reader.

Image Pre-processing: In this study, false-color composite bands were utilized for pre-processing that helps to fulfill the necessity of the developed model. Multiple pre-processing activities such as noise reduction, atmospheric condition adjustment, and radiometric correction are performed on collected images. Furthermore, several data augmentation methods such as

[1]Source: https://scihub.copernicus.eu/

TABLE 3.3: WATER BODIES AVAILABILITY

Sr. No	Type of Class	Definition
1	River	Running water
2	Man Made	still water
3	Pond Water	Still water
4	Lake Water	Still water

clipping, rotating, flipping, shifting, and transforming are used to increase the number of images to address the issue of model over-fitting that aids in the resolution of imbalanced learning (Lan et al., 2019; Xie et al., 2019; Zhang and Montgomery, 1994; Ji, Wei, and Lu, 2019; Ding et al., 2016; Perez and Wang, 2017; Yang et al., 2016; Norouzi, Ranjbar, and Mori, 2009). Moreover, the super-pixel approach is utilized to optimize the prediction performance of the proposed approach. Super-pixels are used in several computer vision and image processing methods. A super-pixel defines the group of pixels with similar characteristics. Hence, Simple Linear Iterative Clustering (SLIC) (Achanta et al., 2012) is utilized to derive the superpixels and helps to eliminate deviated pixels. In this way, the super-pixel technique in satellite images makes the borders around the object that helps in distinguishing every possible small adjacent object.

3.3.2 Fog Space: Water resource prediction

In this section, a Convolutional Restricted model-based technique is utilized for the segmentation of water bodies by analyzing RS images as represented in Fig. 3.2. The first module is responsible to extract spatial characteristics from the RS data by utilizing the feature extraction capability of the Deep Convolutional Restricted Model (DCRM). After extracting features, the structural learning method is used in the second module to analyze the relationship between the artifacts and the environment. At last, a feature fusion layer is introduced to generate more effective image representative functions. The step by step process of each module is discussed below:

Deep Convo-Restricted Model The precise identification of features towards the given object is determined as a key assessment parameter of the proposed approach in the field of RS. Therefore, Deep Convo-Restricted Model extracts spatial features from the given data by utilizing 2d-CNN and RBM techniques. The developed framework is presented in Figure. 3.4 and explained in two layers such as Detection Layer (**DL**) and Visible Layer (**VL**).

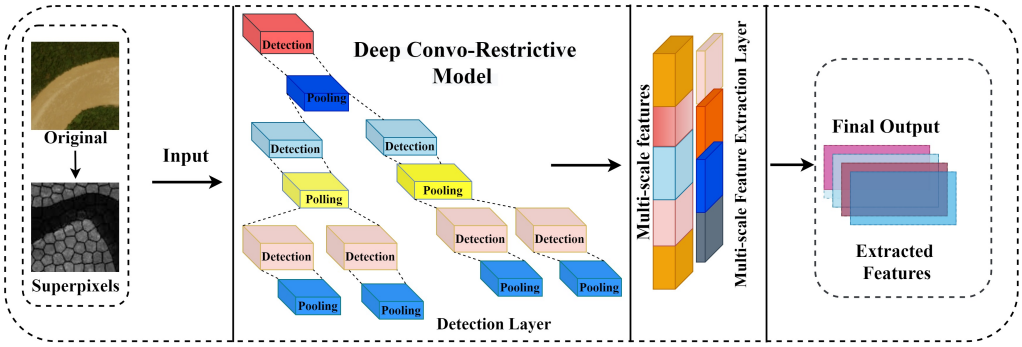

FIGURE 3.4: The DCRM feature learning concept.

In DL, F^k series of kernels are utilized to identify the features from the image and produce D^k dimension matrices indicated with N_d for feature extraction. A dimensional matrix with its weights and bias is indicated by F^k and b^k, respectively. While the dimensional matrix of sub-units are expressed by d_{ij}^k. The variables i and j specify the ratio of convolution process. Using the pooling technique denoted with B_α, the Max-pooling layers marked with **m** are utilized to reduce the dimension of an image. Furthermore, the VL has **K** number of convolutional filters and each filter has n_f dimensional matrix. Convolutional kernels $F^k(k \in [i,k])$ are included to deal with the possibility of comparable characteristics of an image and shared among both DL and VL. The following formula is used to determine the cumulative probabilistic value:

$$m(vl,dl) = \frac{1}{z} exp(-e(dl,vl)) \tag{3.1}$$

Here, the maxpooling operation is denoted by m, detection and visible layer is represented as dl and vl, whereas, the normalised parameter $z = \frac{1}{z} exp\left(-e(vl,dl)\right)$

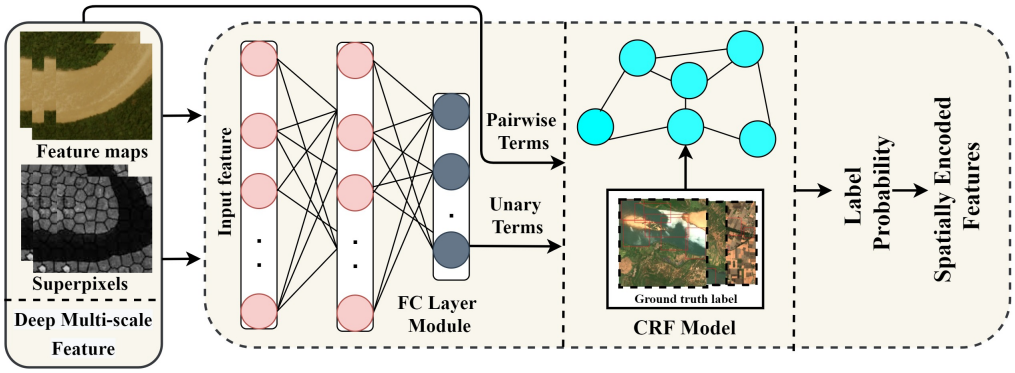

FIGURE 3.5: Representation of structural learning.

and the DCRM energy function is computed as follows:

$$e(l,d) = -\sum_{k=1}^{k} d^k \odot (\tilde{F}^k \star l) - \sum_{k-1}^{k} b^k \sum_{ij} d_i j^k - s \sum_{ij} l_{ij}, \tag{3.2}$$

Here, 2d convolution, element-wise multiplication, and flipping operations are represented by $\star$, $\odot$, and $\tilde{C}^k$, respectively. In this manner, the units of detecting layer **DL** evaluate the overall activation from smaller regions of the satellite image. To minimize the inference process in the proposed solution, the following equation is used:

$$e(vl,dl) = -\sum_{K}\sum_{ij}(d_{ij}^k(\tilde{F}^k \star l)_{ij} + b_k d_{ij}^k) - s\sum_{ij} l_{ij} \sum_{(ij)\beta_\alpha} l_{ij}^k \leq 1, \forall k, \alpha \tag{3.3}$$

Here, the fixed-shape window of the DL is represented as B_α and SGD is adopted to improve the specification of the DCRM (Han et al., 2016). Moreover, the contrastive divergence approach (Hinton, 2002) is employed to optimize the effectiveness of the method over the stochastic gradient descent (SGD).

Structural Learning Layer (SLL) Even, CNN has the potential to obtain hierarchical features, these features are ineffective to evaluate the relationship

between artifacts and spatial features. Therefore, the CRF approach is employed for detecting the SIF (Bu et al., 2016) and the procedure of accessing SIF are clearly illustrated in Figure. 3.5. A graph method represented as **g = (v,e)** is introduced to manage high resolution (HR) images, where the edge e is denoted as E and vertex v is denoted as **V**. The vertex unit refers to the image sub-segments and the border refers to the relationship between nearby unit pairs. The weight in the training data is used to generate the conditional probability distribution as follows:

$$x(x\|y,t) = \frac{1}{z(x,t)} \prod_{i \in V} \phi_n(x_i, y_i) \prod_{e_{ij} \in e} \psi_e(x_{ij}, y_i, y_j) \tag{3.4}$$

Here, a constructed graph model pair-wise partitioning function is expressed by $a(y,t)$. The features of a unit are specified as $\psi_e(x_{ije}, y_i, y_j)$. Furthermore, the potentials of $f_n - F_e$ are labeled as log-linear function denoted as e_{ij}. An edge which is composed of v_i, v_j and p represents the units with their respective states y = < y_1, y_2, y_3,....., y_n >. The training procedure has been modified as follows:

$$t^* argmin_t \lambda \|t\|^2 - \sum_{n=1}^{m} (\sum_{i \in V} t_N^T f_N(x_i^n, y_i^n) + \sum_{e_{ij} \in E} t_E^T f_E(x_{ije^n}, y_i^n, y_i^n)) + \sum_{n=1}^{m} \log Z(x^n, t) \tag{3.5}$$

Here, the weight of paired elements is $t = [T_N; T_E]$, where λ is a positve L2-regularizer represented as $t = [TN; TE]$. Additionally, the graphical model is represented as (x_i^n, y_i^n). It has been analyzed that by maximizing the value can imrove the chance of prediction of target class denoted as $x(y \mid y, t^*)$.

Spatially Inferred Features (SIF) As per the literature review, it has been identified that the CRF is considered as one of the optimized approaches in the field of RS. Here, the integration of CRF is done for enhancing the stability of prediction. In parallel, the graphical and SIF models are applied to obtain both super-pixel and spatial features for resolving the learning limitation

of spatial features. The connection in the graph is defined as $G_\mu = (V_\mu, E_\mu)$, where μ is describing as super-pixels. Moreover, $\odot(\mu)$ is used to represent the SIF model and is further calculated as follows:

$$\odot(\mu) = \lambda \sum_{i \in V_\mu} \sum_{j \in V_\mu} \theta_i \theta_j^T \exp\left(-k_d \frac{d(v_i, v_j)}{\sigma_d}\right) \tag{3.6}$$

Here, the density of existence of the adjacent probability of defined vertices i and j is specified by $n \times n$ matrix of $odot$. Moreover, the distance between super-pixels is denoted by $d(v_i, v_j)$. Furthermore, the distance decay rate, vertice distance, and normalised parameter are represented by k_d, σ_d, and λ, respectively.

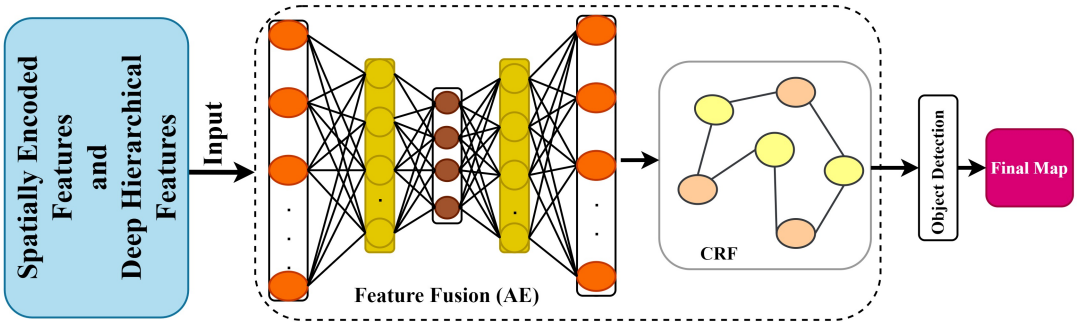

FIGURE 3.6: DSA and CRF model for the extraction of hybrid features.

Multi-layered Feature Fusion (MFF) A multilayer sparse auto-encoder (SAE) is part of a multilayer feature fusion (MFF) neural network that is implemented in the proposed solution. In addition, MFF precisely obtains the hierarchical features with similar attributes from the images. Figure. 3.6 illustrates the complete process of fusing multiple features. In the process of feature and structural learning defined as $[U_p, \odot] \in W^{(N+nxn)}$, two different descriptors such as DHF U_p and SIF $\odot$ are obtained. In addition, DSA is utilized to integrate linked data. Furthermore, the backpropagation approach is applied in the proposed solution to optimize the prediction efficiency.

The sample of SAE is denoted as $X = (x_1, x_2, ..., x_N)^T$. The hidden units n_r in layer **L** are represented as $r_l = (r_1^L, r_2^L ..... r_{nr}^L)$. The sigmoid activation functions utilized in the proposed model are further expressed as follows:

$$r^L = \frac{1}{1 + e^{-x}}(tX + B_r) \tag{3.7}$$

Here, r^L corresponds to the equivalent representation of the modified encoder from the **X** input. The value of $\sigma(z)$ will always be equal to $(1 + \exp(-z))^1, w \in R^{NxN_H}$ and bias value B_H will corresponded to $R^{N_H x1}$. As a result, a $\tilde{X}$ approximation equation can be expressed as follows:

$$\tilde{X} = \frac{1}{1 + e^{-x}}(t^T r^L + B_0), B_o \in R^{nx1} \tag{3.8}$$

To reduce the varince between X and $\tilde{X}$, o is calculated as:

$$o = \frac{1}{n_c} \sum_{i=1}^{n_c} \left\| \tilde{X}^i - X^i \right\|^2 + \beta \|t\|_2^2 + \alpha \sum_{j=1}^{n_r} kl(p \| \tilde{p}_j) \tag{3.9}$$

Here, the average activation fucntion is represented by $\tilde{p}_j$ of j_{th} and p is selected as an activation function.

3.4 Experiments

The efficacy of the proposed model is assessed on the Sentinel-2 image dataset. The system is configured as follows to carry out the experiments: Intel Core i5 2.8GHz CPU, NVIDIA GTX-1080Ti GPU, Ubuntu 18.4 LTS Operating System, Python Programming Language. The implementation of the developed solution is evaluated and presented in distinct subsections as follows;

- Material and Methods
- Evaluation metrics
- Implementation of MDFN
- Prediction Performance

TABLE 3.4: Survey collection from three regions of Punjab

Region	Total responses	Positive Responses	Negative Responses
Dowaba	637	530	107
Malwa	556	412	114
Majha	283	191	92

- Identification Results
- Comparative Analysis

3.4.1 Material and Methods

The degree of happiness index is evaluated by following two processes as follows; (i) Conducting an extensive field survey and (ii) Extraction of water resources from RS data of the targetted areas. A total number of 1476 responses have been conducted according to the three regions of Punjab such as Dowaba, Malwa, and Majha. The number of responses is divided according to the regions of Punjab. The complete detail of responses which are categorized into positive and negative responses is represented in Table 3.4 and illustrated in Figure. 3.7.

3.4.2 Evaluation Metrics

The prediction capability of the developed solution is impossed by calculating F1-score, Recall (R), Precision (P), and IoU performance measures. Moreover, the extraction of water by developed solution is justified by comparing the determined outcomes with the performance of selected state-of-the-art methodologies such as VGG, ResNet, DeepLab V3+, SegNet, NDWI, and MDFN by calculating the similar measures. Furthermore, the specified error metrics are expressed mathematically as follows:

$$P = \frac{TP}{TP + FP} \tag{3.10}$$

$$R = \frac{TP}{TP + FN} \tag{3.11}$$

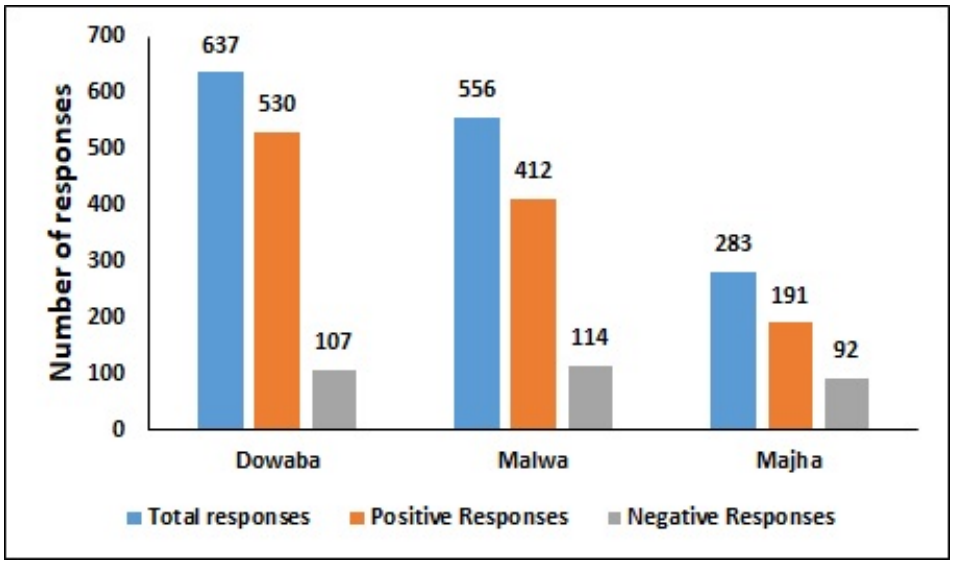

FIGURE 3.7: Number of responses according to positive and negative responses

$$F1 = \frac{2 \times R \times P}{R + P} \tag{3.12}$$

$$IoU = \frac{TP}{TP + FP + FN} \tag{3.13}$$

3.4.3 Implementation Of MDFN

Deep-Restrictive Model (DRM): The Deep Restrictive Model is containing total 6 convolutional layers where Ist, 2nd, and 5th layers of the architecture is responsible to execute convolutional operations. It is imperative to mention that Contrastive Divergence (CD) is utilized to fine-tune the convolutional layers. Furthermore, the 3rd, 4th, and 6th layers of the network perform the Max-pooling operation. Furthermore, the batch gradients are updated during the process of CD by leveraging the momentum from the previous gradients. Similarly, Deep Hierarchical Features (DHF) are utilized to train the Structural Learning Layer without using the method of backpropagation. In this manner, certain experiments are carried out throughout the generation of super-pixels to verify the presented solution's efficiency and

TABLE 3.5: Prediction permorance evaluated on the dataset.

Number of Images	Data Divisioning	Training Samples	Validation Samples	Test Samples	Overall Accuracy
5600	70:30	3920	1176	504	0.826
	75:25	4200	1050	350	0.852
	80:20	4480	896	224	0.899
11090	70:30	5634	2328	2327	0.919
	75:25	6238	2079	2772	0.938
	80:20	7097	1774	2218	0.958

performance. Different parameters such as region size, L2 regularization (λ), and distance factor (kd) with the value of 0.1 are calculated to analyze the spatial correlation among super-pixels. The sparse penalty term α of every hidden layer is evaluated at distant lr such as 0.2, 0.01, and 0.04. Furthermore, the weight (β), activation function (ρ), and the LR are tuned to 0.001, 0.05, and 0.01, respectively. To deal with overfitting, the proposed solution is processed with 50 batches and 100 epochs. The manual data division method is adopted with different ratios to evaluate the performance of the model.

3.4.4 Prediction Performance

In the original dataset, there are a total of 5600 images collected which are further augmented to increase the number of images to satisfy the data-hungry approach of deep learning. In addition to this, different data augmentation techniques such as rotation, clipping, flipping, and transformation are performed on the images to enhance the adaptability of the data that helps to deal with the issue of over-fitting (Ji, Wei, and Lu, 2019; Ding et al., 2016; Perez and Wang, 2017; Yang et al., 2016; Norouzi, Ranjbar, and Mori, 2009). After executing data augmentation processes, a total of 11090 images are collected that allowing for the inclusion of every imaginable real-life scenario. To evaluate the train-set and test-set efficiency, different ratios are used in dataset by utilizing the approach of manual data divisioning as shown in Table 3.5.

TABLE 3.6: The derived result of P, R, F1, mIoU on different resolutions and the highest precision is highlighted.

Model	Ratio	***P***	***R***	***F1***	***mIoU***
MDFN	70 : 30	0.931 ± 0.016	0.912 ± 0.017	0.918 ± 0.016	0.863 ± 0.019
	75 : 25	0.928 ± 0.017	$\mathbf{0.928 \pm 0.017}$	0.909 ± 0.015	0.863 ± 0.022
	80 : 20	$\mathbf{0.958 \pm 0.013}$	0.878 ± 0.016	$\mathbf{0.921 \pm 0.013}$	0.881 ± 0.021

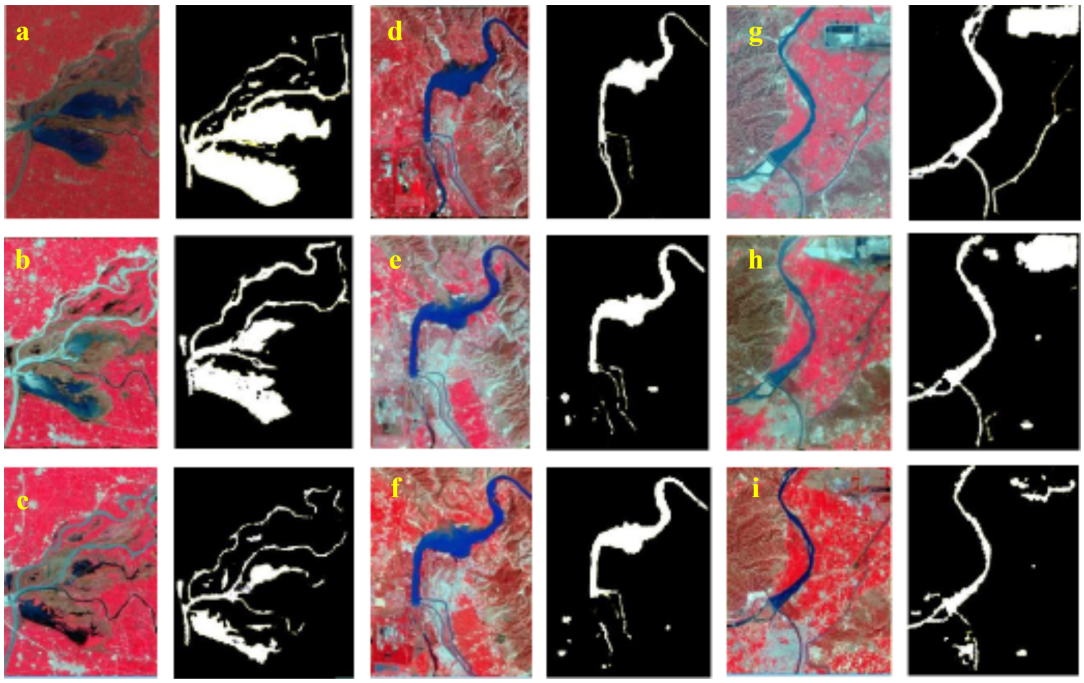

FIGURE 3.8: Comparision of different models on selected wetlands of Punjab.

3.4.5 Identification Results

A set of 940 remote sensing images are selected from the related ground truth images to determine the prediction capability of the proposed solution. The efficacy of the developed method is measured using different ratios as presented in Table 3.6. The water resources from various shapes are present in the dataset that helps to determine the prediction efficiency of the proposed method towards the complex pattern. The method has been considered to be accurate for the classification of water bodies in diverse locations and shapes. Furthermore, the model is capable of accurately distinguishing minor rivers and barriers such as water tunnels. To avoid the biasness in the dataset, the dataset is collected from three different locations of Punjab. The results of each location are illustrated in Figure. 3.8.

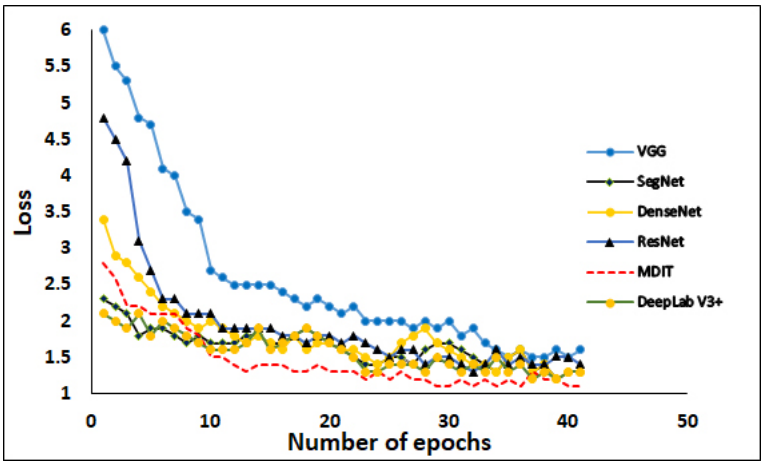

FIGURE 3.9: Training Losses of different models.

3.4.6 Comparative Analysis

The training loss for each selected method is presented in Fig. 3.9. In CNN, the cost function is utilized to compute the variance int he middle of the value of the ground truth of an image. Lower the loss-value means higher the accuracy value of the model. During the comparison, it has been observed that the VGG model has a higher loss value which is fairly similar to SegNet. In the early epochs, the proposed MDFN has registered higher loss. However, less loss has been observed after a certain number of epochs that indicate the stability of the proposed model. Moreover, the comparative analysis based on hyperparameters is illustrated in Table 3.8

Table 3.7 shows the training and testing time taken by the proposed model and selected models. According to the computed results, according to the results the VGG has taken a total of 171.66 minutes of testing which is higher as compared to the others. Additionally, the proposed solution has taken less testing time with 94.37 minutes. In this manner, it can be concluded that the proposed solution has taken less testing and training time as compared to other models as presented in Table 4.13. Moreover, the computed outcomes are also illustrated diagrammatically in Fig. 3.10 for easy understanding.

In addition, the stability of the developed solution is justified by evaluating the P, R, F1-score, and IoU, The calculated outcomes are illustrated in

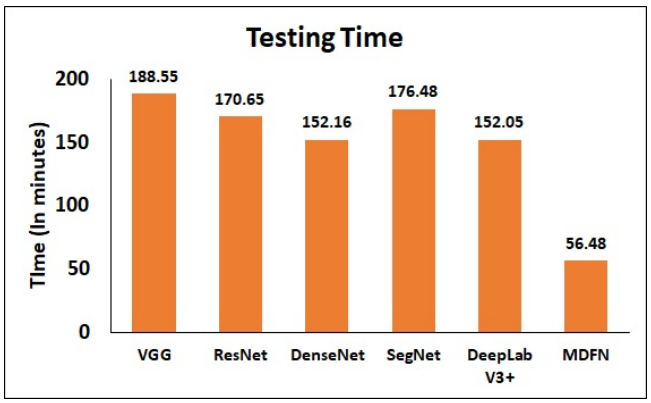

(A) Training

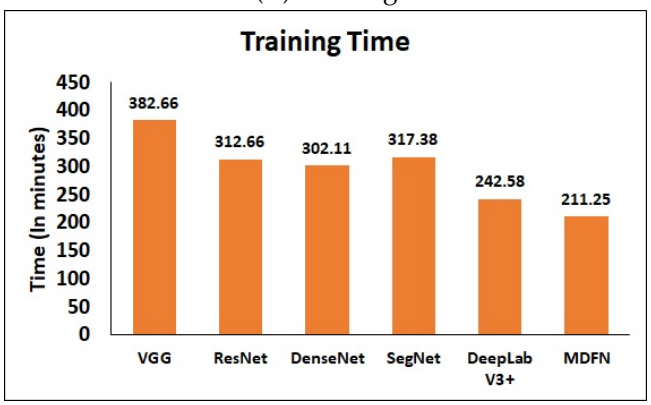

(B) Testing

FIGURE 3.10: Execution time of different models

TABLE 3.7: The execution time of the different models

Models	Training-set		Test-set	
VGG	22,960 s	382.66 m	11310 s	188.55 m
DenseNet	18,120 s	302.11 m	9120 s	152.16 m
ResNet	18,760 s	312.66 m	10239 s	170.65 m
MDFN	12,675 s	211.25 m	3389 s	56.48 m
SegNet	19,043 s	317.38 m	10589 s	176.48 m
DeepLabv3+	14555 s	242.58 m	9123 s	152.05 m

TABLE 3.8: Comparison of hyperparameters

Models	Learning Rate	Activation Function	Batch size	Epochs
MDFN	0.01	ReLU	50	100
VGG	0.001	Sigmoid	70	100
SegNet	0.01	ReLU	40	100
ResNet	0.001	ReLU	40	100
DenseNet	0.01	Sigmoid	50	100
DeepLabv3+	0.01	ReLU	60	100

Table 3.9 and presented in Fig. 3.11 and Fig. 3.12. It has been observed that the proposed solution has registered the highest accuracy of 0.958 as compare to other models. Additionally, the traditional approach NDWI model has achieved a prediction accuracy of 0.719. Furthermore, the F1-score of the developed model acheived the accuracy of 0.928 as compared to VGG (0.892), DenseNet (0.909), SegNet (0.908), DeepLabV3+ (0.907) and ResNet (0.880). Similarly, the proposed model has also achieved a higher IoU value with the value of 0.874% as compare to other models. Therefore, the proposed method surpasses the existing deep learning models for the segmentation of water from RS data. In addition to this, three distinct wetlands in the Punjab region were chosen between 20 August 2019 and 30 November 2019 to assess the prediction performance as presented in Fig.3.11.

Water and vegetation are represented by the blue color and red color in the original image, respectively. The lake is depicted as a pure white color in the prediction image and the dotts indicates the urban area. The developed model effectively extracted the sources of water bodies from RS data

TABLE 3.9: Comparision of different selected models with proposed solution

Metrics	MDFN		VGG		DenseNet		SegNet		ResNet		Deeplabv3+		NDWI	
P	**0.958**	±	0.886	±	0.926	±	0.912	±	0.914	±	0.924	±	0.719	±
	0.012		0.014		0.012		0.018		0.014		0.012		0.029	
R	0.899	±	0.877	±	0.894	±	0.908	±	0.903	±	0.897	±	0.926	±
	0.016		0.014		0.018		0.017		0.013		0.019		0.010	
F1	**0.928**	±	0.892	±	0.909	±	0.908	±	0.880	±	0.907	±	0.896	±
	0.013		0.016		0.014		0.017		0.017		0.014		0.015	
IoU	**0.874**	±	0.833	±	0.868	±	0.842	±	0.854	±	0.862	±	0.758	±
	0.021		0.023		0.023		0.021		0.021		0.021		0.025	

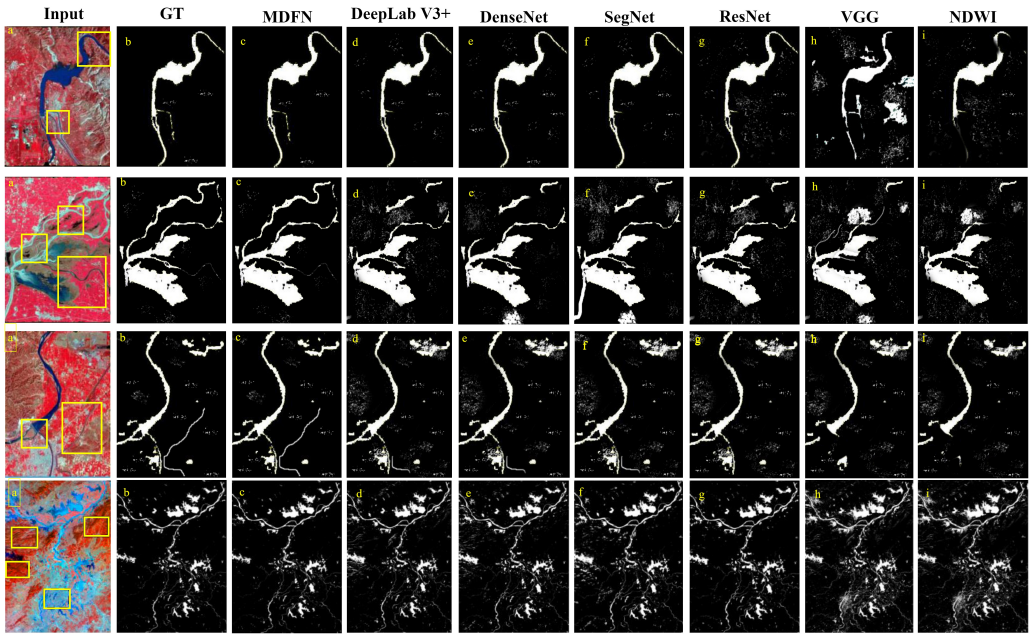

FIGURE 3.11: Water identification results of Punjab from 30 Aug 2017 to 31 Aug 2019.

and also recognized the minor ponds, rivers, and small-lakes during segmentation as presented in Fig. 3.11. Moreover, the stability of the developed model is also better for differentiating the water and clouds. The bare land is depicted with small dots in segmentation images. Moreover, solid lines are depicted as mountain areas and dash lines marked as urban areas in images. The water bodies are isolated from the rest of the image shadows. ResNet and VGG models show various patches in the corresponding areas of the non-water area as water that defines the poor prediction performance. Meanwhile, SegNet, DeepLabV3+ and, DenseNet have also produced some false predictions. The primary water bodies are accurately recognized by the NDWI model. However, certain bare-land and dense areas are also classified as water bodies.

3.4.7 Survey-based prediction performance analysis

The happiness index of the farmers is determined by dividing data into four different classes such as Very Happy (4), Happy (3), Neutral (2), and Not

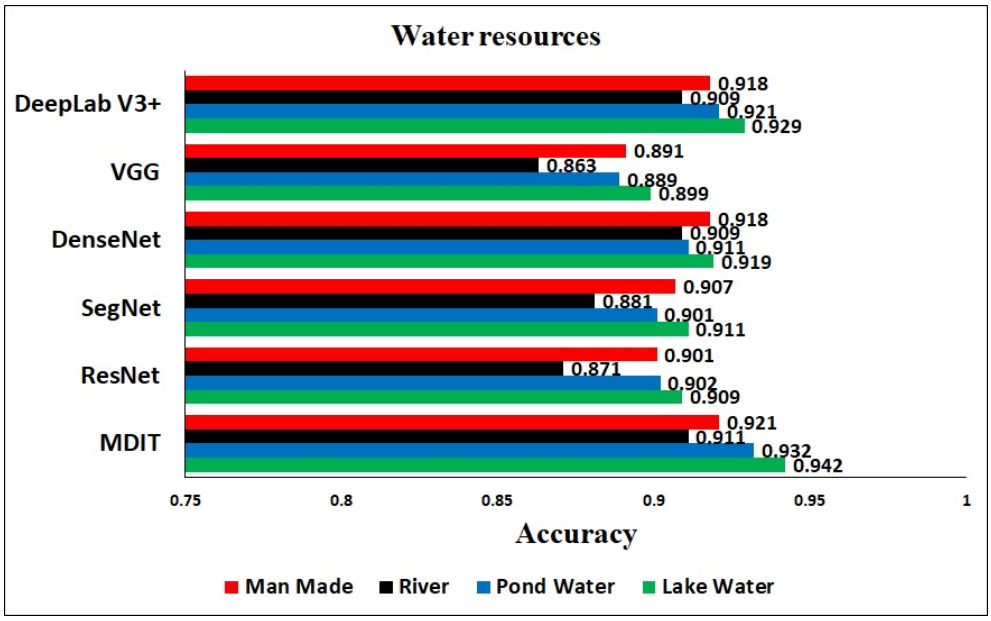

FIGURE 3.12: The prediction performace of defferent models on several wetlands.

TABLE 3.10: KNN perfomance on 4 classes

No of neighbours	k=120	k=100	k=70	k=50	k=20	k=10
Accuracy	63.92%	64.76%	65.23%	65.12%	62.34%	62.78

Happy (1). The degree of happiness is allocated in 4 classes where 1 defines Not Happy and 4 defines Very Happy. Furthermore, the most influential machine learning approaches such as K-Nearest Neighbors, DT, MLP, and NAÏVE BAYES is utilized to evaluate the happiness index of farmers based on the responses of the farmers. The prediction accuracy of each selected model is evaluated and presented in Tables 3.10 3.11 3.12.

It has been observed that the accuracy of each model is improved while decreasing the number of classes. From the calculated outcome, it can be concluded that the MLP model achieved a higher accuracy of 65.25%. However,

TABLE 3.11: Performance of DT on 4 classes

No. of depths	depth=3	depth=5	depth=7	Depth=10
Accuracy	62.67%	63.15%	64.56%	62.43%

TABLE 3.12: Pereformace of MLP and NAÏVE BAYES on 4 classes

Prediction accuracy of MLP					
Hidden Layers	2	2	2	3	4
Hidden Neurons	50	100	150	100	100
Accuracy	61.43	66.23	60.22	65.25	64.45
Prediction accuracy NAÏVE BAYES					
No of folds	1	2	3	4	5
Accuracy	60.43%	65.13%	59.42%	64.78%	63.34

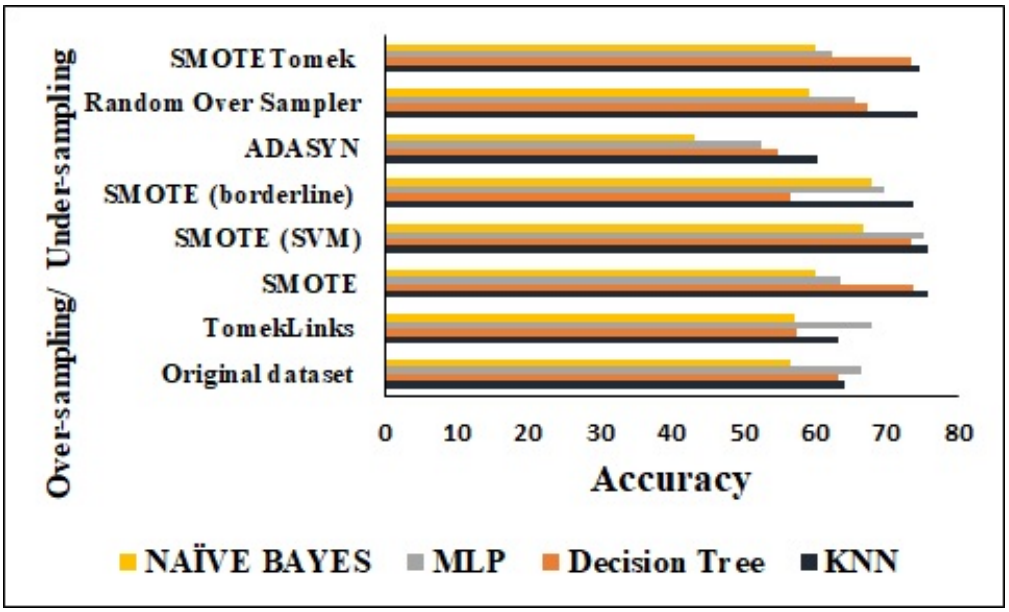

FIGURE 3.13: Comaparative analysis of different models

the achieved results are not satisfactory due to class imbalance in the dataset. To solve the issue of class imbalance, two major approaches are opted such as over-sampling and under-sampling. The over-sampling techniques such as SMOTE, SMOTE based on SVM, SMOTE based on borderline, RandomOver-Sampler, and ADASYN, and the under-sampling approaches such as Tomek-Links and TomekLinks are employed. Furthermore, the calculated outcomes with respect to over-sampling and undersampling are shown below.

From the results, it has been realized that the MLP model has acheived a better accuracy of 78.35% towards the 4 classes as presented in Table 2.5 and Figure 3.13. On the other hand, the KNN, NAÏVE BAYES, and Decision Tree registered the accuracy value of 68.26%, 60.53%, and 70.17%, respectively. In this manner, a direct correlation has been observed between the availability of water and the scale of happiness of the farmers. The higher availability of water defines the higher index of happiness in farmers of that specific region. It has been observed that the Malwa and Majha regions of Punjab are containing a large number of manmade water resources as compared to the Dowaba region. Therefore, a higher degree of happiness index has been calculated in the farmers of the Majha and Malwa regions. However, due to the less availability of water resources in the Dowaba region, a less degree happiness index is observed in farmers.

3.5 Conclusion

Advanced hardware and data processing solutions have provided the capability to analyze the frames to identify common patterns effectively. In this manner, a multi-layer data fusion approach is developed for the segmentation of water sources in a specific area by utilizing multispectral data. The purpose of this study is to analyze the degree of happiness index in the farmers of different regions of state Punjab towards the availability of water at their specific location. The maximum prediction accuracy is achieved by integrating DSA that evaluates spatial features from the data. Furthermore, the DRCM-assisted unsupervised learning solution is also integrated with the proposed solution for the extraction of complex characteristics from the

TABLE 3.13: Comparative analysis for the calculation of hapiness index by applying differnt models

Approaches	Original dataset	TomekLinks	SMOTE	SMOTE (SVM)	SMOTE (border-line)	ADASYN	Random Over-Sampler	SMOTETomek
KNN	68.26%	67.33%	78.61%	76.78%	76.67%	70.39%	78.43%	75.53
Decision Tree	70.17%	61.44%	77.69%	76.40%	60.54%	60.92%	69.45%	73.57%
MLP	78.35%	79.78%	74.42%	80.19%	70.53%	67.50%	68.58%	66.48%
NAÏVE BAYES	60.53%	65.11%	64.13%	68.65%	70.78%	52.22%	58.24%	66.15%

labeled data. The determined outcomes define the efficacy of the developed solution for the prediction of the source of water from different RS samples by registering the higher rate of F1 (0.928), IoU (0.874), Recall (0.899), and Precision (0.958). Moreover, the higher accuracy in the performance measures achieved by the proposed solution has outperformed the selected models concerning the prediction of the sources of water from Rs images. Furthermore, the conducted survey defines the higher correlation between the degree of happiness in farmers towards the availability of water resources in that specific location. In this manner, the proposed solution can be considered to analyze the degree of happiness of the individuals related to the other social aspects such as urban development, food security, and many others. Howover, the proposed model is not able to identify the small water bodies due to the presence of cloud. In future work a multi-spectral high resolution satellite images need to pe utilized for the prediction of small water bodies in the domain of remote sensing.

Chapter 4

Water Bodies Identification

4.1 Introduction

Identification of water resources from satellite images has become a primary domain of research in the area of remote sensing. As water is helping in the overall development of humans, it also adds to economic development by affecting nearly every industry such as agriculture, petroleum refineries, melting facilities, and many others (Feng et al., 2015; Famiglietti and Rodell, 2013). Over the last few decades, the constant expansion of companies in metropolitan areas has resulted in substantial changes in urban water management (Du, Ottens, and Sliuzas, 2010; Xie et al., 2018). It has been hypothesized that inefficient water management has an impact not only on sustainability but also on the normal role of ecosystems (Shuster et al., 2005). Moreover, it has been analyzed that the large need for water and constantly increasing temperature has become the key challenge of climate change. Therefore, the development of empirical and reliable urban water management is essential for efficient sustainability.

4.1.1 Problem Identification

The mapping of water resources is considered as one of the crucial applications for resource surveys, flood assessments, and environment monitoring. From the last few decades, numerous studies have been suggested for the identification of water resources. Researchers from different domains have proposed several strategies to address the issue of misclassification of water

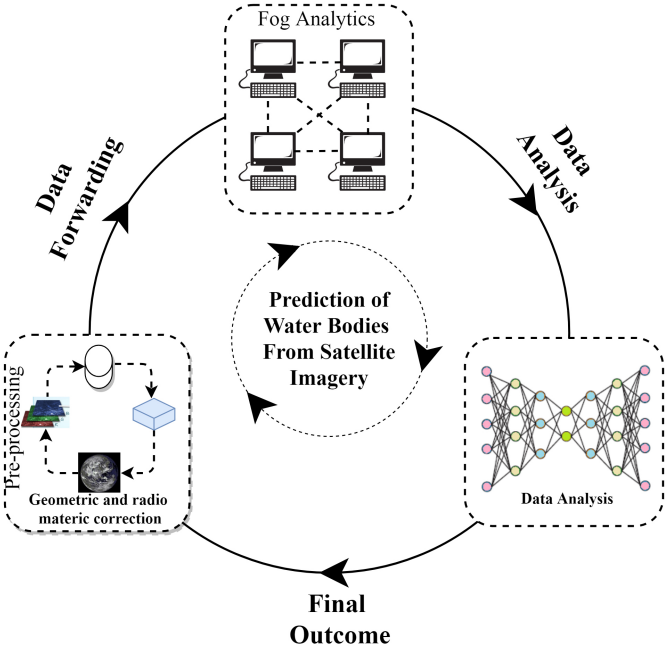

FIGURE 4.1: The conceptual framework of the proposed framework

indexes. However, due to the unique features of water spectral reflectance, precisely analyzing the dynamics properties of water from a sequence of images is difficult to analyze (Fisher, Flood, and Danaher, 2016). Therefore, the water indexes were incorrectly categorized using traditional data processing methods. In this manner, several limitations have been observed with respect to the identification of water resources in the previously developed identification approaches.

4.1.2 Motivation and Contribution

At present, satellite images have shown a considerable outcome in the field of remote sensing (Shuster et al., 2005). By considering the advancement in data acquisition and processing techniques, satellite images are widely used in several domains such as environmental conservation, geography, military identification, mapping, many others (Yang et al., 2017b). Moreover,

advanced data processing techniques and high computational resources allow more effective and precise analysis of the objects from satellite images. In this manner, remote sensing has been widely used for natural resource mapping by considering its capability of collecting a large number of observations with low cost (Du et al., 2016; Wu et al., 2019a; Zhou et al., 2014). Therefore, the ability of a high scope of perceptions from remote sensing made it possible to map the water resources in a frequent and effective manner (Zhou et al., 2014). Hence, the extraction of water resources from the targeted area is illustrated in Figure.4.1. In this manner, to achieve the goal of the prediction of water resources, the objectives of the proposed chapter are listed as:

1. To analyze the area by identifying the underlying relationship among the smaller areas with the help of the proposed Deep Convolutional-Restrictive Model (DCRM).

2. To improvize the concept of inferencing and structural learning in an explicit manner with the help of the proposed Multi-scaler Data Integration Technique (MDIT).

3. To increase spatial deviations by computing the data of the designated areas by adding Spatial Inferred Features (SIF) in the proposed MDIT.

4. To evaluate the non-direct relationship among the features of the data by utilizing Deep Sparse Auto-encoder (DSA) module.

4.1.3 Chapter Structure

The rest of the chapter is organized into multiple sections. In Section 4.2, the primary literature of review is made on traditional and modern approaches for the detection of water. Every possible aspect of the proposed architecture is discussed in Section 4.3. Experimental results are discussed in Section 4.4. At last, primary conclusive remarks with possible future directions are discussed in Section 4.5.

4.2 Related Work

In this section, extensive literature is reviewed and presented by dividing it into the following subsections: (i) Conventional approaches and (ii) Deep Learning approaches.

TABLE 4.1: Comparative analysis based on the specific parameters

Authors	Description	Satellite Data	Fog	Technology	Real Time
(Feyisa et al., 2014)	To identify the water bodies from satellite imager an automatic approach for the identification of water is proposed while taking various types of environmental noise.	Yes	No	Traditional	No
(McFeeters, 1996)	To detect the patterns of open water features an NDWI method is proposed.	Yes	No	Traditional	No
(Huang et al., 2015)	To identify the surface water an exploratory evaluation is carried out on VIR satellite images.	Yes	No	Traditional	No
(Xu, 2006)	To enhance the water identification accuracy the modified version of NDWI and MNDWI is proposed for the identification of water bodies.	Yes	No	Traditional	No

(Kang et al., 2016)	The Hybrid approach is proposed to identify the multi reservoir water supply in dry years.	Yes	No	Traditional	No
(Katz, 2016)	Three special issues are presented in this study (1) Change detection, (2), Remote sensing classification, (3) Fusion of diverse types of images.	Yes	No	Modern	No
(Fang et al., 2019)	To detect the global reservoir from Landsat-8 images a convolutional neural network framework is proposed.	Yes	No	Modern	No
(Chen et al., 2018b)	For the extraction the of urban water bodies from a deep learning architecture is proposed.	Yes	No	Modern	No
(Yu et al., 2017a)	A deep-learning-based hybrid approach is proposed for the identification of water bodies from Landsat-8 images.	Yes	No	Modern	No
(Isikdogan, Bovik, and Passalacqua, 2017)	To segment water bodies a Fully Convolutional Neural Network is developed for Landsat 8 images.	Yes	No	Modern	No

Proposed Solution	In this proposed study, a novel Multi-scaler Data Integration Technique (MDIT) is proposed to identify the availability of water resources from a targeted location using sentinel-2 images	Yes	Yes	Modern	Yes

4.2.1 Conventional approaches

Numerous techniques have been developed to recognize water resources by utilizing the techniques of remote sensing such as single and multi-band threshold approaches, water bodies index methods, and water mapping methods using sub-pixels (Li et al., 2015; Yan et al., 2018b). McFeeters and (McFeeters, 1996) developed a Normalized Water Difference Index (NDWI) approach to identify the targeted object. However, the proposed model fails to identify the difference between shadows and water resources. (Xu, 2006) proposed an approach that deals with the gap between shadows and water by employing a mid-infrared band for the normalization as compare to the green band. The proposed model has shown the utmost result for urban water bodies extraction. On the other hand, several machine learning approaches such as k-mean clustering, support vector (Kang et al., 2016; Katz, 2016) have been developed by multiple researchers to identify the water bodies in an accurate manner. These approaches were generally utilizing remote sensing images with limited spatial resolution. Furthermore, the selection of appropriate combinations of features such as spectral, texture, and shapes played are playing a crucial role in these approaches. Therefore, the process of feature extraction is time-consuming and difficult (Kang et al., 2016).

4.2.2 Deep Learning approaches

Deep learning has shown significant efficacy in the domain of image processing that overcomes the limitations of standard data processing approaches (Huang et al., 2017; Badrinarayanan, Kendall, and Cipolla, 2017; Zhu et al., 2017; Afaq and Manocha, 2021a). Convolutional Neural Network (CNN) is one of the most prominent deep learning image processing techniques that is primarily used to extract features and perform classification operations (Han et al., 2020). The ability to generate multi-level features is considered the fundamental advantage of the CNN technique. Researchers employed CNN models to extract water from images by successfully distinguishing water, shadow, and ice/snow from cloud shadows and ground shadows without utilizing additional resources (Fang et al., 2019; Chen et al., 2018b; Yu et al., 2017a; Isikdogan, Bovik, and Passalacqua, 2017). Moreover, a Multi-scale fully convolutional Network (MFCN) was proposed by (Weinstein and Ebert, 1971; Geng et al., 2020; Wang et al., 2020a) to extract multiple features from the satellite images. However, most of the experiments had minimal or short-term dimensions.

As a majority of studies have been developed, researchers have incorporated high-dimensional image processing algorithms for the better prediction of environmental resources. However, several limitations have been observed from the previously discussed literature that is presented in Table 4.1. This research aims to build an innovative method that can be implemented into remote sensing to address those limitations and gaps.

4.3 Proposed Work

The proposed solution aims to determine the availability of water resources by utilizing the advanced image processing principles of deep learning. The proposed solution is discussed into two different phases such as Data collection and Water resource determination as illustrated in Fig. 4.2.

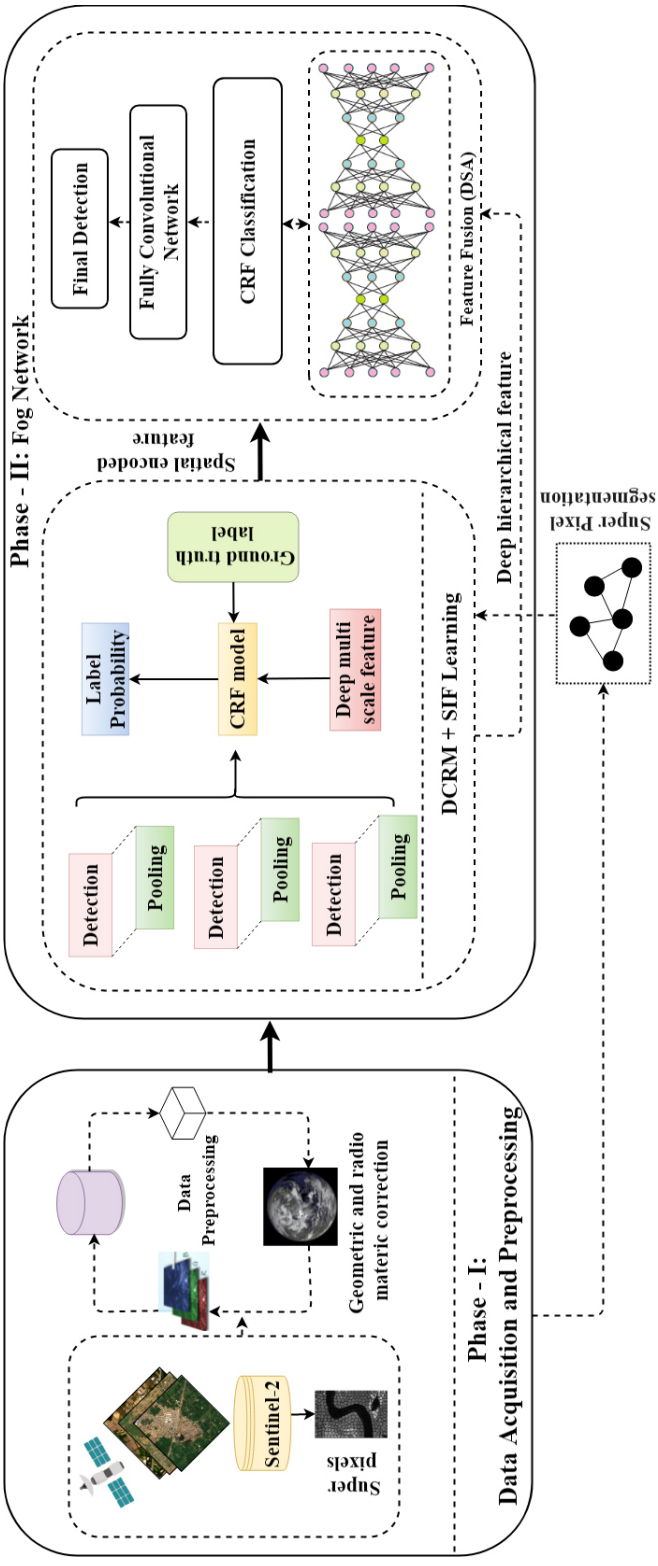

TABLE 4.2: Overview of the proposed framework (MDIT)

4.3.1 Data Collection

The real-time identification of the water resources from satellite images is considered one of the most effective methods of remote sensing. In the proposed study, a total of 9 man-made wetlands with an area of 14739 km^2 and 12 distinct natural wetlands with an area of 839 km^2 are considered to analyze the status of water resources (Kumar and Singh, 2020; Ladhar, 2002). The targeted area is illustrated in Fig. 4.2. The wetlands such as rivers, reservoirs, and ponds/tanks are covering the 69%, 14%, and 17% percentage of area, respectively. In the proposed study, three wetlands of Punjab such as Roper, Harike, and Kanjli are considered to analyze the status of water as illustrated in Fig. 4.3. The data with respect to the targeted location are acquired from the Copernicus Open Access Hub (COAH) [1]. Moreover, the detailed specification of the data is presented in Table 4.3.

Data Pre-processing: In the proposed study, Sentinel-2 images are utilized with 4 different bands such as VNIR, Blue, Green, and Red. Therefore, the need for the process of data normalization is realized to adapt to change the specification of data according to the input requirement of the proposed model. Several preprocessing operations such as Geometric correction (Lan et al., 2019), Correction of atmospheric condition (Xie et al., 2019), and Radiometric correction (Zhang and Montgomery, 1994) are performed on the data to normalize the sentinel-2 images. Geometric corrections are utilized to determine the location of the image by performing several geometric registrations are considered such as geo-referenced, co-registration, and orthorectification. To deal with undesirable atmospheric conditions, object subtraction and disturbance adaptive methods are utilized to correct the atmospheric conditions. Moreover, radiometric correction such as histogram matching, overlapping regions between images, and pseudo-invariant features are also performed on the dataset. In addition to this, different data augmentation techniques such as rotation, clipping, flipping, and transformation are performed on the images to enhance the adaptability of the data that helps to

[1]Source: https://scihub.copernicus.eu/

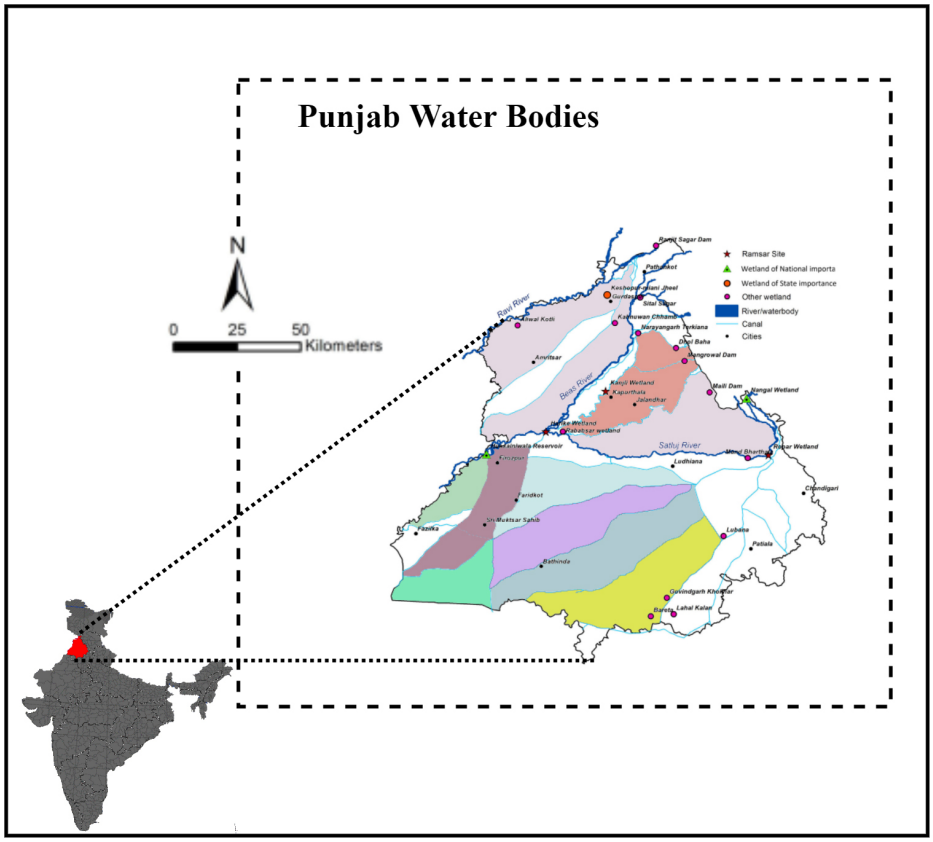

FIGURE 4.2: Distribution of wetland and other man-made lakes in Punjab Pandey and Khare, 2017

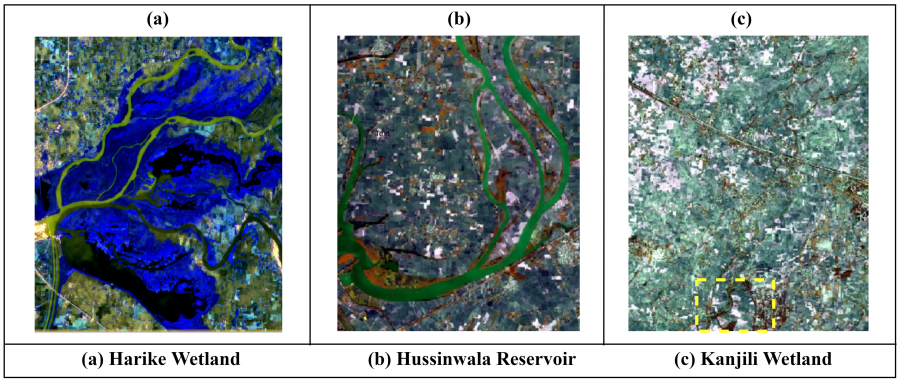

FIGURE 4.3: Selected wetlands from Punjab situated on Sentinel-2 images

TABLE 4.3: The detail description of the image dataset

Dataset Type	Satellite technology	Image Specification	Class	Description
Image Dataset	False-color composite images from sentinel-2	Pixel Density: 256×256, resolution: 10m Bands: False-color composite (VNIR, Blue, Green, and Red)	River, Pond Water, and Reservoir Man Made, Water,Lake	Satellite image data from sentinel-2 with False-color composite.

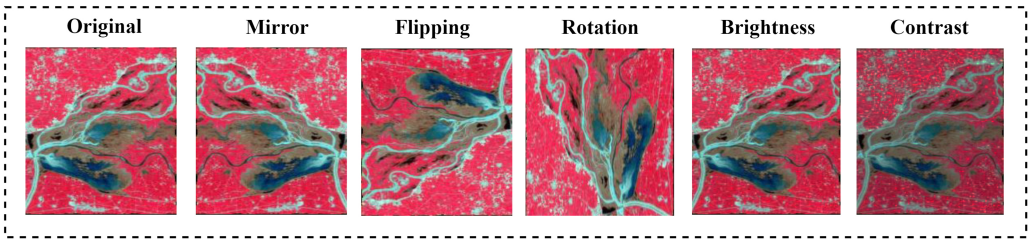

FIGURE 4.4: Examples of different data augmentation operations

deal with the issue of over-fitting (Ji, Wei, and Lu, 2019; Ding et al., 2016; Perez and Wang, 2017; Yang et al., 2016; Norouzi, Ranjbar, and Mori, 2009) as illustrated in Fig. 4.4. Furthermore, super-pixel segmentation is considered to improve the overall accuracy of prediction. In this manner, the Simple Linear Iterative Clustering (SLIC) (Achanta et al., 2012) technique is employed to extract super-pixels from an image to remove the deviated pixels. For each super-pixel, the average features are calculated as $t_p \in r^r$, where t_p is defined as super-pixel and r^n is defined as the selected area of each super-pixel.

4.3.2 Fog Module: Water bodies source prediction

In this section, the Convolutional Restrictive Machines-assisted multi-layered prediction method is proposed to identify the availability of water resources from the satellite images. The overall working process of the proposed approach is illustrated in Fig.4.2. In the first space, Deep Convolutional Restrictive Model is proposed to extract the spatial features from the satellite images. In the second space, the relationship between artifacts and the environment is calculated by utilizing the structural learning process. At last, to produce the efficient feature from input data, a feature fusion layer is included at the top of the prediction model. The complete process for each space is explained ahead.

Feature Extraction: Deep Convolutional-Restrictive Model It is determined that the accurate prediction of features related to a specific object is a significant assessment parameter in the domain of computer vision. In this manner,

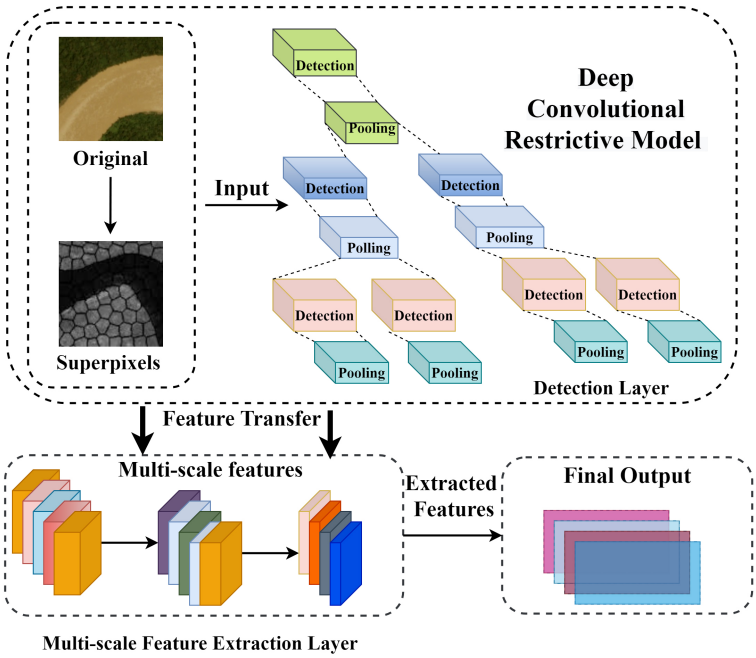

FIGURE 4.5: DCRM feature learning concept

a hybrid Deep Convolutional-Restrictive Model (DCRM) is proposed to extract the local scale-invariant features from images. It extracts the features from both 2-Dimensional (2D) Convolutional Neural Networks (CNN) and Restricted Boltzmann Machines (RBM). The overall architecture of the proposed DCRM is presented in Fig. 4.5 and discussed by dividing it into two different layers such as Detection Layer (**T**) and Visible Layer (**U**).
Detection Layer: In the detection layer, c^K number of filters are employed for feature extraction to convolve an image and create T^K dimensional matrix represent with n_t. The weights and Bias values of a dimensional matrix are represented by c^K and B^K respectively. On the other hand, the sub-units of a dimensional matrix are represented with T_{ij}^K. The ratio value of the convolution process is defined with i and j. Moreover, the dimensionality reduction of an image is calculated by including the max-pooling layer denoted with **m** and the pooling operations are denoted as b_α.

Visible Layer: In the visible layer, the **K** number of convolutional filters

are considered in a single layer where each filter is containing N_c dimensional feature matrix. The convolutional kernels $c^K(K \in [i, K])$ are processed over the entire region of an image and divided between the detection and visible layers to deal with the probability of similar features appearing in an image. The mathematical calculation of cumulative probabilistic value are as follows:

$$M(t,u) = \frac{1}{Z} exp(-e(t,u)) \tag{4.1}$$

Here, a normalised parameter of the separation function is denoted as $Z = \sum_u \sum_t exp\,(-e(u,t))$ and the DCRM energy function is determined as:

$$e(T,U) = -\sum_{k=1}^{K} T^K \odot (\tilde{c}^K * U) - \sum_{K-1}^{K} B^K \sum_{ij} T_i j^K - S \sum_{ij} U_{ij}, \tag{4.2}$$

Here, the signification of the 2D convolution is represented with $*$, element-wise multiplication is represented as $\odot$, and flipping operation is denoted as $\tilde{C}^k$. In this manner, the components of detection layer **t** are utlized to calculate the total activation from a descrete areas of an image. In this manner, the energy function of the proposed model is calculated as:

$$e(T,U) = -\sum_{k} \sum_{ij} (T_{ij}^K (\tilde{c}^K \star U)_{ij} + B_k T_{ij}^K) - S \sum_{ij} U_{ij} \sum_{(ij)\beta_\alpha} L_{ij}^K \leq 1, \forall U, \alpha \tag{4.3}$$

Here, the pooling window of a detection layer is denoted as β_α. Stochastic Gradient Descent (SGD) is used to optimize DCRM parameters (Han et al., 2016). Furthermore, the Contrastive Divergence (CD) solution (Hinton, 2002) is utilized to enhance the performance of the network as compared to the Stochastic Gradient Descent algorithm (SGD). In this manner, a total of 6 convolutional layers are implemented in DCRM. The first, third, and fifth layers of the model are performing the operation of convolution. The convolutional layers are fine-tuned with Contrastive Divergence (CD) to optimize the performance of feature extraction. On the other hand, the second, fourth, and sixth layers is performing the function of Max-polling. In addition, the

batch gradients are modified by using the extra momentum of the preceding gradients during CD. However, the changes in the dynamic rates caused the elimination of meaningful features. The process of feature extraction is performed on different learning rates to extract optimal features by selecting the optimal learning rate.

Structural Learning Layer (SLL) While CNN may generate hierarchical features, these features are still inadequate for calculating the correlation between spatial features and objects. The super-pixel-based CRF model is proposed to deal with this issue that is used to identify the Spatially Inferred Features (SIF) (Bu et al., 2016). The overall process of extracting the spatial inferred features from an image is illustrated in Fig. 4.6. Moreover, a graph-based **o = (V,E)** approach is proposed in which vertex v is defined as **V** and the edge e is defined as E. The vertex unit of an image is composed of its sub-segments, whereas the edge is composed of the relationship between adjacent unit pairs. The conditional probability distribution is evaluated by considering the weight in the training data. SLL is containing deep hierarchical features which are working without backpropagation. For evaluating the efficiency and performance of the proposed system, few experiments are conducted during the establishment of super-pixels. Region size (every superpixel), L2-regularizer parameter (λ), and distance factor (k_d) with the value of 0.1 are opted for calculating the spatial relationship between super-pixels.

$$x(x\|y,w) = \frac{1}{Z(x,w)} \prod_{i \in V} \phi_N(x_i, y_i) \prod_{e_{ij} \in E} \psi_E(x_{ij}, y_i, y_j) \tag{4.4}$$

Here, the pair-wise partition function of a created graph model is representd as $Z(x,w)$. The features are denoted as $f_N = \theta_N(x_i, y_i)$ and $f_E = \psi_E(x_{ije}, y_i, y_j)$. Moreover, the non-linear features are the sequence of $f_N - f_E$ that are indicated as log-linear. The e_{ij} sign described an edge composed of vertex v_i, v_j and p is represented as the components with their respective states $y =< y_1, y_2, y_3, ..., y_N >$. The process of training is reformed as:

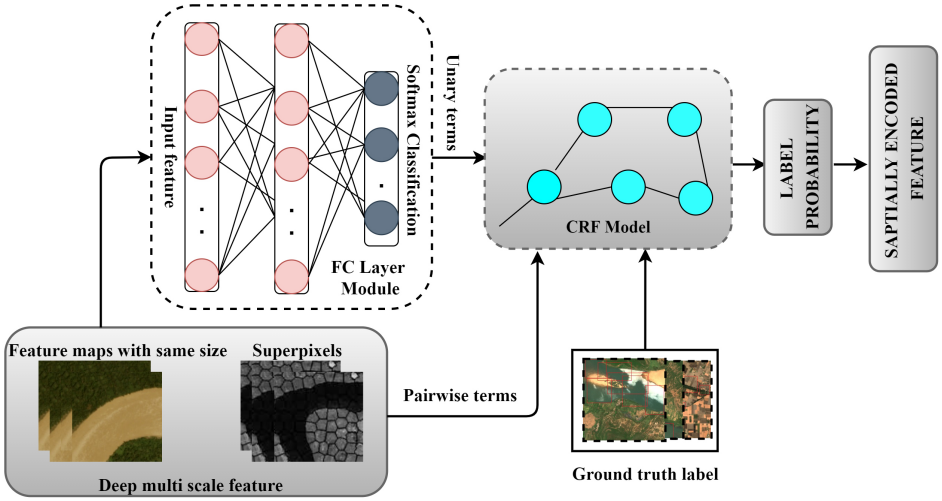

FIGURE 4.6: Representation of structural learning

$$w^* argmin_w \lambda \|w\|^2 - \sum_{n=1}^{M} (\sum_{i \in V} w_N^T f_N(x_i^n, y_i^n) + \sum_{e_{ij} \in E} w_E^T f_E(x_{ije^n}, y_i^n, y_i^n)) + \sum_{n=1}^{M} \log Z(x^n, w) \tag{4.5}$$

Here, λ, $w = [W_N; W_E]$ is defined as a non-negative L2-regularizer parameter and the weight of pairwise elements. Furthermore, the training sample of a graphical model is described as (p_i^n, q_i^n). It has been found that by maximizing the value of $x(y \mid y, w^*)$, the conditional probability distribution over the target class can be obtained.

Spatially Inferred Features (SIF) The structure of CFR is included in the proposed SIF to improve the prediction accuracy. The proposed DCRM model is showing a lack of spatial relationships from the super-pixels. To overcome the constraint of spatial feature learning, SIF models is utilized to access both spatial and super-pixel features at the same instance of time. The connection in the graph is denoted as $o_\mu = (V_\mu, E_\mu)$. Here, μ described the super-pixels and $\odot(\mu)$ defined the SIF model which is further calculated as:

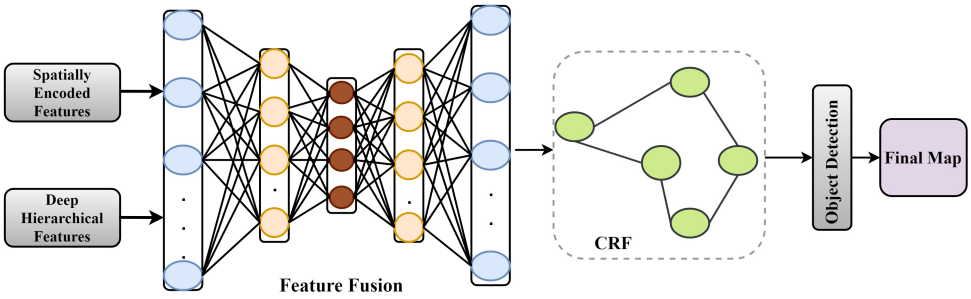

FIGURE 4.7: Procedure to extract hybrid feature using Feature fusion (DSA) and CRF model.

$$\odot(\mu) = \lambda \sum_{i \in V_\mu} \sum_{j \in V_\mu} \theta_i \theta_j^h \exp\left(-k_t \frac{t(v_i, v_j)}{\sigma_t}\right) \tag{4.6}$$

Here, $\odot$ is $n \times n$ matrix that represents the frequency of the availablility of neighbouring probability defined as i and j . The distance of super-pixels are represented as $t(v_i, v_j)$. Moreover, σ_t k_t, , and λ denoted the distance of the vertices, distance decay rate, and the normalized parameter, respectively.

Multi-layered Feature Fusion (MFF) In the proposed solution, multilayer Feature Fusion (MFF) is a form of neural network with multilayer Sparse Auto-Encoder (SAE). In addition, the hierarchical features are learning through MFF by rembling the features from the image. The overall process of the MFF is illustrated in Fig. 4.7. Furthermore, DHF S_p and SIF $\odot$ are two different descriptors that are included during the process of structural and feature learning that are represented as $[S_p, \odot] \in R^{(N+nxn)}$. On the other hand, the linked features are fused by applying DSA. After finishing the unsupervised pretraining phase, supervised backpropagation with limited labeled data is used to optimize the network for optimal parameters.
Let every training sample of SAE represented as $A = (a_1, a_2, ..., a_r)^d$. The hidden units r_f in layer **I** are represented as $f_i = (f_1^I, f_2^I ..... f_{rf}^I)$. The linear and nonlinear sigmoid activation functions are represented as follows:

$$f^d = \frac{1}{1 + e^{-x}}(wA + B_f) \tag{4.7}$$

Here, f^I represents the altered encoder from in the input **A**. In this manner, the value of $\sigma(Z)$ is always be equal to $(1+\exp(-Z))^1, w \in G^{rxr_f}$ and the value of bias B_f is correspond to $G^{r_f x1}$. Therefore, an approximation equation of $\tilde{A}$ can be written as follows:

$$\tilde{A} = \frac{1}{1+e^{-a}}(w^D f^I + B_0), B_o \in G^{rx1} \tag{4.8}$$

o is calculated to minimize the error between A and $\tilde{A}$ as follows:

$$o = \frac{1}{r_s}\sum_{i=1}^{r_S}\left\|\tilde{A}^i - A^i\right\|^2 + \beta\|w\|_2^2 + \alpha\sum_{j=1}^{r_f} kl(x\|\tilde{x_j}) \tag{4.9}$$

Here, $\tilde{x_j}$ describe the average activation of the j_{th} hidden unit and the activation function x is selected. In MFF, three Stacked Auto-Encoders (SAEs) with the size of 1200, 700, and 500 hidden units are applied for constructing DSA. The sparse weights (α) are calculated in each hidden layer at different learning rates such as 2, 0.1, and 0.05. Furthermore, the activation function (ρ) with the weight (β) of 0.05 is adjusted to 0.001, and the learning rate is tuned to 0.01. To address the problem of overfitting, a batch of 20 is trained on 100 epochs.

4.4 Experiments

In this section, the complete working process of the proposed framework is illustrated in Fig. 4.8 and different performance measures have been calculated to evaluate the prediction performance of the proposed solution. Therefore, the performance is evaluated into different subsections as follows:

- Data Modulation
- Water Identification result of MDIT
- Working efficiency of MDIT, ResNet, VGG, SegNet, and DenseNet
- Evaluation metrics

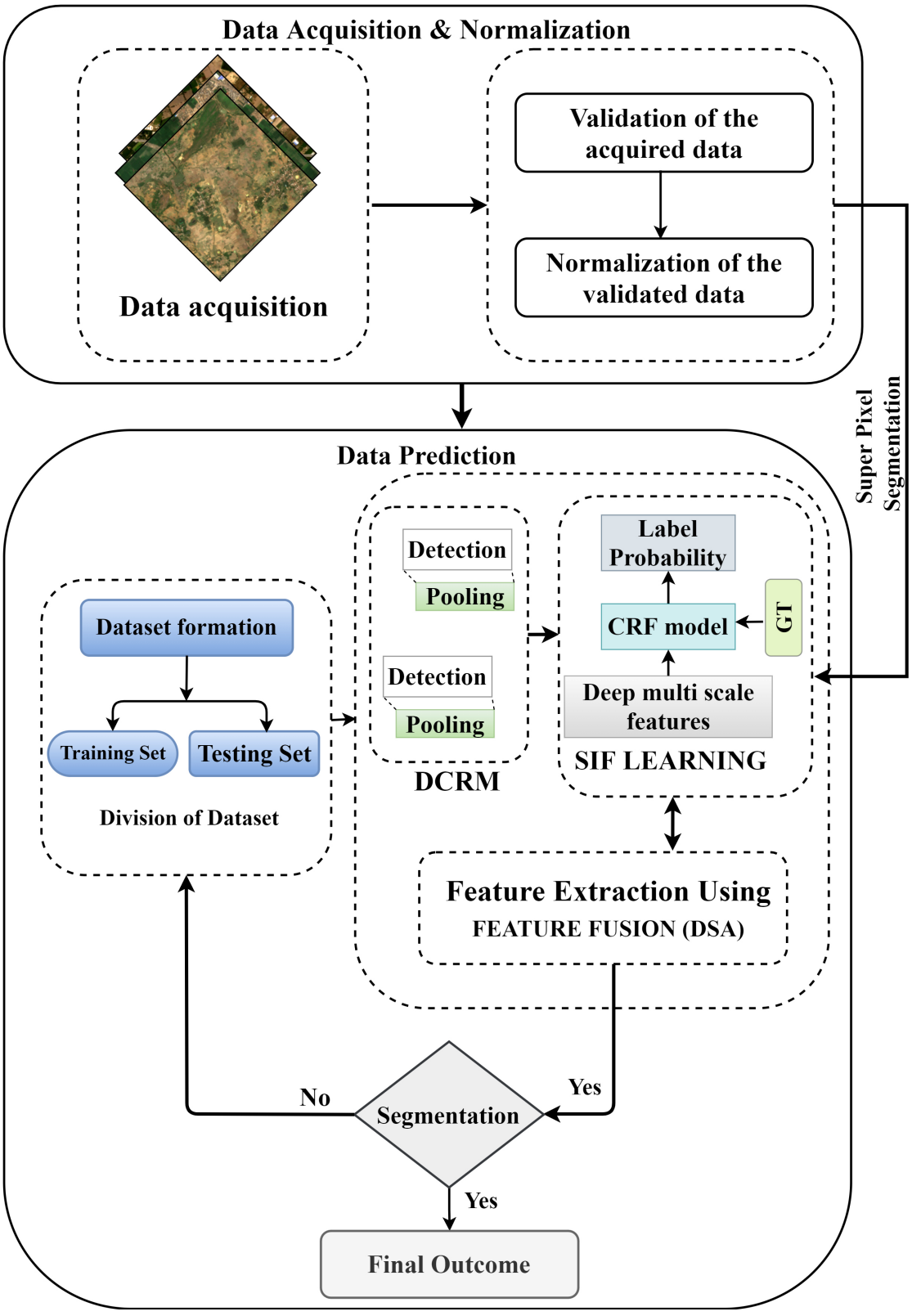

FIGURE 4.8: The overall working process of the proposed framework

TABLE 4.4: Water bodies prediction evaluation on different ratios of the dataset.

Total Images	Ratio	Training	Validation	Test	Accuracy
5600	70:30	3920	1176	504	0.845
	75:25	4200	1050	350	0.873
	80:20	4480	896	224	0.902
11090	70:30	5634	2328	2327	0.929
	75:25	6238	2079	2772	0.934
	80:20	7097	1774	2218	0.945

- Comparison of Identification results
- Fog-based performance evaluation

4.4.1 Data Modulation

A total number of 5600 images are selected in the original dataset. As deep learning algorithms need a huge amount of data for training, different data augmentation approaches are applied to the original dataset to increase the size of the dataset and 11090 augmented images are generated. Moreover, the manual data splitting method is applied to the datasets to generate training and testing sets. The dataset is divided into three different ratios as 70:30, 75:25, and 80:20. The overall accuracy calculated on both of the datasets is presented in Table 4.4.

4.4.2 Water Identification Results Of MDIT

To check the prediction performance of the proposed model, a total number of 1050 images are selected. As the evaluation is carried out on different ratios, the calculated results are presented in Table 4.5. It has been observed that the proposed model is performed better on the augmented dataset as compared to the original dataset with an 80:20 ratio. In this manner, the ratio of 80:20 is selected for further performance evaluation of the proposed model

The calculated results of the proposed solution are illustrated in Fig. 4.9 and Fig. 4.10. From the calculated outcomes, it has been realized that the

TABLE 4.5: Prediciton performance analysis of MDIT

Model	Resolution	***P***	***R***	***F1***	***IoU***
MDIT	70 : 30	0.929	0.902	0.911	0.853
	75 : 25	0.934	0.897	0.919	0.861
	80 : 20	0.945	0.919	0.929	0.871

proposed model is successfully identified the water bodies with different shapes from multiple areas even small lakes, ponds, obstacles. Three different wetlands such as Harike, the Hussainiwala reservoir, and the Kanjili were selected and the images are captured at different time instances to remove the biases from the dataset. Furthermore, the performance of the proposed model is evaluated by utilizing a 5-fold based leave one out a testing protocol to check the prediction efficiency. In each iteration, out of 5 folds, 4-folds are used for training and the remaining fold is used for testing the prediction performance. In this manner, each fold gets a chance to be in a test set. The evaluated outcomes are shown in Table 4.6.

Table 4.6 represents the average prediction outcome of water identification for 5 folds. It has been observed that confusion usually occurs between rivers and lakes. A total of 8% rivers are misclassified as lakes. The reason for misclassification can be the less number of training samples that can be avoided by increasing the samples related to the particular class in the training phase. In this manner, the average prediction accuracy of the proposed model with respect to the k-fold cross-validation technique is achieved by 0.943% of accuracy with the standard deviation of $\pm$0.94.

4.4.3 Working Efficiency Of MDIT, ResNet, VGG, SegNet, and DenseNet models

The performance of each model such as ResNet, VGG, DenseNet, Deeplab v3+, SegNet, and MDIT is illustrated in Fig. 4.11. The loss function is utilized in the convolutional neural network to evaluate the difference between the value of the ground truth of an image and the prediction results of the model. The performance of the model is directly dependent on the value of

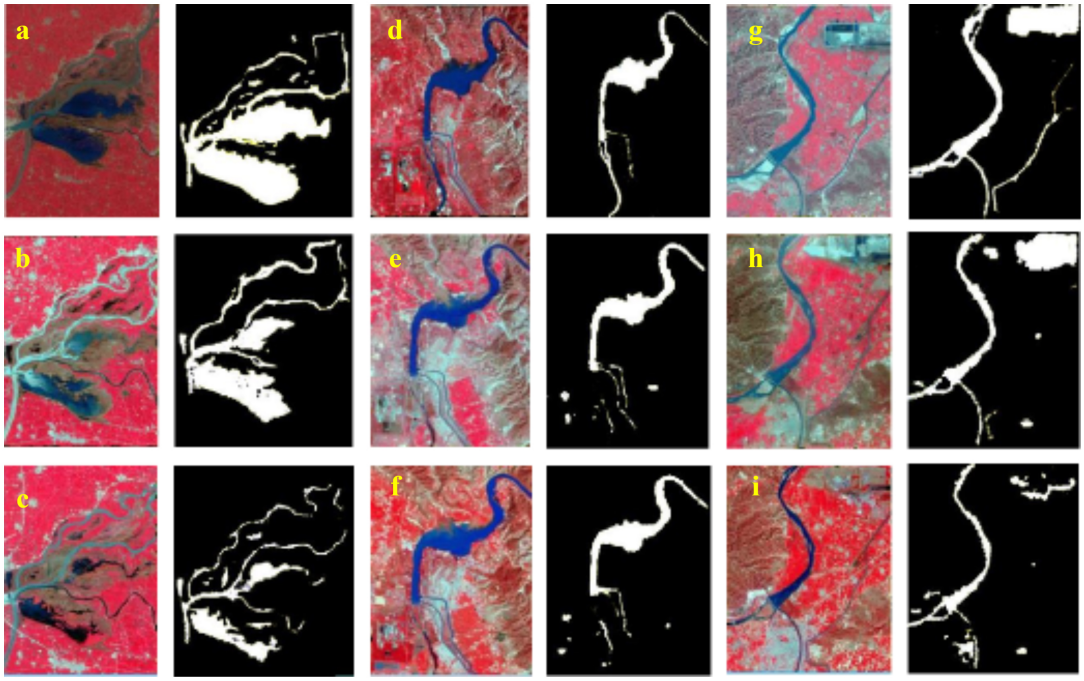

FIGURE 4.9: Examples of the recognition of water bodies of the proposed model. Original images False-color composite remote sensing images of different wetlands and the water bodies detection is shown in black and white images of each wetland.

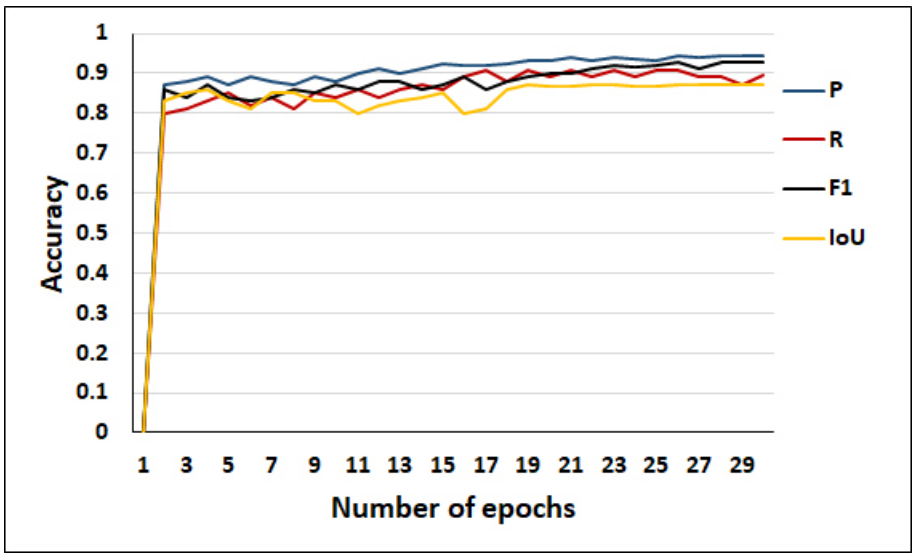

FIGURE 4.10: The performance evaluation of MDIT on 256 × 256 resolution sentinel-2 images.

TABLE 4.6: 5-Fold Cross Validation River (A), Lake(B), Man-made (C), Ponds (D), and Reservoir (E). The prediction accuracy of the propsed model is highlighted with bold values in the table.

TABLE 4.7: Fold-1

	A	B	C	D	E
A	**0.938**	0.024	0	0	0
B	0	**0.947**	0	0	0
C	0	0	**0.969**	0	0
D	0.034	0	0	**0.939**	0.018
E	0	0	0	0	**0.948**

TABLE 4.8: Fold-2

	A	B	C	D	E
A	**0.936**	0.022	0	0	0.014
B	0	**0.942**	0	0	0
C	0	0	**0.955**	0.021	0
D	0	0	0	**0.934**	0
E	0.008	0	0	0	**0.941**

TABLE 4.9: Fold-3

	A	B	C	D	E
A	**0.969**	0.035	0	0	0
B	0	**0.942**	0	0	0
C	0	0	**0.947**	0.001	0.021
D	0.021	0	0	**0.938**	0
E	0	0	0	0	**0.948**

TABLE 4.10: Fold-4

	A	B	C	D	E
A	**0.945**	0	0	0	0.021
B	0	**0.942**	0	0	0
C	0	0	**0.955**	0.02	0
D	0	0	0	**0.934**	0
E	0.022	0	0	0	**0.941**

TABLE 4.11: Fold-5

	A	B	C	D	E
A	**0.974**	0.015	0	0	0.022
B	0	**0.959**	0	0	0
C	0	0	**0.946**	0.013	0
D	0.003	0	0	**0.948**	0
E	0	0	0	0	**0.957**

TABLE 4.12: Overall Accuracy

k-fold (5 folds)	Overall Accuracy
Fold-1	0.948%
Fold-2	0.941%
Fold-3	0.935%
Fold-4	0.938%
Fold-5	0.956%
Mean	0.943%
Standard deviation	$\pm$ 0.94

the loss. The lower value of loss means the higher accuracy of the model. It has been observed that the VGG model has registered higher loss as compare to MDIT and DeepLab v3+. From the calculated outcomes, the proposed model registered a lower value of loss as compared to other state-of-the-art models that define the outstanding performance of the proposed MDIT.

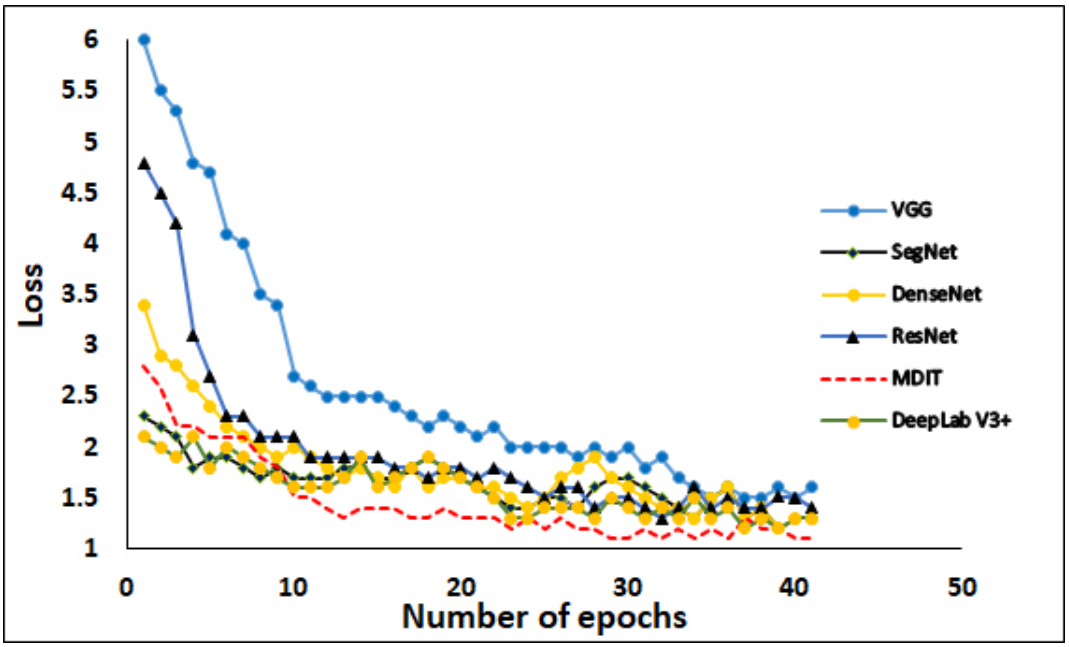

FIGURE 4.11: Training Losses of different models.

Furthermore, the training and testing of each sate-of-the-art model are presented in Table 4.13. It has been observed from the calculated outcome that VGG has higher training and testing time as compare to other models. On the other hand, the proposed model takes considerably less time for training and testing. The proposed model takes a total training time of 212 minutes, where the VGG, Deeplab V3+, DenseNet, ResNet, and SegNet have taken the training time of 380.75 minutes, 240.44 minutes, 332.92 minutes, 320.72 minutes, respectively.

As presented in Table 4.13, it has been observed that the proposed model took less training and testing time as compare to all state-of-the-art models. Moreover, the calculated result of each model is represented in Fig. 4.12 for

TABLE 4.13: The training time of different models on sentinel-2 images.

Models	Training		Testing	
VGG	22,845 s	380.75 m	12340 s	205.66 m
DeepLab V3+	14426.4 s	240.44 m	4819.8 s	80.33 m
DenseNet	18,054 s	300.91 m	9430 s	157.16 m
ResNet	19,375 s	322.92 m	10920 s	182 m
MDIT	12,774 s	212.91 m	3289 s	54.81 m
SegNet	19,243 s	320.72 m	10789 s	179.81 m

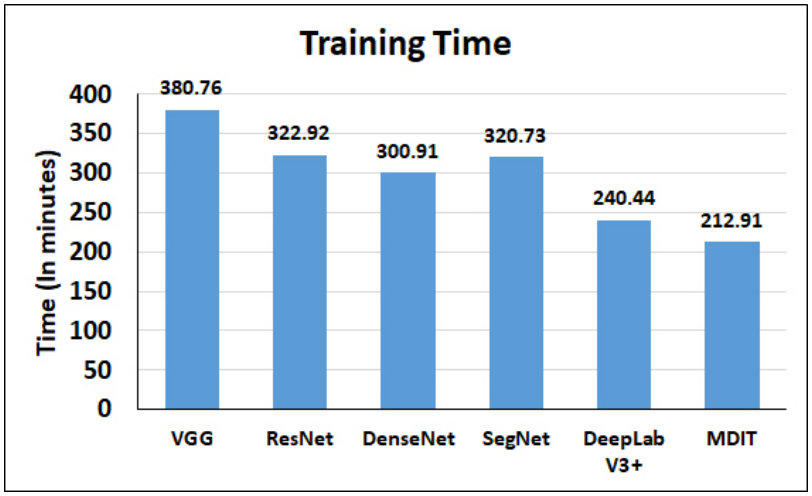

(A) Training

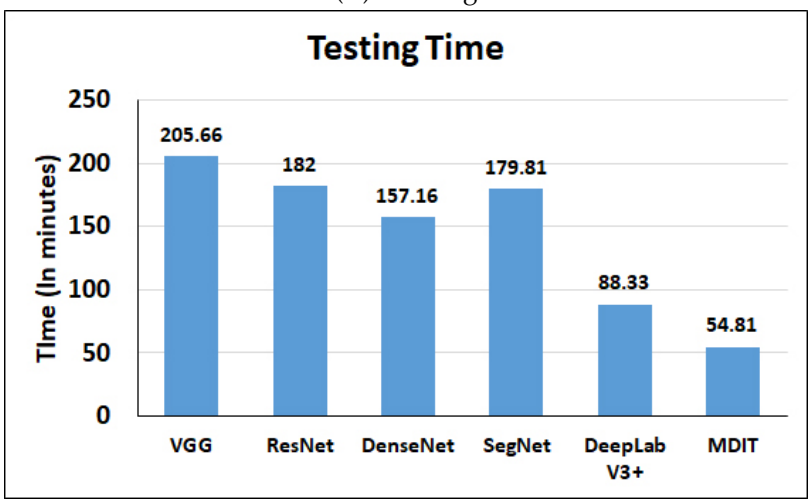

(B) Testing

FIGURE 4.12: The Training and Testing time of different models for the prediction of water bodies from sentinel-2 images.

better understanding.

4.4.4 Evaluation Metrics

In the proposed study, four performance measures such as F1-score, Recall (R), Precision (P), and intersection over union (IoU) are used to analyze the prediction performance of the proposed solution. Moreover, the selected measures are mathematically represented as follows:

$$P = \frac{TP}{TP + FP} \tag{4.10}$$

$$R = \frac{TP}{TP + FN} \tag{4.11}$$

$$F1 = \frac{2 \times R \times P}{R + P} \tag{4.12}$$

$$IoU = \frac{TP}{TP + FP + FN} \tag{4.13}$$

Here, IoU defines the intersection of the two sets of predicted outcomes and its ground truth values. The efficiency of the ResNet, VGG, DeepLab V3+, DenseNet SegNet, NDWI, and MDIT is evaluated by utilizing the same performance metrics. The precision refers to the proper recognition of water pixels defines by (TP) in relation to overall water pixel prediction (TP + FP). Moreover, recall defines the pixels that are correctly detected (TP) in comparison to the actual pixels are defined as (TP + FN). The F1-score is used to describe the scale of accuracy by addressing the occurrences of recall and precision discrepancies.

It has been realized from the results that the proposed solution achieved a better Precision with the value of 0.945 as compared to DeepLab V3+ 0.914, DenseNet 0.911, ResNet 0.909, SegNet 0.913, and VGG 0.899. In addition, the traditional method NDWI has registered a precision of 0.709. Moreover,

in terms of F1-score, the proposed solution has registered the value of F1-score is 0.919 which is higher than other state-of-the-art models such as VGG, DeepLab V3+, DenseNet, SegNet, and ResNet with the values of F1-score 0.864, 0.896, 0.894, 0.891, and 0.881, respectively. On the other hand, the prediction performance of the proposed model is also observed based on the IoU and the proposed model registered the higher value of 0.872 as compared to VGG, Deeplab V3+, DenseNet, SegNet, ResNet, and NDWI with the values of 0.832, 0.868, 0.865, 0.843, 0.850, and 0.759, respectively. All the calculated results are presented in Table 4.14 and illustrated in Fig. 4.15 and Fig. 4.13 for better understanding. It has been determined that the proposed approach outperforms other deep learning models in terms of prediction performance. Furthermore, the prediction performance of the proposed solution is evaluated on three different wetlands of Punjab within the period of 1 Aug. 2018 to 30 Oct. 2019 as illustrated in Fig. 4.15.

The blue and red colors in the False composite color image represent water and vegetation, respectively. In the images, the water is represented as a solid white color, while the dotted line represents the urban area. From the sentinel-2 false-color composite images, the proposed method correctly identified the water and also distinguished the tiny rivers and lakes during prediction. The water bodies are separated from all other shadows but ResNet and VGG have wrongly identified the water bodies from the images and these two approaches show the non-water area as water that defines the false prediction of such models. Similarly, in Deeplab V3+, DenseNet, and SegNet some false identified results have been recognized. Moreover, the performance of the traditional approach such as NDWI has successfully identified the main water bodies from images but some urban areas and bare land are also recognized as water bodies by such model.

4.4.5 Fog-based Performance Evaluation

Resource optimization is a crucial method for decreasing computing costs while attaining the required data processing capabilities. Due to a lack of computational power and network capacity, the fog nodes processed the

TABLE 4.14: Comparison result evaluation of different networks the optimum values in the table are highlighted.

Metrics	MDIT		VGG		DeepLab V3+		DenseNet		SegNet		ResNet		NDWI	
Precision	0.945	±	0.899	±	0.914	±	0.911	±	0.913	±	0.909	±	0.709	±
	0.013		0.014		0.011		0.012		0.018		0.014		0.030	
Recall	0.897	±	0.871	±	0.884	±	0.887	±	0.887	±	0.882	±	0.929	±
	0.016		0.015		0.018		0.018		0.017		0.015		0.009	
F1-Score	0.929	±	0.864	±	0.896	±	0.894	±	0.891	±	0.881	±	0.899	±
	0.013		0.016		0.017		0.014		0.017		0.017		0.015	
IoU	0.872	±	0.832	±	0.868	±	0.865	±	0.843	±	0.850	±	0.759	±
	0.021		0.023		0.024		0.023		0.021		0.021		0.025	

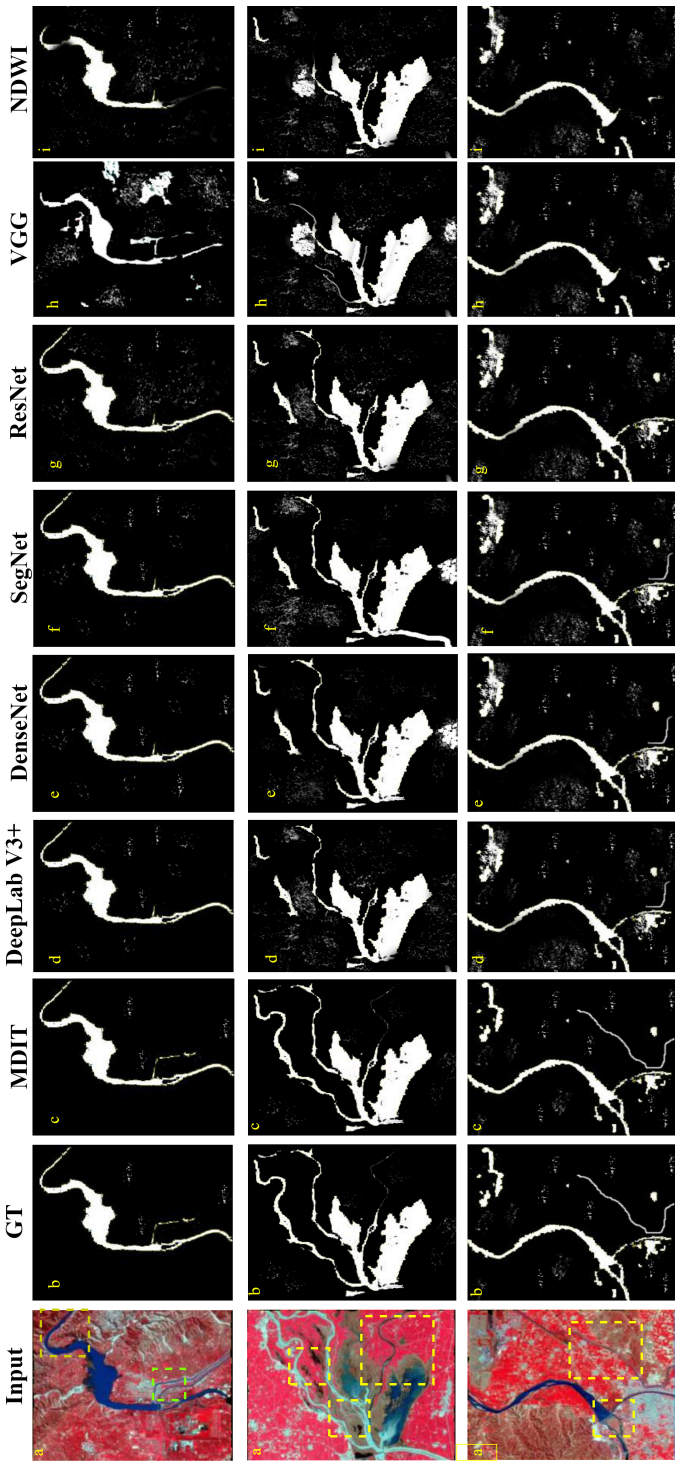

TABLE 4.15: Comparison of water detection effect of different models on three different wetlands of Punjab on 30 Aug 2018. **(a)** False-color composite and the detection of water bodies results from **(b)** the ground truth, **(c)** the MDIT **(d)** the Deeplab V3+ **e** the DenseNet, **(f)** the SegNet, **(g)** the ResNet, **(h)** the VGG, **(i)** the NDWI models.

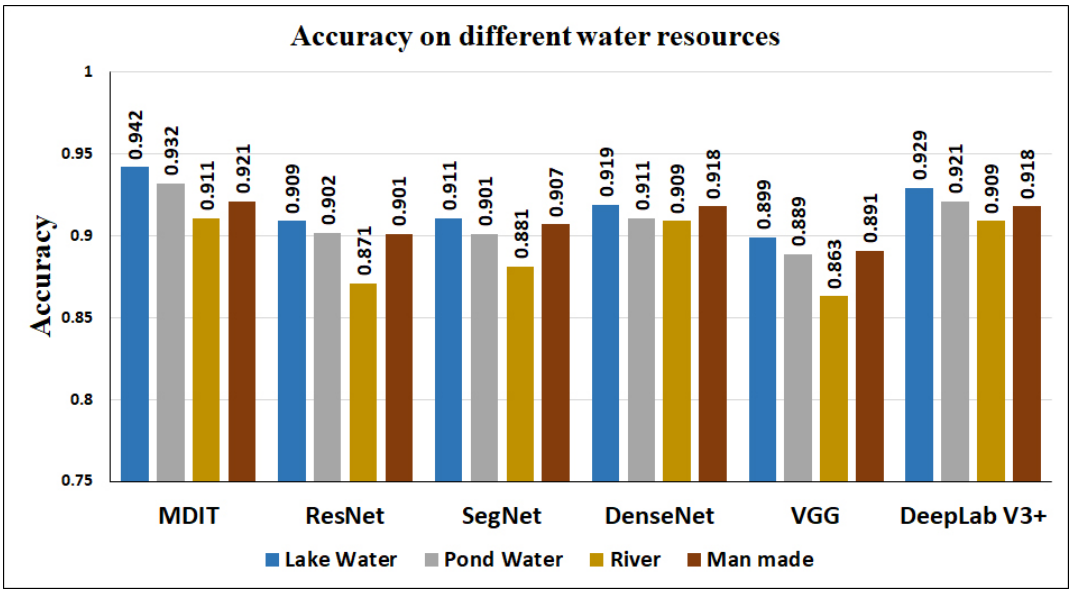

FIGURE 4.13: Comparative result of different models for the recognition of water bodies.

data in the local environment rather than transmitting it to the cloud. In this manner, three measurements are calculated to determine the utilization of the resources as follows:

- Image Segment processing time
- Overall Processing time on fog and cloud layer

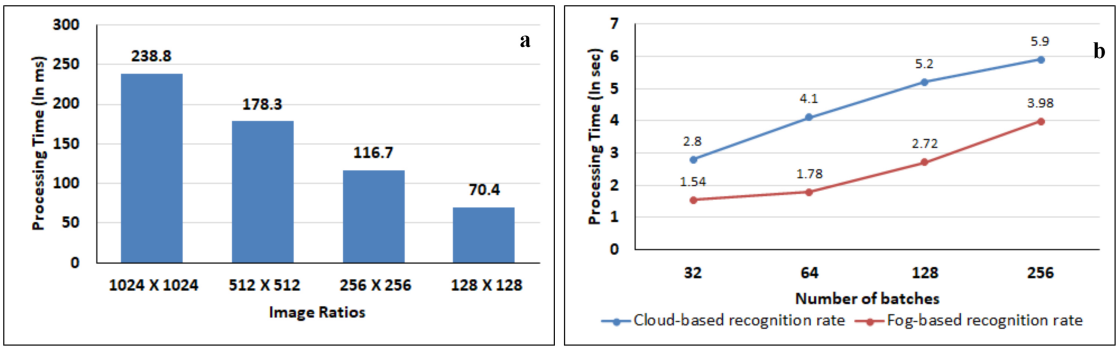

FIGURE 4.14: Fog nodes processing time

In comparison to the original data, Fig. 4.14(a) represents the processing time difference between the original and downsampled image segments on the fog node with the different number of image batches. The system has been evaluated using downsampled data with a resolution of 256×256. It has been determined that the model executed the downsampled data run four times faster as compared to the original data. The model took 62.4 milliseconds to process a single downsampled image segment. The optimal number of image segments is determined by forwarding the image segments on fog and cloud servers as presented in Fig. 4.14(b). A different number of image batches have been forwarded on both fog and cloud servers to evaluate the processing time. From the calculated outcomes, it has been observed that fog servers have taken less processing time as compared to cloud servers. It can be realized that the fog server has taken 1.54 seconds to process the 32 batches as compared to the cloud server which took 2.8 seconds for the number of batches. Similarly, a relevant increment in the processing time is observed with the different number of batches. In this manner, it has been observed that the fog layer is performed considerably better by taking less processing time as compared to the cloud layer for the prediction of water bodies from the satellite images. The reason behind the less data processing time consumption on fog servers is, images are processed on local machines that save the transmission delay. Therefore, it has been concluded that data processing is more effective by following the distributed data processing principles of fog analytics.

4.5 Conclusion

The continuous progression in the data acquisition and processing methods has brought significant enhancement in the field of remote sensing. Several conventional and modern remote sensing techniques are directly dependent on the base methods of deep learning such as CNNs for the extraction of essential features from the thousands of RGB color values. However, to examine the low-level pixels, it is compulsory to access the high-level information from the satellite images. In this manner, a multi-layered framework is

proposed to detect the presence of different water resources from sentinel-2 images in a targeted area. The purpose of predicting the water resources from the target location is to determine the level of happiness index of that specific region towards the availability of water. To analyze the complex patterns of sentinel-2 images, the DSA-based approach is utilized in the proposed study to analyze the spatial information from the images. Furthermore, an unsupervised deep learning-based DCRM technique is utilized to extract features from the annotated images. The calculated outcomes justified the performance of the proposed framework by achieving the higher accuracy of precision, recall, F1-measure, and IoU with the value of (0.945%), (0.868%), (0.929%), and (0.871%), respectively. Furthermore, the comparative analysis has shown the correctness in the prediction performance of the proposed solution by achieving the precision of 0.945% as compared to the selected state-of-the-art approaches such as NDWI (0.709%), ResNet (0, 909%), VGG (0.899%), DeepLab V3+ (0.914%), DenseNet (0.911%), and SegNet (0.913%). Moreover, several limitations with respect to the prediction of shadows, clouds, small lakes, and rivers have been observed in the conventional methods that have been overcome in the proposed solution.

Chapter 5

Rice Monitoring from Satellite Images Using Deep Learning

5.1 Introduction

Monitoring Land Use and Land Cover (LULC) is considered an essential task in the domain of agriculture for yield prediction, food security, export planning, crop estimation, and many others (Jesús Rubio, 2018; Papageorgiou, Markinos, and Gemtos, 2011). The monitoring of LULC from satellite images can provide an effective solution for crop management that is considered as one of the primary objectives of agribusiness for the rapid growth of population (Kontgis, Schneider, and Ozdogan, 2015). Earlier, the crop fields were monitored manually and it was considered one of the most tedious and time-consuming tasks. Moreover, the dynamics in the weather condition is also considered as one of the most prominent challenges in the cultivation of crop (Wuebbles et al., 2017). As the population is rapidly growing, the production and management of food need to be achieved (Alexandratos, 2009). Over the past few years, several solutions have been developed by the researcher for generating field maps by utilizing satellite images (Liu et al., 2017a). In this manner, remote sensing has proved a prominent solution for the monitoring of agricultural or non-agricultural land (Zhang et al., 2018a). However, there are still some limitations such as the complex spectral channels of satellite images and atmospheric conditions that need to be considered for effective monitoring.

5.1.1 Research domain

Several techniques are developed by researchers for monitoring the fields from satellite imagery (Kavzoglu and Colkesen, 2013). Random Forest (RF) is one of the traditional machine learning models in the field of remote sensing and achieved a higher accuracy with minimal training time (Ok, Akar, and Gungor, 2012; Belgiu and Drăguţ, 2016b). Other traditional classifiers such as canonical correlation forest (CCF) (Rainforth and Wood, 2015), extreme gradient boosting (XgBoost) (Chen and Guestrin, 2016), Support Vector Machine (SVM) (Park et al., 2018), and Light Gradient Boosting Machine (LightGBM) have been developed by the researchers for the classification (Ke et al., 2017). Moreover, the LGBM approach has shown a better result among these machine learning approaches and has achieved a better accuracy so far in the field of remote sensing (Ustuner and Balik Sanli, 2019). Nowadays, several modern classifiers such as InceptionNet and VGG are developed to classify RGB images (Albert, Kaur, and Gonzalez, 2017), DeepLabV3+ (Chen et al., 2018a; Niu et al., 2018), and Convolutional Neural Network (CNN) (Zhang et al., 2018a) approaches have been developed to achieve the complex dependencies among temporal information and spectral bands. Moreover, DeepLabV3+ is also utilized to extract the spatial features from hyperspectral images. However, with a lot of salt and pepper noise, the categorization findings are generally limited. The following challenges are most common in the domain of remote sensing.

- Satellite images have a very low spatial resolution and the inexact measurement of a substantial geographic region due to the traditional sensors.
- The influence of adverse environmental conditions such as cloud shadows and solar radiation on satellite images.
- Current spectral indices for recognizing crop fields from satellite images are often exploratory. Moreover, it requires additional domain measurements and validation processes at the time for applying to distinct locations.

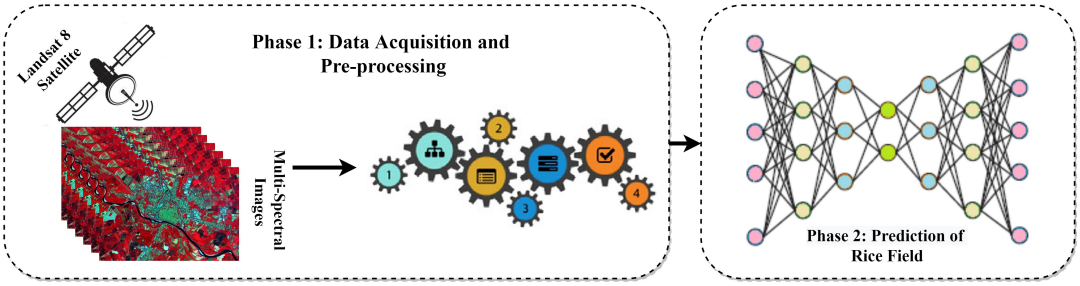

FIGURE 5.1: Conceptual framework for the prediction of rice field from satellite imagery.

5.1.2 Contribution

In the proposed study, an advanced multi-stream deep learning approach is proposed to overcome the above-discussed challenges and to map rice fields through satellite images in a precise manner. The proposed model has the capability to access multispectral information from satellite images. Therefore, the Landsat 8 satellite images are used in the proposed study. The proposed solution is orthogonal to area-specific spectral indices. In this manner, the proposed approach can retrieve the paddy features directly from the input data. The conceptual framework for the prediction of rice fields from satellite images is illustrated in Figure 5.1. The overall contribution of the proposed study is listed below:

1. Development of a pipeline for the collection of Landsat 8 satellite images of the rice field with respect to a specific area for the boundary prediction and classification.

2. A Bi-GRU technique-based Multi-streaming Deep Neural Network (MR-DNN) approach is proposed to evaluate the temporal dependencies related to multiple timestamps.

3. For enabling pixel-based mapping at different temporal resolutions, a multi-temporal spatial resolution solution is embedded in the proposed framework.

5.1.3 Chapter Structure

The remaining chapter is organized into different sections. In Section 5.2, some of the imperative studies related to the traditional and modern monitoring approaches are discussed. Section 5.3 is containing every possible working detail of the proposed framework. The calculated outcomes are discussed in Section 5.4 to evaluate the performance of the proposed framework. Lastly, the chapter is concluded with its primary findings in Section 5.5.

5.2 Related Word

This section discusses the previous literature based on the traditional approach for rice mapping and modern approaches for remote sensing.

5.2.1 Traditional Approach

Many traditional approaches have been developed by the researchers for classifying the rice field from satellite imagery such as Normalised Difference Vegetation Index (NDVI) (Rouse et al., 1974), Enhanced Vegetation Index (EVI)(Huete et al., 2002), Rice Growth Vegetation Index (RGVI) (Nuarsa, Nishio, and Hongo, 2011), Land Surface Water Index (LSWI) (Xiao et al., 2006), Soil Adjusted Vegetation Index (SAVI) (Huete, 1988) and many other. The main purpose of developing NDVI is to detect the living crop by utilizing the light which is reflected from the vegetation. However, there are some limitations with respect to the misclassifications (Rouse et al., 1974). To overcome this issue, the EVI method was developed that improved the performance of the NDVI including light distortion, reflection, and solar incidence angle. As these traditional approaches worked only on three spectral bands (red, blue, infrared), it is considered as a primary limitation of these models (Kontgis, Schneider, and Ozdogan, 2015). To overcome these limitations, some advanced computer vision techniques have been developed for rice field classification, feature extraction, object detection from satellite imagery.

TABLE 5.1: Compatrative analysis based on specific parameters

Study	Description	Method	Limitations
(Rouse et al., 1974)	In this study a method is developed for measure the vegetated area using ERTS-1 MSS data	Traditional	The proposed techniques is sinsitive to chlorophyll, but developed for flourish vegetations. Mostly the proposed approch is used for vegetation health and dynamics.
(Huete et al., 2002)	The analysis of MODIS NDVI and EVI performance from biophysical radiometric is evaluated	Traditional	EVI is only saturated for growing seasons and MODIS data is available after 2000
(Nuarsa, Nishio, and Hongo, 2011)	Landsat images are used by author for rice plant mapping and spectral features	Traditional	However, the developed approach is limited to cloudless and high resolutions images. Obtaining cloudless images throughout the rice-growing season is difficult in some areas due to severe climate constraints.

(Xiao et al., 2006)	A technique is developed for paddy rice monitoring using time series data with three vegetations indices LSWI, EVI, and NDVI	Traditional	MODIS pixels typically include a mix of different crop types due to their low spatial resolution. Croplands have a wide range of field sizes, especially in mountainous areas where crops are generally smaller than one MODIS pixel, resulting in sub-pixel variability in crop type and intensity.
(Huete, 1988)	To reduce the soil brightness a transformation approach is developed by the author	Traditional	The fundamental nonlinearity of ratio-based indices, as well as the influence of additive noise factors such as air path radiances, is the NDVI's primary drawbacks
(Ball, Anderson, and Chan Sr, 2017)	In this study, some challenges in remote sensing using deep learning are analyzed	Modern	Limitations of different modern approaches are highlighted in the proposed study.
(Albert, Kaur, and Gonzalez, 2017)	A Convolutional Neural Network is utilized to analyze the pattern in urban land use using large scale satellite imagery data	Modern	The proposed approach is limited to high-resolution satellite imagery which is not publically available.

(Pareeth et al., 2019)	Landsat 8 images and Random Forest approach is utilized for post-processing to extract the Land Use Land Cover (LULC)	Modern	Creating a time series data is a challenging part for many domains of satellite imagery.
(Yue et al., 2015)	A Deep Learning-based framework Restricted Boltzman Machine with Deep Belief Network is developed for feature extraction	Modern	The do not acquire spatial contextual information like the normal shape of a class objects.
(Yue et al., 2015)	A hybrid approach is proposed for classification from spectral and spatial resultion	Modern	The proposed approach is unable to learn spatial contextual features.
Proposed Model	In the proposed solution, a Bidirectional Gated Recurrent Unit is (Bi-GRU) proposed to monitor rice field from Landsat 8 satellite imagery	Modern	In the proposed approach, the above-mentioned challenges are overcome by developing multi-streaming based deep learning approach.

5.2.2 Modern Approaches

Deep learning approaches are utilized in numerous domains of remote sensing such as Image Classification, Object Detection, and semantic segmentation (Ball, Anderson, and Chan Sr, 2017). Moreover, deep learning approaches are also applied for image classification. By analyzing the considerable outcomes of the deep learning methods, several researchers have utilized the principles of deep learning for various remote sensing domains

such as Land Use Land Cover (LULC) classification and Urban Planning Albert, Kaur, and Gonzalez, 2017; Pareeth et al., 2019. A broad variety of statistical learning methods have been explored for target identification and image recognition through spectral images (Mittal et al., 2019). Furthermore, the authors proposed a Deep Belief Network (DBN) to classify the land cover from aerospace spectral images (Li, Zhang, and Zhang, 2014). However, due to the deployment of multiple Full Connected Layers (FCL), the performance of DBN was suffered due to the limited resources. Moreover, the production of spectral images by utilizing satellite images has become a different challenge in the field of classification for spectral images. The adversarial condition of an image is also considered as one of the most common challenges that makes object classification difficult (Yue et al., 2015). Moreover, a deep learning-based Convolutional Neural Network was proposed by Slavkovikj et al. (Slavkovikj et al., 2015) that was used to collect the spatial pattern from multiple spectral bands. However, due to the limited amount of training data, the proposed techniques did not perform better and misclassified the temporal dimension. In this manner, Table 5.1 Illustrates the comparison of traditional, modern, and proposed approaches.

5.3 Proposed Model

As the objective of the proposed study is to monitor the land related to rice field from satellite images, the complete process of the proposed solution is illustrated in Figure 5.2. The process of land prediction is divided into two sub-modules:

1. Input module
    (a) Data acquisition
    (b) Data preprocessing
2. Prediction the status of rice fields
    (a) Feature extraction module
    (b) Rice field mapping

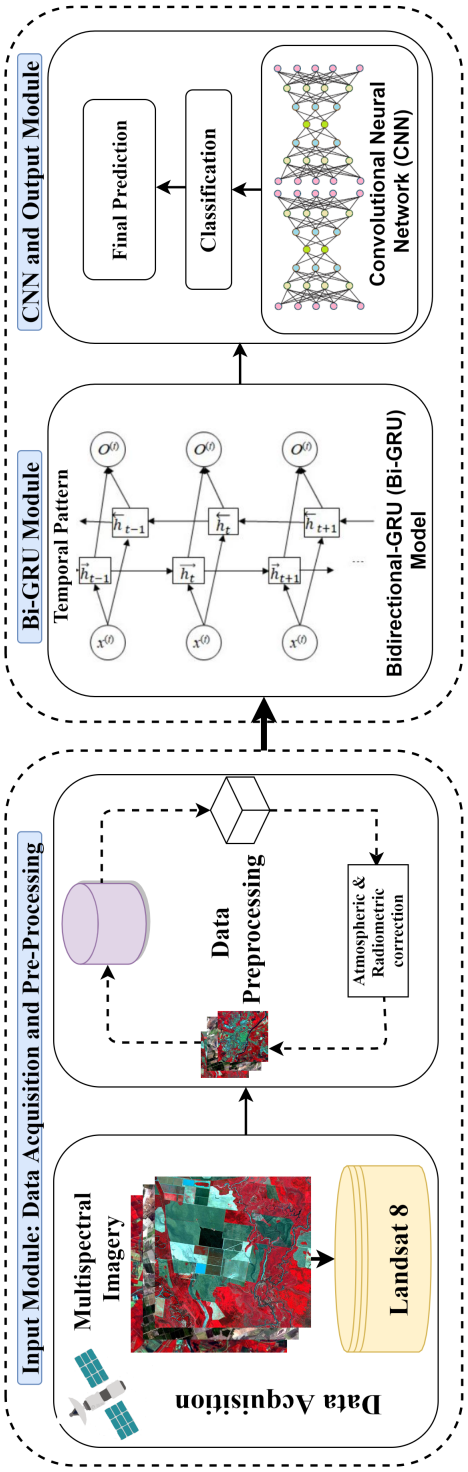

FIGURE 5.2: Overall framework of proposed approach

5.3.1 Input module

The input module is dealing with the process of data acquisition and pre-processing as follows:

Data Acquisition

Initially, the Landsat 8 satellite images are primarily obtained from the Earth Explore platform [1]. These images are essentially a digital map of the output radiance with infrared, visible, thermal infrared values at the top of the Earth's atmosphere. Landsat 8 images are containing multiples regions with 11 spectral bands for 16 days. After acquiring the images, the images are compressed into small sizes and transferred into the ground station database and again retransferred and converted into calibrated pixels. The captured images are categorized into multiple levels based on the quality of data and types of pre-processing as follows: (i) High-quality geometric information is containing data with respect to less cloud, accurate orbit information with time-series data at level 1. (ii) In level 2, the geometric requirements are not confirmed such as cloud shadow, older sensors, insufficient ground control. However, the requirement of data preprocessing in level 2 is required to enable more real-time analysis [2]. Similarly, both the level are required to ensure the completion and accuracy of the data. If the data is not available in level 1, level 2 data will be used.

Data Pre-Processing

In satellite images, the atmospheric condition and Spatio-temporal differences are considered as one of the most common challenges for remote sensing. In the proposed solution, some common pre-processing stages are followed as follows:

1. For geometric correction, the georeference and co-registration technique is utilized (Huete et al., 2002).

[1] source: https://earthexplorer.usgs.gov/
[2] source: https://www.usgs.gov/landresources/nli/landsat

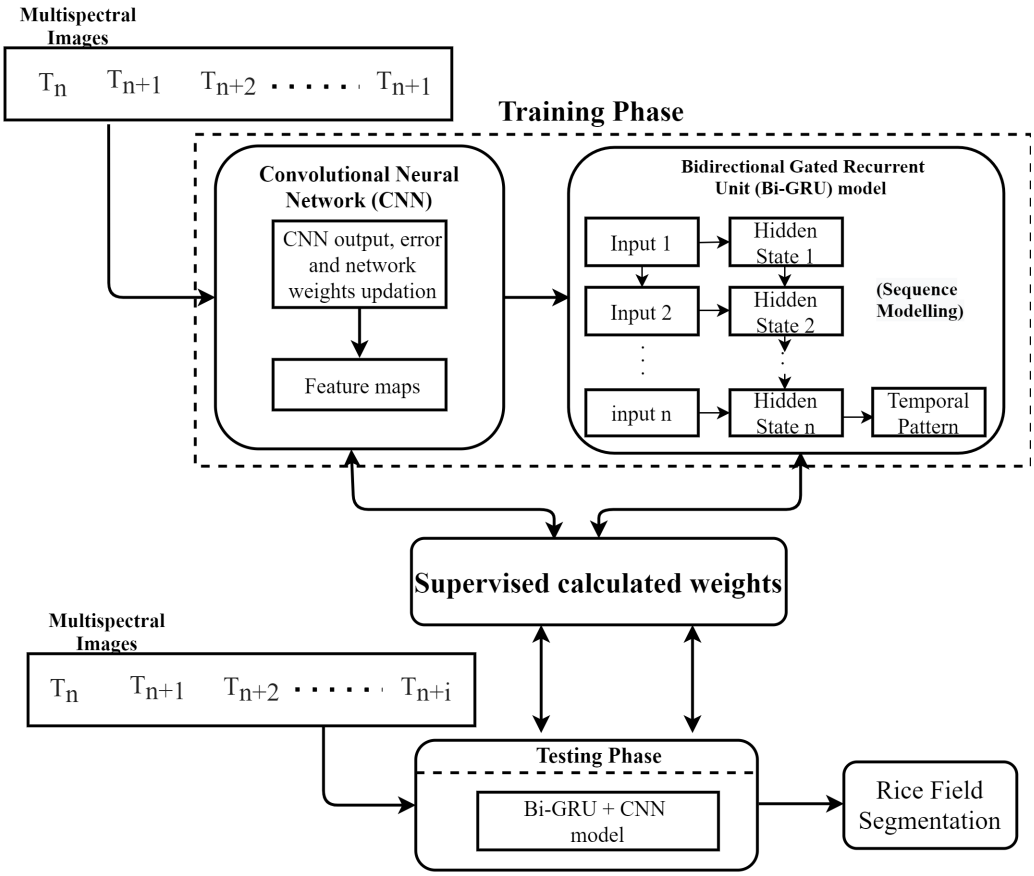

FIGURE 5.3: Deep Neural Netowrk temporal resolution architecture for rice mapping

2. To correct the atmospheric effects, the disturbance adaptive process and dark object subtraction approaches are utilized in the proposed solution (Nuarsa, Nishio, and Hongo, 2011).

3. To collect the temporal and spectral pattern, multiple radiometric approaches such as histogram matching, overlapping regions, etc (Mittal et al., 2019) are utilized.

4. The re-scaling coefficients are used to convert the digital numbers into radiance values. (Zhang, Gong, and Chan, 2018)

5.3.2 Prediction the status of rice fields

The major difference between satellite images and normal images is, satellite images are containing multicolor bands. On the other hand, normal images are containing 3 bands of color (Red, Green, and Blue). In this manner, satellite images are specifically known as multispectral images. Therefore, the extraction of spatial features from satellite images is difficult as compared to the normal image. To achieve this limitation, a deep learning-assisted multispectral feature extraction approach is proposed to segment the target area for better classification.

In the proposed study, two classes of fields such as rice field and non-rice field are carried out which are labelled with two integer values i.e. P=1,2. The input image $A = (a_{11}, a_{1n1}, ...a_{n1n2})$ is a set made up a feature vector $V = V_1 \times V_2$. Moreover, the Landsat 8 image is containing 11 spectral bands, therefore, all bands are denoted with M with the value of 11. More specifically, each satellite image is denoted as $a = A_1, A_2, ...A_t$. Where t denotes the time taken for capturing the particular image. In the proposed study, the value of time t is set to 28 which defines 28 tiles of an image for a year to monitor the rice cultivation. Moreover, the problem of zoning and monitoring (Xiao et al., 2006) is also considered in the proposed study.

1. **Rice field Zoning:** Full time RZS is a mapping procedure of full-time fuction $F_1 : S^{n*m*t} \rightarrow S^{n*2}$ from the pair of image a to the set of label vectors.

$$Z = F_1(a) \tag{5.1}$$

   Where Z defines N vectors that correspond the number of pixels $z_1, ..., z_n, ..., z_N$ in an image. Every element is a 2-dimensional vector z denoted as $\{z^1, z^2\}$. Where z^1, z^2 denotes the value of prediction probability that defines the relation of an image with the targeted class such as rice field or non-rice field. Moreover, the aggregation function $Z^* = agg(z^1, z^2)$ is used to decide the belongingness of Z^* label to the pixel of an image.

Furthermore, to maximize the classification performance, the definition of classification model F_1 and an aggregation function are primarily required.

2. **Rice field monitoring:** The function $F_2 : S^{n*m*T} \rightarrow S^{n*T*2}$ represent the process of rice field monitoring from pair of images a. Mathematically, it is calculated as;

$$z = F_1(a) \tag{5.2}$$

Where $z = \{z_1, ...z_t\}$ represent the labelled information for a point t. At last, the aggregation function is utilized to decide the final label for every pixel. Here, the label Z_t has the same meaning in rice zoning segmentation. Similarly, Rice Monitoring Segmentation needs to be described with the function model F_2 and an aggregation function.

Feature extraction module

Based on the above-mentioned two problems, a deep learning-assisted modular approach is proposed to combined temporal, spectral, spatial features for final classification in a simultaneous manner. In the proposed model, the input layers are used to feed the satellite data to the proceeding layers and Bidirectional-Gated Recurrent Unit (Bi-GRU) is utilized for handling the temporal patterns of the input data. Moreover, Convolutional Neural Network (CNN) is used to classify the spatial and spectral dependencies from the pixel values. At last, the final prediction is achieved by the output layer. The complete overview of the proposed model is illustrated in Figure 5.3.

Bi-GRU Space: Initially, a 2D Convolutional Neural Network (2D CNN) (Huete, 1988) is utilized to obtain pixel-wise features from satellite imagery and Gated Recurrent Unit (GRU) model is utilized to capture temporal dependencies Golilarz, Gao, and Demirel, 2019. The advantage of the Bi-GRU model over the most widely used LSTM technique is processing the temporal dependencies. GRU's working process is quite similar to the Long

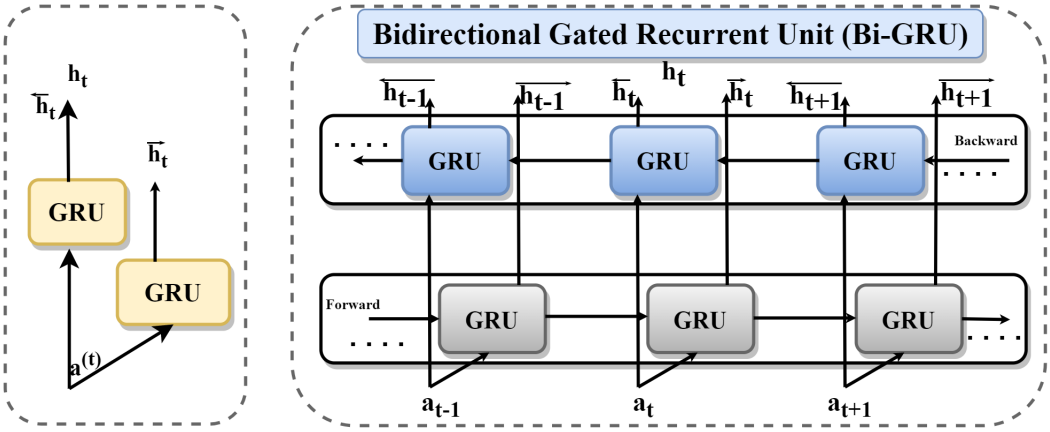

FIGURE 5.4: The proposed structure of Bi-GRU architecture

Short-Term Memory (LSTM), however, there are some structural differences (Pareeth et al., 2019; Mittal et al., 2019). The Bi-GRU model is used to capture temporal interdependence in both past and future directions across several time steps. Because there are fewer parameters in the GRU model as compared to LSTM, it can deal with less training data and take less time to train. Moreover, it has the capability to deal with the problem of vanishing gradient (Pareeth et al., 2019). In this manner, Bidirectional Gated Recurrent Unit (Bi-GRU) (Mittal et al., 2019) approach is utilized in the proposed study to calculate future probabilities which is essential for long-term classifications such as the cultivation of rice. The proposed approach effectively obtained the temporal dependencies from satellite images before feeding data to the convolutional layers. Moreover, the Bi-GRU model is able to combine the previous and next feature information by processing the data in forward and as well as backward direction simultaneously with two different hidden layers. The traditional GRU is made up of three different gates reset gate (e_t), update gate (v_t), and output gate (h_t). Under the control of input (a_t) and previous state (h_{t-1}) ,the output gate is determined and calculated as:

$$e_t = \sigma(w_e a_t + U_e h_{t-1} + b_e) \tag{5.3}$$

$$v_t = \sigma\left(w_v a_t + U_v h_{t-1} + b_v\right) \tag{5.4}$$

$$\tilde{h}_t = \tanh\left[W_h a_t + U_h\left(r_t \odot h_{t-1}\right) + b_h\right] \tag{5.5}$$

$$h_t = (1 - z_t) \odot h_{t-1} + z_t \odot \tilde{h}_t \tag{5.6}$$

Where e_t denotes the reset gate, v_t represents the update gate, and $\tilde{h}_t$ is used to add new memory information. On the other hand, W_e, U_e, w_v, U_v are the wight metrics. To stable the memory value into -1, 1 tanh activation function is used that defines the dependency of the current state of the GRU on the previous state in the current memory. The proposed Bi-GRU model is able to learn the information from previous and future data while processing current data and focused on two GRUs that are unidirectional in opposite direction illustrated in Figure 5.4. This enables the future and previous knowledge to influence the current states and calculated as:

$$\overrightarrow{h_t} = gru_{fwd}\left(a_t, \overrightarrow{h_{t-1}}\right) \tag{5.7}$$

$$\overleftarrow{h_t} = gru_{bwd}\left(a_t, \overleftarrow{h_{t+1}}\right) \tag{5.8}$$

$$h_t = \overrightarrow{h_t} \oplus \overleftarrow{h_t} \tag{5.9}$$

Where $\overrightarrow{h_t}$ denotes the forward state of GRU and $\overleftarrow{h_t} = gru_{bwd}$ represent the backward state of the GRU. While $\oplus$ defines the integration of the two different features. Multiple images with respect to different periods are required to train the Bi-GRU model. In this manner, the group of 28 images was used for a targeted area with a sample rate of 16 days per year that is the hidden unit of the Bi-GRU module (T = 28). Due to Equation 4, the input is flattered before entering into the Bi-GRU module. The output vector is transformed into 2D to maintain the spatial structure information. Finally, the outcome obtained from Bi-GRU is further transferred to Convolutional Neural Network Layer.

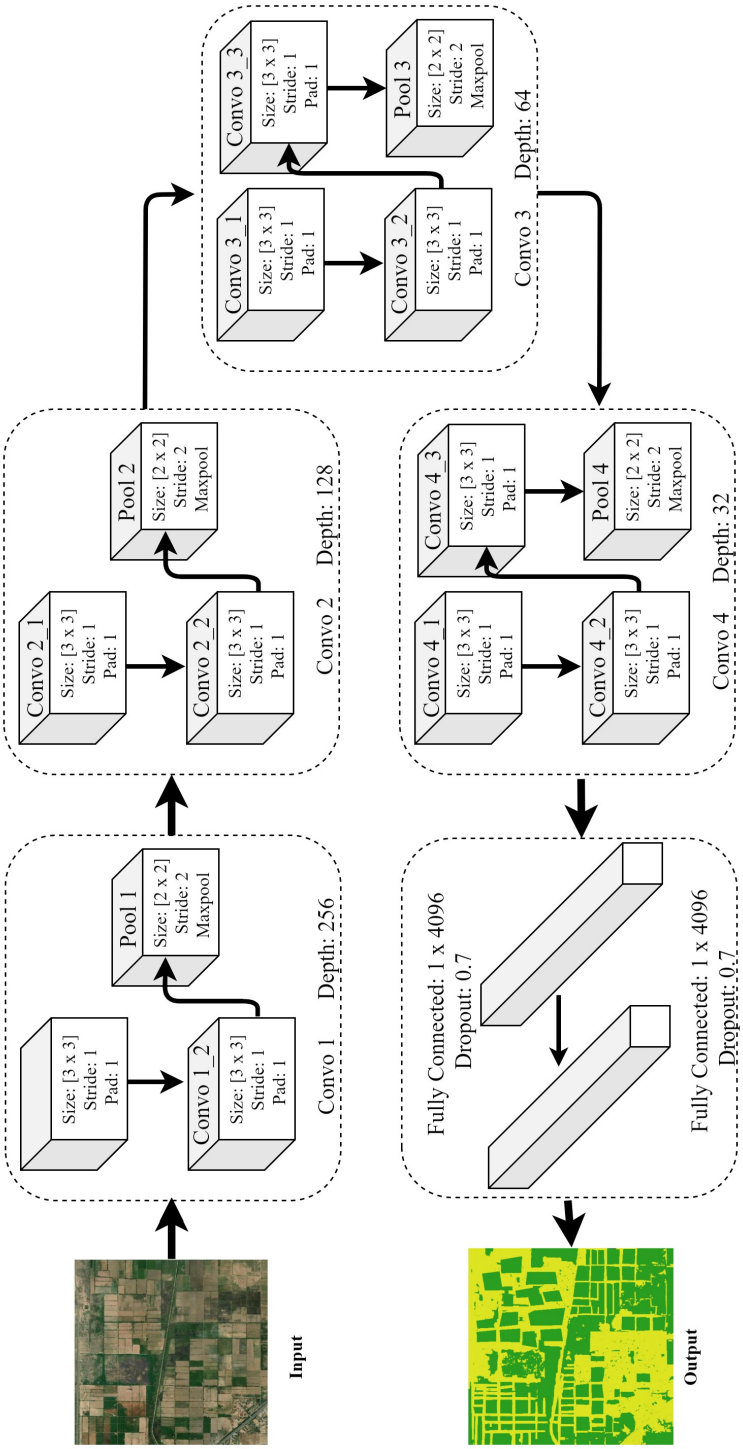

FIGURE 5.5: Structure of Convolutional Neural Network

Convolutional Neural Network Space: To capture the spatial dependencies among the multiple bands, a Convolutional Neural Network is designed in a proposed study. In this space, two different types of temporal resolutions are carried out (i) Full-time temporal resolution (FTTR) and (ii) Real-time temporal resolution (RTTR). The full-time resolution took the temporal dimension as a whole into its consideration. For that reason, we use filters on the first convolutional layer to aggregate the outputs of Bi-GRU blocks over many times. The same number of filters and kernel sizes are used in convolutional layers for real-time temporal resolution. In first convolutional layer process $L_0 = 128 \times 28$ spectral bands to $L_1 = 256$ with $b_c = 3$ size of the kernel. The filters in second layer of convolution is $L_2 = 128$ and $b_c = 3$ is the size of kernel. Similarly, the third convolution also include $L_3 = 64 filters$ with a kernel size of $b_c = 3$.
In Real-time temporal resolution, the outcome generated by the proposed Bi-GRU is directly fed to the convolution layer and the neuron of one layer is linked only with neurons of another layer in receptive area (Li, Zhang, and Zhang, 2014). When the layers are at a deep level, they become small and extract more accurate and descriptive features. The concentration of the model will remain on the local spatial dependencies among the pixels instead of the actual targeted area of an image. Across the entire input representation, the actual field area of an image is changed. On the other hand, the spatial dependencies as well spectral dependencies of the previous layer are captured by the neurons of the succeeding layer. The computational efficiency of the convolutional network is high as compared to a fully connected network in terms of weight sharing. The same weight and biases are shared by the neurons that are in the same layer with their weighted sum formation in the respective area of the observed neurons (Yue et al., 2015).

$$V_{ij} = \phi\left(b_i + \sum_{k=1}^{K} W_{ik} Z_{j+m-1}\right) = \phi(b_i + W_i Z_j) \tag{5.10}$$

Where the number of bands/filters are denoted by K, V_i, ϕ are the output of the j_{th} neuron and neural activation function, respectively. The overall shared bais of filter i is denoted by b_i. The shared weight with vector is

calculated as $W_i = [W_{i1}, ...W_{iK}]$. Moreover, the actual area of an images is calculated as $Z_j = [Z_j, ...Z_{j+k_c-1}]$. The three different types of convolutional layers are designed in the proposed solution and also multiple numbers of filters are assigned to each layer due to different spatial features. The complete process of convolution layers with their respective weights is represented in Figure 5.5. According to spatial resolution (30m) of Landsat 8, the same and small kernel sizes are used for each layer.

Convolutional layers assume strongly spectral dependencies by simultaneously taking into account all spectral bands. In practice, partial dependencies may be present because of the high difference between the spectral bands. Therefore, the pooling layer is used after every convolutional layer to deal with this issue and soothes the performance of the architecture by subsampling. The selected size of the pooling layer is $AP_{size} = 2$ with stride= 2. In the proposed solution, the average pooling technique is utilized instead of Max Pooling to deal with rice field features because rice field features are not sharp as compared to other features.

Rice field mapping

The dimensionality reduction of a source image is performed and the final convolutional output must be transformed into the source input size for pixel-level segmentation (Yue et al., 2015). To achieve this, bi-linear upsampling layer is utilized on 2D data for generating g $\times$ n_1 $\times$ n_2 pixels. In the g_{th} proposal, pixels *ij* from nearby pixels are interpolated.

$$P_{ik}^{g} = \frac{V_{i-1,k}+V_{ik}+Vi+1,k}{3} forj-1 \leq k \leq j+1 \tag{5.11}$$

$$P_{kj}^{g} = \frac{V_{kj-1}+V_{kj}+Vkj+1}{3} fori-1 \leq k \leq 1+i \tag{5.12}$$

At last, the upsampling is converted by mapping to classify the score Wang et al., 2018a.

$$Y = WP + B \tag{5.13}$$

Where the scores for non-rice field and rice field is denoted by $P = [P^1, ..., P^g]$ and W, B are trainable parameters. Moreover, the output of the above-mentioned technique is finally transferred to the softmax layer that does not linearize the projection and normalize the classification values for class comparison. The mathematical calculation of the aggregation function is as follows:

$$F_{ij}^{C} = \frac{expF_{ij}^{C}}{\sum_{C' \in s} exp(F^{C'}ij)} \tag{5.14}$$

Where the score of the value of the pixels is denoted by F_{ij}^{C}. The final pixel label is determined as $F_{ij}^{*} = argmax_{C \in sFCij}$ during the test period.

Hyperparameter Optimization: To effectively address the rice zoning and rice monitoring segmentation, two-loss functions such as former K_f and latter K_r are utilized to determine the scale of loss. A loss-share α ratio is defined for a specific part of the model to calculate the full-time and real-time loss. This also makes it possible for users to control the model flexibility. Mathematically, the calculation of loss is represented as:

$$K = \alpha K_f + (1 - \alpha)K_r - \sum_{1 \leq i \leq N_1, 1 \leq j \leq N_1} \sum_{C \in K} 1_{F_{ij}^{*}} \log(F_{ij}^{*}) \tag{5.15}$$

Where K_f and K_r represents the loss function that is used to increase the value of true class for every image pixel. To enhance the efficacy of the proposed model, the following training parameter is tuned accordingly:

1. Optimization of Parameters: In the proposed study, the Adam optimization technique is applied to train the network. This technique has shown better results in terms of theoretically and empirically on momentum and RMSProp (Ball, Anderson, and Chan Sr, 2017).

2. Tuning of Hyperparameter: The hyperparameters are fine-tuned by following some parameters such as Momentum coefficient μ, learning Rate n, regularisation λ, and the batch size b. There are enhanced by using the Bayesian approach (Li, Zhang, and Zhang, 2014).

3. Avoid Overfitting: Training data are limited based on the requirement of expert knowledge (e.g. rice-paddy labeling) and real-world experiences for specific applications as rice mapping (e.g. low sampling rate). However, due to the limited amount of data, the rice field monitoring led to overfitting. To deal with the overfitting problem, several strategies are applied to the dataset.

    - Data Argumentation: The transformation technique is used to increase the size of the dataset without losing accuracy. In this manner, some transformations are applied to the proposed dataset to increase the sample into eight multiple samples by combining $k = \pi/2$ rotations, $k = 0....3$, and verticle direction. The transformed images have the same class and label.
    - Regularization: To avoid the overfitting of the proposed model, some regularization techniques are also applied such as pooling, batch normalization, and drop-out.

5.4 Performance Evaluation

In this section, the utmost performance of the proposed framework is evaluated on the Landsat 8 image-based dataset. The performance of the proposed solution is evaluated and presented in different subsections:

1. Study area and dataset
2. Monitoring performance evaluation
3. Comparative analysis

5.4.1 Study area and dataset

As India is one of the largest countries for cultivating rice, we have opted Punjab state for the experimental study. During the past few years, Punjab is the second largest popular state of India for rice production and it is also known as the "Rice Bowl of India". Punjab has located between 29'30" N to

TABLE 5.2: Seasons for rice cultivation

Season	Sowing	Harvesting
Rainy Season	May- August	September -November
Autumn Season	June - July	October - November

32′32″ N latitude and 73′55 E to 76′50 E longitude in Northern India. The altitude of Punjab varies between 230 m to 700 m from the mean sea level. The cultivable area is 4.20 million hectares (83.4%of total geographical area) and the net area sown is 4.023 million hectares (95.7% of cultivable area). The gross cropped area is 7.739 million hectares and the area sown is 3.704 million hectares with a cropping intensity of 186 %. The net irrigated area is 4.019 million hectares (by canals- 26.2%, by Tube wells- 72.5%, and by others – 1.3%). The gross irrigated area is 7.442 million hectares and the percentage of the net irrigated sown area is 96.17%. The total number of landholdings is 10.93 lakh out of which 2.04 lakh (18.7%) are marginal farmers, 1.83 lakh (16.7%) small farmers and 7.06 lakh (64.6%) farmers hold land above 2 hectares [3]. It can be cultivated on a range of low permeability and pH soil ranging between 5.0 and 9.5. Different varieties of rice are cultivated in Punjab. The annual average temperature is 16 to 30°, showing the temperature is 20-30°, and harvesting temperature is 16 to 27°. [4]. The rice cultivation seasons in Punjab are summarized in Table 5.2. The complete source code of the proposed solution can be found by accessing the given link of GitHub repository [5].

Dataset: For rice cultivation two different types of real-world Landsat 8 satellite image-based dataset is created by specifying the region of interest. In order to check the efficiency of the proposed model, the two largest places from India are selected to build the real-world rice dataset such as Punjab and West Bengal.

[3]Source: https://www.apnikheti.com/rice-TypesofVarieties
[4]Source: https://www.apnikheti.com/en/pn/agriculture/crops
[5]Source: https://github.com/yasir2afaq/Multi-resolution-deep-neural-network.git

TABLE 5.3: Important features of both datasets

Dataset	Time Stamp	Number of Images	Resolution	Class distribution	Cloud Coverage
Punjab Rice	01-05-2017 to 30-05-2019	70	30m/pixels	130,110,720 : 43,969,464	<10%
West Bengal Rice	01-06-2017 to 30-12-2019	70	30m/pixels	37,296,336: 138,529,580	<10%

- *Punjab rice:* The whole rice farming is concentrated in the State's high productivity zone. After Tamil Nadu, Punjab ranks second in the country in rice productivity. Punjab's average three-year productivity (3337 kg/ha) is 71% higher than that of the nation's average three-year productivity (1,947 kg/ha). Indeed, the rice area in Punjab is lower, although overall productivity is higher [6].

- *West-Bengal Rice:* With average productivity of 2.6 tons/ha, the State has the cultivation of 5.8 million ha in rice, covering irrigated and rainfed areas. This is the largest state of India which is producing a high amount of rice [7]. As the rice-growing season is monsoon, the presence of clouds is a challenging task in the field of remote sensing for crop monitoring. In the proposed study, only the images which are containing <10% clouds are downloaded from Earth Explorer. Furthermore, preprocessing techniques are applied to the proposed dataset to remove further noise from the selected images. The main features of both datasets are shown in Table 5.3.

To conduct the experiments, the configuration of the system is as follows: CPU: Intel Core i5 2.8-GHz CPU, GPU: NVIDIA GTX-1080Ti GPU, Operating System: Ubuntu 18.4 LTS, and Programing Language: Python. The complete configuration of the proposed model is presented in Table 5.4 for

[6]Source: http://www.drdpat.bih.nic.in/PA-Table-19-Punjab
[7]Source: https://icar.gov.in/files/state-specific/chapter/125.htm

TABLE 5.4: Proposed architecture configuration

Space	Model Components	Size of Input	Size of Output
Rice Zoning	Input	$28 \times 64 \times 64 \times 14$	$4096 \times 28 \times 14$
	Bi-GRU	$4096 \times 28 \times 14$	$28 \times 64 \times 64 \times 128$
	CNN	$28 \times 64 \times 64 \times 128$	$28 \times 64 \times 64 \times 2$
Rice Monitoring	Output	$28 \times 64 \times 64 \times 2$	$28 \times 64 \times 64 \times 2$
	CNN	$28 \times 64 \times 64 \times 128$	$1 \times 64 \times 64 \times 2$
	Output	$1 \times 64 \times 64 \times 2$	$1 \times 64 \times 64 \times 2$

better understanding which includes 40747689 parameters including weight and biases.

5.4.2 Monitorng performance evaluation

To improve the performance of the proposed model, a k-fold cross-validation process is followed for training and testing. K-fold cross-validation is utilized in the proposed study to divide the dataset equally into a training set and test set. More specifically, the data is randomly divided into k-equal subsets for model training using $k - 1$ subsets and for model testing the single remaining subset is used. The whole process is performed k times and the observed test accuracy is averaged 10 results. k = 10 is frequently applied to reach the utmost performance between the training data and sufficient invisible samples to evaluate accurately. To avoid the problem of overfitting in the model, the training data is divided into learning rates i.e. k -2 subsets, and the tuning set is 1 subset. The whole process is repeated k -1 time and selected the best performance. In case the model is assured to perform well on unseen data (via the tuning system), an optimal setting can be set and thus avoids over-fitting in the test set. In total, 80% for preparation, 10% for validation, and 10% for testing are divided between labeled data. Moreover, an early stoppage process is followed during training that helps to prevent the overfitting as well as speed up the training by calculating model convergence on the tuning set instead of the learning set (Li, Zhang, and Zhang,

TABLE 5.5: Seasonal imapct on rice mapping

Problem	Year	Precision	Recall
Rice Zoning	2017	95.61%	95.89%
	2018	93.33%	94.43%
	2019	90.77%	93.61%
	Overall	91.12%	94.11%
Rice Monitoring	2017	94.78%	90.23%
	2018	93.23%	89.12%
	2019	90.33%	91.89%
	Overall	86.22%	89.11%

2014).

Spatio-temporal Condition effects: To check the Spatio-temporal condition, the proposed model is evaluated on two different temporal resolutions namely Rice Zoning Segmentation and Rice Monitoring Segmentation. Moreover, the performance is evaluated on Spatial datasets by training the selected models. The Rice Zoning Segmentation and rice monitoring results on the Punjab rice dataset are illustrated in Figure 5.6 and Figure 5.7.

The proposed model has achieved a better performance as compared to other baseline models in terms of F1-score 95.32% on the Punjab Rice dataset. On the other hand, the comparison is also done on Rice monitoring Segmentation on the same datasets and the proposed model again achieved better performance with the F1-score 93.12% which is higher than other selected models. However, the models have not shown better results on the West-Bengal Rice dataset. The result of each model is illustrated in Figure 5.8 and Figure 5.9.

Moreover, the efficacy of each selected model is tested by choosing a different model design. Here, (i) Bi-GRU: changed Bi-GRU block with GRU or LSTM to check the impact of temporal data on future and past monitoring, (ii) CNN: changed the CNN clocks with multilayer perceptrons (MLP) to know the impact spectral and spatial features, (iii) Upsampling: changed the bilinear upsampling with Deep Neural Network (DNN) with the same

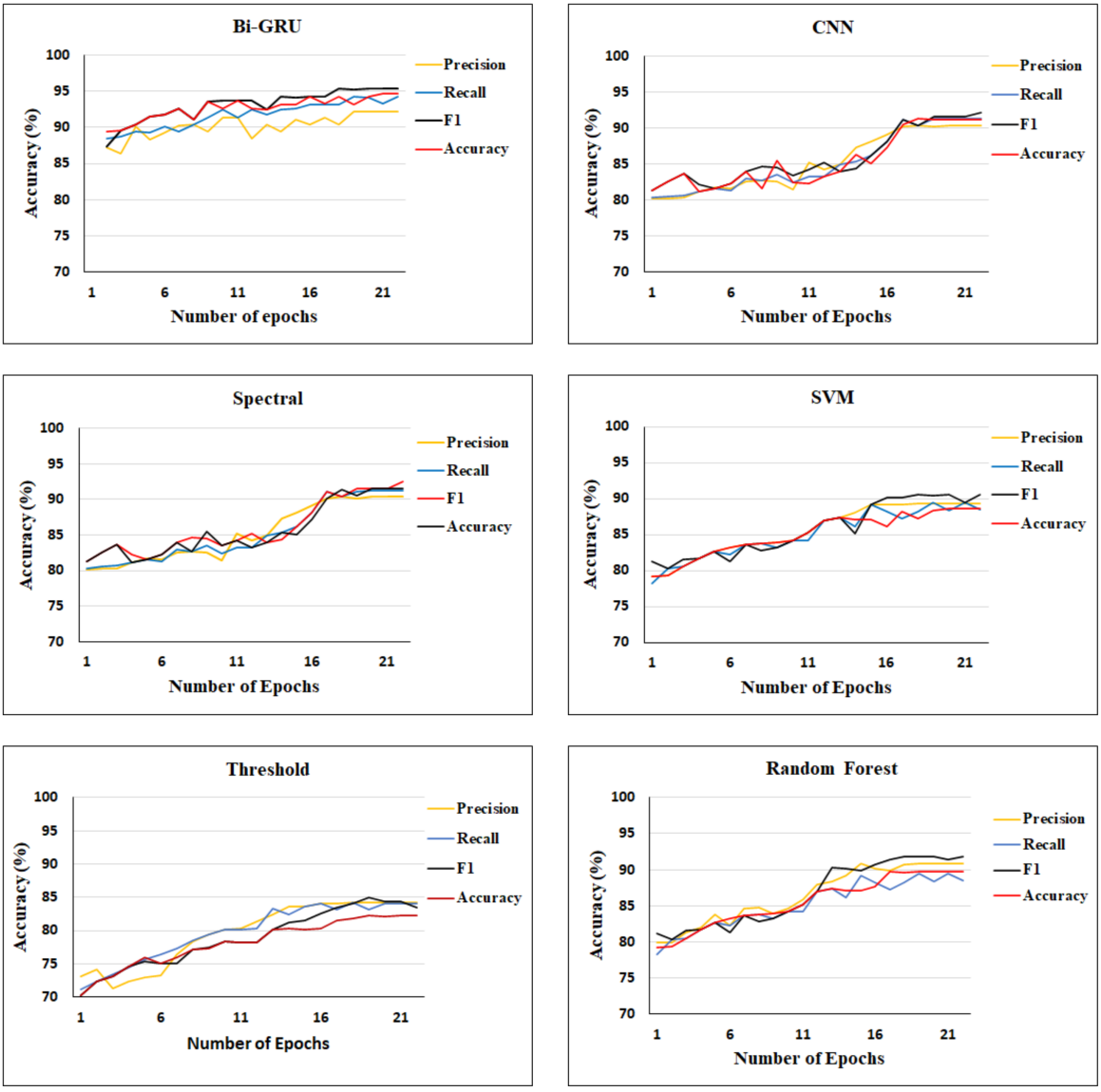

FIGURE 5.6: Comparative analysis of rice zoning segmentation on punjab dataset.

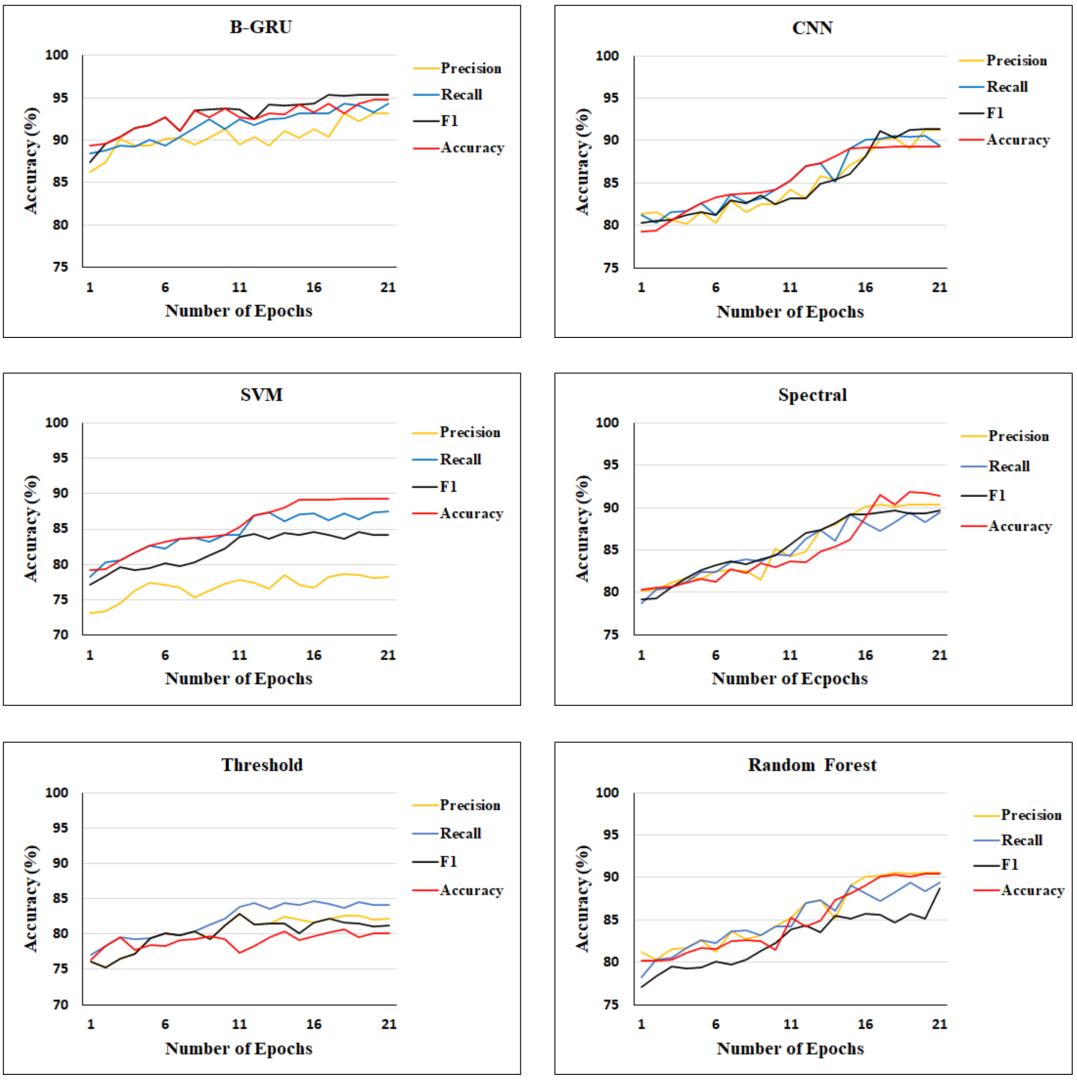

FIGURE 5.7: Comparative analysis of rice Monitoring segmentation on punajb rice dataset.

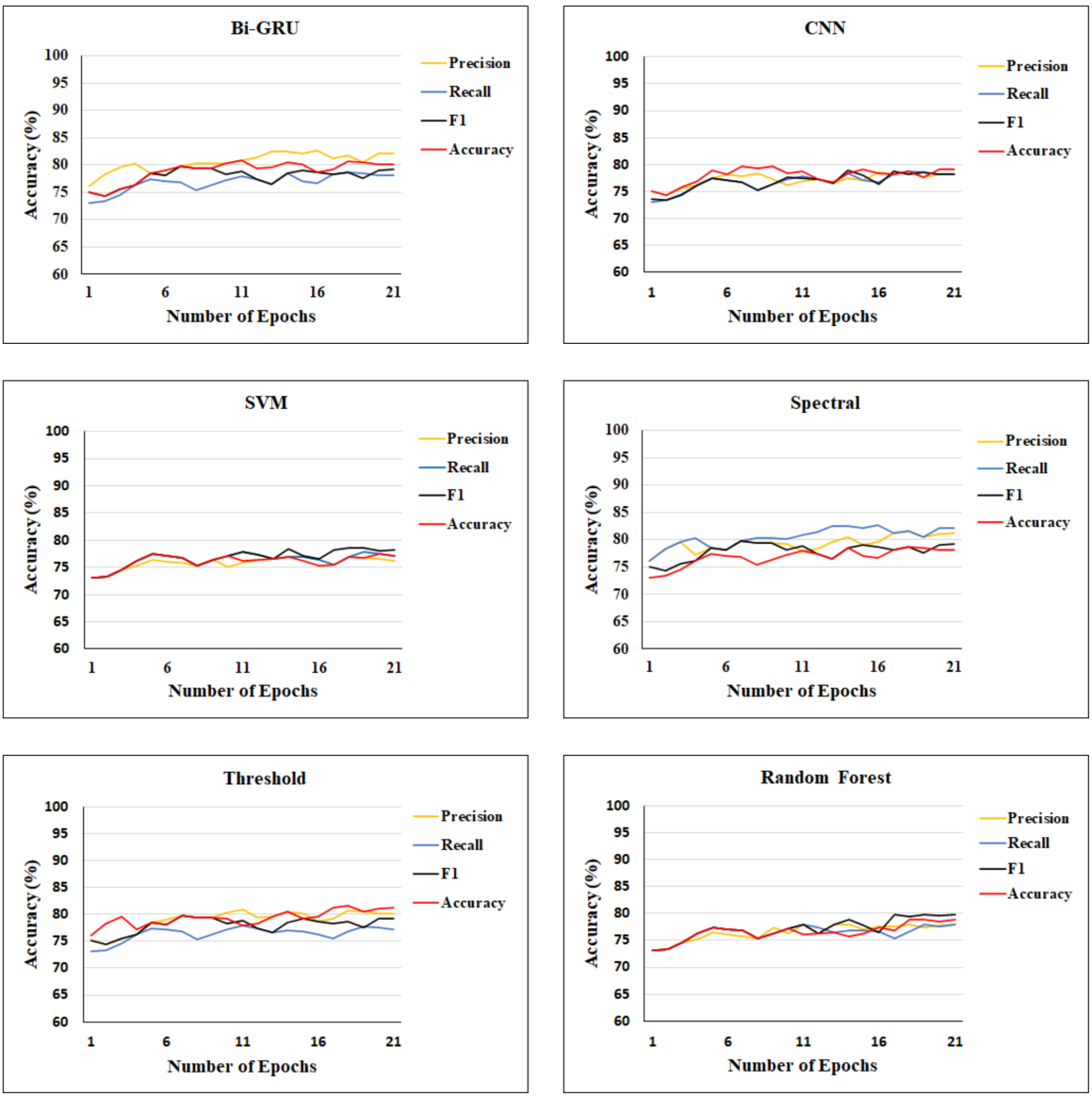

FIGURE 5.8: Comparative analysis of rice zoning segmentation on West-bengal rice dataset.

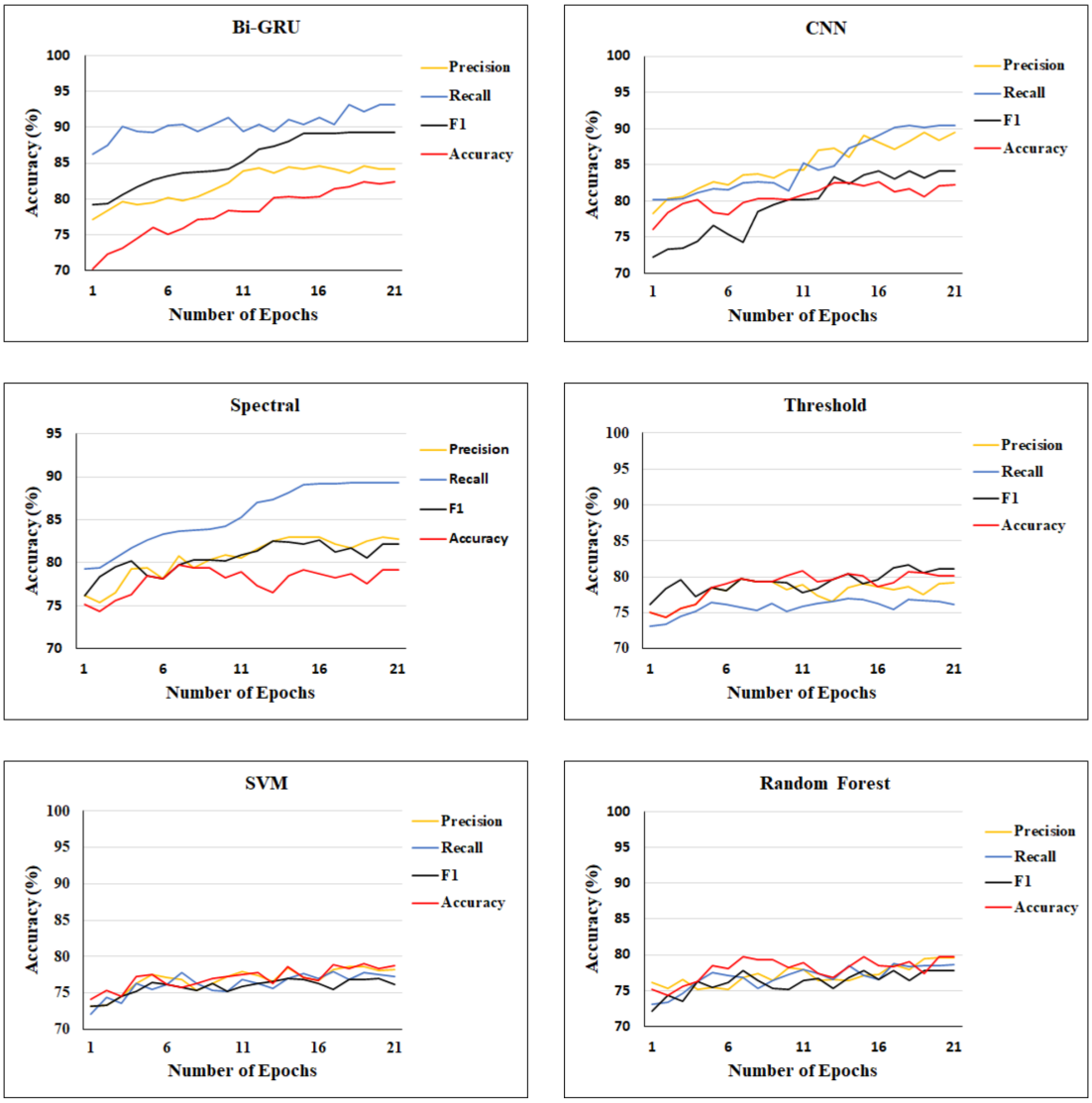

c

FIGURE 5.9: Comparative analysis of rice monitoring on West-bengal rice dataset.

kernel size as the CNN space to measure the segmentation performance upsampling effect. The final result of each model is evaluated on both datasets and illustrated in Table 5.6 in terms of F1-score and training and testing time. The calculated outcomes revealed that the model *Bi-GRU + CNN + Upsampling* has shown a better result as compare to other models. The highest results are highlighted for easy understanding.

Analysis of Seasonal effects: In this section, the performance of the model is analyzed against the seasonal impact. The model is evaluated on two different seasonal effects such as annual cultivation and different type of crops. As there will be different types of crops in Punjab namely Wheat, Paddy, Basmati, Cotton, etc. [8]. Moreover, the dataset is further divided into three different cultivation periods (2017, 2018, and 2019). The evaluated results in terms of Precision and Recall are compared with other selected models and illustrated in Table 5.5. It has been realized that the performance of the model is not effective in 2017 just because of climate change which can affect the spectral bands and may change the important features in spectral channels.

In addition, rice cultivation in Punjab has different durations that are ranged from *100-120* days to *130-140* days in a district of Punjab state named Amritsar. In this manner, the input data vary the size of the window with T = 7, 14, 28 to activate the zoning and monitoring with multiple periods.

The results of Rice Zoning segmentation and Rice Monitoring segmentation in terms of Precision and Recall for different window sizes are illustrated in Table 5.7. The results for larger window sizes are low as compared to the other two window sizes. The degradation in results occurred due to the confusion generated at the time of differentiation of the smaller fields with another area.

[8]Source: https://pbplanning.gov.in/pdf/COCbriefreport.pdf

TABLE 5.6: Content of each model and their imparative result with training and testing in seconds

Models	Rice Zoning (F1-Score)	KAPPA	Rice Monitoring (F1-score)	KAPPA	Training (Sec)	Testing (Sec)
Bi-GRU + CNN + Upsampling	95.4 ± 0.009	0.91	92.3 ± 0.011	0.89	1245	15
Bi-GRU + MLP + Upsampling	95.1 ± 0.009	0.90	91.4 ± 0.012	0.86	710	15
GRU + CNN + Upsampling	94.2 ± 0.009	0.90	89.4 ± 0.014	0.83	550	9
LSTM+ CNN + Upsampling	93.3 ± 0.010	0.89	86.5 ± 0.020	0.82	450	9
Bi-GRU + CNN + DNN	91.6 ± 0.012	0.86	90.3 ± 0.012	0.86	1230	16

TABLE 5.7: Effect of multiple crops on model performance for rice mapping

Problem	Window Size	Precision	Recall
Rice Zoning	7	93.22%	95.23%
	14	84.23%	95.12%
	28	82.11 %	94.12 %
Rice Monitoring	7	94.21 %	92.77 %
	14	86.23%	86.33%
	28	83.55 %	84.18 %

5.4.3 Comparative analysis

The performance of the proposed model is justified by comparing it with the selected models such as SVM, LGBM, XGboost, Threshold, Convolutional Neural Network (CNN), DeepLabV3+, Spectral, VGG, Random Forest, and InceptinnNet. The final result is summarized in Table 5.8. From the calculated outcomes, it has been observed that the proposed model took less training time and test time on Landsat 8 images as compared to other deep learning models illustrated in Table 5.9.

From Table 5.8 and 5.9, It can be analyzed that the proposed model has achieved a better result on Landsat 8 images as compared to another selected model by achieving 95.12% on rice zoning and 92.67% on rice monitoring. Furthermore, the evaluation of classification efficiency was done at a fine-tuned level with the calculation of true/false positive and true/false-negative results. The confusion matrices are generated on the proposed model and other selected models for Rice Zoning Segmentation on the Punjab rice dataset. Table 5.10 represents the normalized confusion matrices-based results on different models.

Moreover, the interpretation of the proposed model for rice field segmentation is done by visualizing the outcomes of the model based on the region of interest. The true-color image as illustrated in Figure 5.10(a) can easily understand. The segmentation results based on the true-color image and the ground truth image with the combination of 11 spectral bands are illustrated in Figure 5.10. After visualizing the segmentation results, it can be seen that

TABLE 5.8: Compartive analysis results on differnt models

Models	F1 Score (Full-time resolution)	KAPPA	F1 Score (Real-time resolution)	KAPPA
Threshold (Meng et al., 2019)	86.21 ± 0.018	0.81	87.19 ± 0.020	0.82
Spectral (Ursani et al., 2011)	89.87 ± 0.014	0.82	88.41 ± 0.014	0.83
SVM (Mansaray et al., 2019a)	90.60 ± 0.012	0.86	89.44 ± 0.014	0.83
VGG (Sethy et al., 2020)	85.23 ± 0.021	0.78	85.12 ± 0.021	0.81
InceptionNet (Kiratiratanapruk et al., 2020)	83.12 ± 0.023	0.79	84.15 ± 0.021	0.80
CNN (Zhang et al., 2018b)	91.76 ± 0.012	0.87	90.21 ± 0.012	0.86
RF (Mansaray et al., 2019b)	90.81 ± 0.012	0.88	88.75 ± 0.020	0.84
Light-GBM (Lv et al., 2020)	91.96 ± 0.012	0.87	89.77 ± 0.019	0.83
XGboost (Nagaraju, Mohandas, et al., 2021)	91.45 ± 0.012	0.87	89.65 ± 0.014	0.83
DeepLabV3+ (Heryadi et al., 2020)	92.44 ± 0.013	0.89	90.12 ± 0.012	0.86
Proposed Model	95.12 ± 0.009	0.91	92.67 ± 0.010	0.89

TABLE 5.9: Traning time and test time of differnt models

Models	Traning (In Seconds)	Testing (In Seconds)
Threshold	80	81
Spectral	1390	26
SVM	1265	17
VGG	1432	21
InceptionNet	1478	22
CNN	1260	13
RF	1129	15
Light-GBM	1012	17
XGboost	1190	78
DeepLabV3+	1250	14
Proposed Model	**940**	**12**

the proposed model performed better for segmenting the ground truth pixels as compared to other selected models.

The prediction efficiency of the proposed solution is evaluated by comparing the results with conventional and modern selected approaches such as Threshold, Spectral, RF, SVM, LGBM, XGboost, CNN, and DeepLabV3+. Images from the West-Bengal dataset are selected for testing the prediction performance of the proposed solution. The selected image for prediction analysis is captured on 01-Aug-2018. The calculated performance measures such as P, R, F1, Kappa, and Accuracy is presented in Table 5.11 to justify the prediction performance of the proposed solution. Moreover, the segmented outcomes are shown in Figure 5.11 for better understanding. It has been observed that the proposed (MR-DNN) tends to have a maximum F1-Score with the value of 96.33% as compare to DeepLabV3+ (92.13%), CNN (91.22), RF (88.43%), Light-GBM (89.77%), XGboost (89.67%), SVM (88.33%), Spectral (84.44%), and Threshold (85.46%). Similarly, better prediction efficiency has been observed from the outcome on the West-Bengal dataset on different dates. Therefore, it has been concluded that the proposed model is robust than other deep learning and machine learning models. Furthermore, the calculated outcomes illustrated in Figure 5.11 and Figure 5.12

Extracting the crop field from satellite imagery is considered one of the most imperative task for accurate planning the food. In this manner, the

TABLE 5.10: Normalized Confusion Matrices. Rice field classification: RFC, Non-rice field classification: N-RFC

Classification Models	Class	RFC	N-RFC	OA	KAPPA
RF	Rice Field	93.78%	4.45%	88.59 ± 0.018	0.84
	Non-Rice field	19.67%	80.22%		
Threshold	Rice Field	90.45%	9.21%	66.46 ± 0.029	0.62
	Non-Rice field	59.24%	45.21%		
Spectral	Rice Field	92.21%	3.2%	85.46 ± 0.022	0.81
	Non-Rice field	24.92%	73.12%		
SVM	Rice field	93.14%	4.65%	88.77 ± 0.021	0.73
	Non-Rice field	19.77%	82.11%		
CNN	Rice field	81.45%	21.34%	79.84 ± 0.026	0.75
	Non-Rice field	20.12%	82.76%		
Light-GBM	Rice field	93.87%	3.65%	88.87 ± 0.021	0.83
	Non-Rice field	18.67%	84.56%		
XGboost	Rice field	93.43%	3.98%	88.25 ± 0.021	0.84
	Non-Rice field	19.52%	83.11%		
DeepLab V3+	Rice field	85.66%	19.56%	83.52 ± 0.023	0.79
	Non-Rice field	14.67%	87.78%		
Proposed Model	Rice field	**96.23% (TP)**	3.10% (FN)	89.33 ± 0.014	0.85
	Non-Rice field	18.34% (FP)	83.21% (TN)		

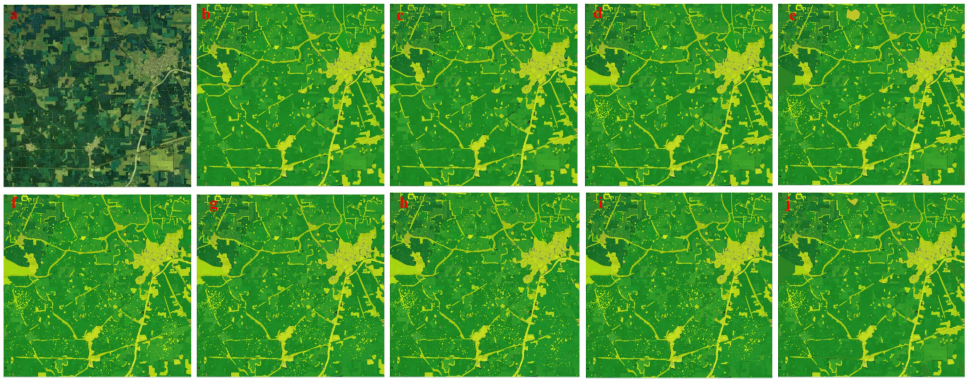

FIGURE 5.10: Segmentation result of different models (a) Natural color (b) Ground truth (green pixel= rice field,and yellow pixel= non-rice field). (c) Proposed model. (d) CNN. (e) DeepLab V3+.(f) SVM. (g) Spectral. (h) Threshold. (i) Random Forest. (j) Light-GBM.

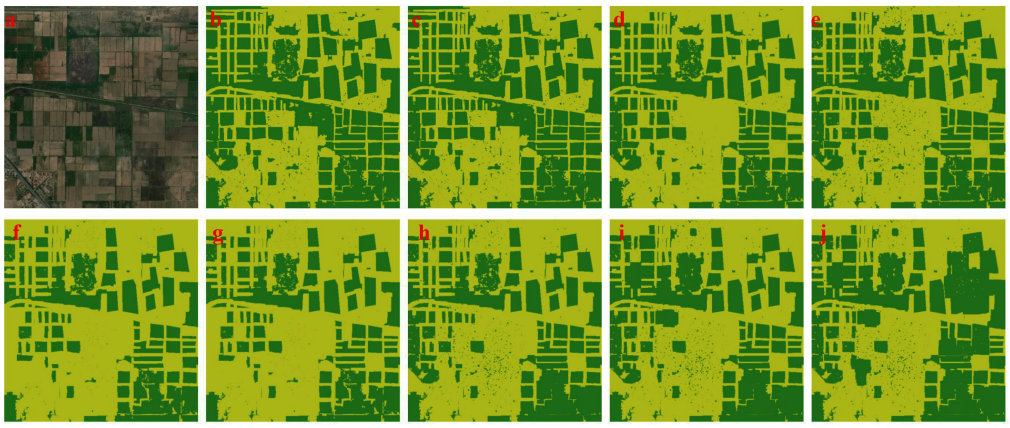

FIGURE 5.11: Segmentation results of differnt models on Westbengal datatset on 01-Aug-2018. (a) Natural color. (b) Ground truth. (c) Proposed model. (d) DeepLab V3+ (e) CNN. (f) SVM. (g) Light-GBM. (h) Random Forest. (i) Spectral. (j) Threshold.

TABLE 5.11: Comparative analysis of diffent models on west-bengal dataset; A: Modern Approaches, B: Traditional Approaches.

	Classifier Type	P	R	F1-Score	Acc	KAPPA	Training Time (s)	Testing Time (s)
A	Proposed	93.15 ± 0.009	90.12 ± 0.012	96.33 ± 0.005	94.13 ± 0.008	0.90	1023	9
	DeepLabV3+	90.77 ± 0.012	89.23 ± 0.014	92.13 ± 0.009	90.44 ± 0.010	0.87	1250	10
	CNN	90.11 ± 0.012	90.10 ± 0.012	91.22 ± 0.012	89.33 ± 0.013	0.85	1180	14
B	RF	87.65 ± 0.016	84.67 ± 0.018	88.43 ± 0.012	88.12 ± 0.014	0.84	1297	45
	Light-GBM	88.12 ± 0.021	85.43 ± 0.019	89.77 ± 0.019	89.22 ± 0.013	0.85	1329	36
	XGboost	88.16 ± 0.021	85.21 ± 0.020	89.68 ± 0.019	89.21 ± 0.013	0.85	1312	37
	SVM	87.33 ± 0.021	84.43 ± 0.025	88.33 ± 0.019	88.10 ± 0.016	0.84	789	34
	Spectral	83.34 ± 0.023	82.34 ± 0.023	84.44 ± 0.022	84.12 ± 0.022	0.80	1467	66
	Threshold	84.54 ± 0.022	81.37 ± 0.022	85.46 ± 0.021	85.92 ± 0.021	0.81	80	98

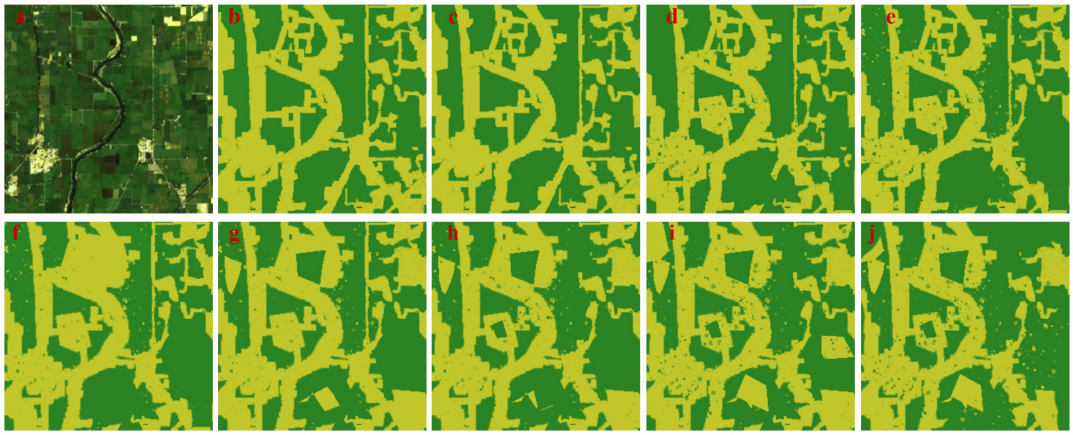

FIGURE 5.12: Segmentation results of differnt models on West-bengal datatset on 01-Aug-2018. (a) Natural color. (b) Ground truth. (c) Proposed model. (d) DeepLab V3+ (e) CNN. (f) SVM. (g) Light-GBM. (h) Random Forest. (i) Spectral. (j) Threshold.

distance metric is used to evaluate the localization ability of the rice mapping approach. Two binary images (a) True-color and (b) Ground-truth (b) were selected for the detection of result: $a = (a_1, ..., a_{lw})$ and $b = (b_1, ..., b_{lw})$. Here, a_1 and b_1 represent the binary value 0, 1 of an image in which 0 represent the rice-negative and 1 represent the rice-positive. The length and width of each pixel of an image is denoted by l *and* w. Furhtermore, the Image Euclidean Distance (IMED)Fytsilis et al., 2016 technique is utilized to check the spatial relationship between the image pixels which is mathematically calculated as:

$$d(a,b) = \frac{1}{a\pi} \sum_{i,j=1}^{lw} \exp\left\{ \frac{-|p_i(a) - p_j(b)|^2}{2} \right\} (a_i - b_i)\,(a_j - b_j) \tag{5.16}$$

The position of *ith* pixel (a) and *jth* pixel (b) is denoted by $p_i(a) = (l, w)$ and $p_j(b) = p_j(b) = (l', w')$,respectively. Moreover, the IMED between two spatial pixels is represented by $|p_i(a) - p_j(b)| = \sqrt{(l-l')^2 + (w-w')^2}$. It has been observed that the performance of the proposed model is much better than the other selected approachs. The proposed model has achieved the distance of 27.786 px in image. On the other hand, CNN with 41.51 px, SVM

TABLE 5.12: Overall accuracy on SAR data

	Models	Overall Accuracy(OA)	Kappa	IoU
Conventional	SVM	0.672 ± 0.030	0.59	0.601
	RF	0.876 ± 0.018	0.77	0.798
	Light-GBM	0.863 ± 0.018	0.79	0.804
	XGboost	0.853 ± 0.019	0.77	0.783
Modern	VGG	0.731 ± 0.028	0.63	0.682
	InceptionNet	0.821 ± 0.021	0.77	0.793
	CNN	0.883 ± 0.018	0.79	0.802
	DeepLabv3+	0.912 ± 0.013	0.83	0.882
	Proposed	0.942 ± 0.011	0.89	0.895

with 77.04 px, RF with 5.03 px, Spectral with 33.982, and Threshold with the distance value of 74.675. Moreover, Mean square error (MSE) and Mean absolute error (MAE) based error measures are calculated to justify the sensitiveness of the proposed model towards outliers. It has been observed that the proposed model has calculated the less value of MSE with the value of 0.96 ± 0.21 and MAE with the value of 0.74 ± 0.08. The calculated error values define the ability of accurate prediction of the rice field from the satellite images.

In addition, the SAR data were captured from European Space Agency (ESA) under Sentinel-1. The data is publically available with multiple resolutions. In order to check the prediction efficiency, the proposed model is evaluated and compared on time-series Synthetic Aperture Radar (SAR) data. The results of the proposed approach and other selected approaches are presented in Table 5.12. It has been observed from the calculated outcome that the proposed model has achieved a better overall accuracy value of 0.942% and Intersection of Union (IoU) 0.895% as compare to the 0ther selected model on SAR images. On the order hand, the DeppLabv3+ model also shows better performance as compared to conventional and modern approaches for the prediction of rice fields from SAR images. The DeepLabv3+, CNN, InceptionNet, XGboost, Light-GBM, RF, and SVM models registered the overall accuracy of values 0.912%, 0.883%, 0.821%, 0.853%, 0.863%, 0.876%,

TABLE 5.13: Normalized Confusion matrix on SAR data

Models	Class	Rice field	Non-rice field	OA
Proposed Model	Rice field	**93.23% (TP)**	6.33% (FN)	
	Non-Rice field	21.54% (FP)	82.56% (TN)	86.31%
DeepLabv3+	Rice field	84.78% (TP)	11.34% (FN)	
	Non-Rice field	26.98% (FP)	80.67% (TN)	81.22%
CNN	Rice field	79.23% (TP)	10.43% (FN)	
	Non-Rice field	34.54% (FP)	79.52% (TN)	77.93%
XGboost	Rice field	90.33% (TP)	16.93% (FN)	
	Non-Rice field	42.24% (FP)	77.22% (TN)	73.90%
Light-GBM	Rice field	90.76% (TP)	19.43% (FN)	
	Non-Rice field	39.54% (FP)	83.34% (TN)	74.77%
SVM	Rice field	91.53% (TP)	5.13% (FN)	
	Non-Rice field	44.14% (FP)	80.22% (TN)	77.71%
RF	Rice field	92.53% (TP)	6.13% (FN)	
	Non-Rice field	44.14% (FP)	80.22% (TN)	77.46%
Threshold	Rice field	89.19% (TP)	10.44% (FN)	
	Non-Rice field	60.12% (FP)	67.12% (TN)	68.90%
Spectral	Rice field	86.56% (TP)	2.13% (FN)	
	Non-Rice field	34.14% (FP)	65.22% (TN)	80.71%

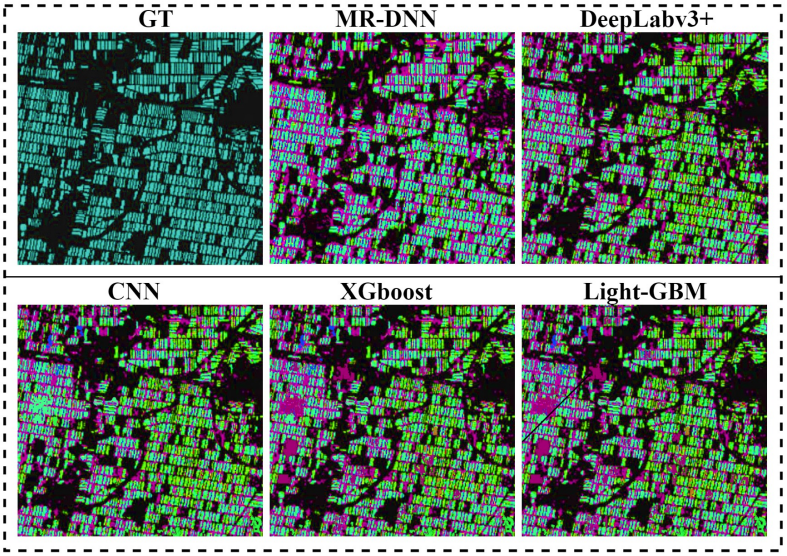

FIGURE 5.13: Segmentation results of different models on Sentinel-1 SAR dataset. (a) Ground Truth (GT). (b) MR-DNN. (c) DeepLabv3+. (d) CNN. (e) XGboost. (d) Light-GBM.

0.672%, respectively. The IoU values of SVM (0.601%), RF (0.798%), Light-GBM (0.804%), XGboost (0.783%), InceptionNet (0.793%), CNN (0.802%), and DeepLabv3+ (0.882%). Moreover, the confusion matrix is created for each selected model to check the prediction accuracy of rice field and non-rice field from SAR images. The calculated outcome is presented in Table **??** for better understanding. The classification results of each selected method are further compared with the proposed MR-DNN and illustrated in Figure 5.13. The Pink color in the image referred to the area of the rice field that is not identified by the model (FN). On the other hand, the blue color is not a rice field but identified as a rice field by the proposed model (FP). At last, the green color is a rice field and the model has correctly identified as rice field (TP) and the black is color non-rice field and the model has segmented it as a non- rice field (TN).

5.5 Conclusion

Developing a suitable technique for monitoring land from satellite imagery has become a central topic for research in the agriculture domain from the last few years. Earlier findings have reported the adequacy of satellite images to fulfill the purpose of land monitoring with some limitations such as low or medium spatial resolution, neglection of high spatial resolution, and many others. In this manner, a Multi-streaming Deep Neural Network (MR-DNN) is proposed for the collection of data and for monitoring the boundaries of rice fields from Landsat 8 satellite images. The proposed solution is having the capability for capturing the pixel-based rice field from satellite images automatically. In the proposed model, Bi-GRU is utilized to extract the temporal dependencies from satellite imagery before feeding data to the CNN model. Furthermore, the CNN model is used to capture spatial dependencies among the multiple bands. The performance analysis is done on two different real-time Landsat 8 satellite datasets. The proposed model has achieved the high prediction performance in terms of F1-score by achieving the accuracy value of 95.32% on the Punjab rice dataset and 93.12% on the West-Bengal rice dataset. Furthermore, the prediction performance of the

proposed solution is justified by comparing the calculated outcomes with selected solutions such as DeepLabV3+, CNN, SVM, RF, LGBM, XGBoost, Spectral, and Threshold. From the calculated outcomes, it has been observed that the proposed model has achieved the higher mean accuracy of 95.32% as compared to DeepLab V3+ (92.44%), CNN (91.81%), SVM (90.60%), RF (90.81%), LGBM (91.86%), XGBoost (89.68%), Spectral (89.87%), and Threshold (86.21%). In this manner, the proposed solution can help Government bodies and other decision-makers to monitor the production of other food crops such as wheat, corn, sugarcane, etc.

Chapter 6

Conclusion and Future Work

6.1 Thesis Summary

The overall goal of this thesis is to utilize advanced innovative approaches to satellite images to resolve practical remote sensing problems such as classification, object detection, and urban development monitoring. In this thesis, we have explored and developed some innovative approaches such as Computer Vision, Satellite Images, Fog computing, and Deep Learning in the field of remote sensing. Advanced classification concepts based on deep learning have been demonstrated to be effective for classifying multiples classes from satellite imagery. The use of Deep learning and satellite imagery for the prediction of the happiness index based on the development and basic fundamental rights provided by the Government to the people of Punjab is explored in this thesis. The satellite images contain a lot of information about the earth and extracting such information is a challenging task. This dissertation proposed three different solutions to extract important information from satellite images for the prediction of the Happiness index of farmers by applying a deep learning approach. Furthermore, survey data is also collected from different regions of the state of Punjab to check the satisfaction level of the people of Punjab. In order to overcome the challenges of multi-resolution satellite imagery, in chapter 5, we have utilized spatio-spectral-temporal resolution satellite imagery. The proposed model has the capability to access multispectral information from multi-resolution images. Therefore, the Landsat 8 satellite images are used in the proposed study. The

proposed solution is orthogonal to area-specific spectral indices. In this manner, the proposed approach can retrieve the paddy features directly from the input data.

Findings:

- In chapter 3, we have proposed a novel deep learning-based Multi-data Fusion Network (MDFN) to identify the water resources from Sentinel-2 images. This research aims to predict the degree of happiness index in farmers of Punjab by correlating the survey data and the satellite data. In this manner, MDFN is proposed to identify the different sources of water from Sentinel-2 satellite images. Furthermore, multi-structural feature fusion layers are utilized in the proposed solution to extract the spatial features from remote sensing images to predict the sources of water. The calculated outcomes of the proposed solution are further compared with the state-of-the-art models such as NDWI, ResNet, VGG, SegNet, DeepLabv3+, and DenseNet. According to the calculated results of the proposed methodology, it has been observed that the proposed model defines better prediction performance by registering the higher values of Precision, F1-score, Recall, and IoU with the value of 0.958%, 0.928%, 0.899%, and 0.874%, respectively. In order to check the correlation between the survey data and the satellite data for the prediction of the degree of happiness index among the farmers four different models such as K-Nearest Neighbour (KNN), Decision Tree (DT), Multi-layer perceptron (MLP), and NAÏVE BAYES are evaluated on the survey data. The calculated outcomes show that the MLP has achieved a higher accuracy value of 78.35% out of all other selected models. Furthermore, the collected survey and the evaluated results define the high correlation between the degree of happiness towards the availability of water resources in a specific location.

- By extending the complexity of multi-spectral satellite images for classification, object detection, and segmentation. Water resources identification become a hot topic in the field of remote sensing to deal with

the problem of water scarcity. In this manner, a novel Multi-layered Data Integration Technique (MDIT) is proposed to identify the sources of water from RS images. Moreover, a Deep Convolutional Restrictive Machine (DCRM) is proposed to extract the deep hierarchical features from Sentinel-2 satellite images. By the use of DCRM, meaningful patterns among the features are calculated. Moreover, the Deep Sparse Auto-encoder (DSA) and Spatial Inferred Features (SIF) modules are employed in the proposed model to enhance the inference among the spatial features and calculate the indirect relationship among the extracted features. Furthermore, the proposed methodology is compared with state-of-the-art methodologies such as ResNet, VGG, DenseNet, DeepLabv3+, SegNet, and NDWI to check the prediction efficiency of the proposed solution. It has been overserved from the calculated results that the proposed approach has outperformed by registering the precision value of (0.945%), which is higher than other selected models.

- By reviewing the literature related to Remote Sensing and satellite imagery for classification and object detection, it has been observed that there is no work has been done by applying Spatiotemporal-spectral resolution. In the above-mentioned studies, only false-color composite images are utilized to identify the water resources from Sentinel-2 images. The main goal of this study is to utilize Sapatio-temporal-spectral images to predict the rice field by applying deep learning approaches. A novel deep learning-based Multi-Resolution Deep Neural Network (MR-DNN) approach is proposed to predict the rice field by performing the multi-streaming classification from Landsat 8 images. The proposed solution can automatically capture the pixel-based rice field from satellite images. To check the prediction efficiency of the proposed solution, the proposed model is evaluated on two different real-time datasets. It has been observed from the results that the proposed model has achieved the highest F1-score accuracy value of 95.32% on the Punjab rice dataset and 93.12% on the West-Bengal

rice dataset. Furthermore, a comparative analysis is done with state-of-the-art models such as DeepLabV3+, CNN, SVM, RF, LGBM, XGBoost, Spectral, and Threshold to justify the prediction performance of the proposed solution. From the calculated outcomes, it has been observed that the proposed model has achieved a higher mean accuracy of 95.32% as compared to DeepLab V3+ (92.44%), CNN (91.81%), SVM (90.60%), RF (90.81%), LGBM (91.86%), XGBoost (89.68%), Spectral (89.87%), and Threshold (86.21%). In this manner, the proposed solution can help Government bodies and other decision-makers to monitor the production of other food crops such as wheat, corn, sugarcane, etc.

6.2 Future work

Due to advancements in hardware as well as algorithms, remote sensing technology received attention in the last few years. The proposed models have achieved satisfactory results but still, some improvements could be made.

- **Hyperspectral and Multispectral Satellite Images:** Hyperspectral images contain very rich spatial and spectral information and compare to multispectral images because in hyperspectral images there are more than 200 bans and multispectral images are having more than 3 bands. In the future, we can utilize hyperspectral images instead of multispectral for the detection of development changes by applying a large deep learning-based multi-resolution approach.

- **Computational Complexity:** However, because the computing difficulty of processing hyperspectral data is so high, it would be extremely beneficial if the spectral dimensionality could be decreased while maintaining the same knowledge from the hyperspectral bands.

- **Data and Pre-processing:** In the domain of remote sensing, there is a lack of hyper-spectral, multi-spectral, and SAR datasets. In future

work, we will create datasets that will help researchers to extract important information from satellite images. Moreover, climate and weather changes, such as snow and cloud, have a significant influence on RS images. Further study in my future work will be aimed at removing the influence of weather variations in the classification of RS images.

In the field of remote sensing, manual data collection and pre-processing are considered an imperative aspects to justify the findings. In this manner, a survey has been conducted based on different parameters such as Good Governance, cultural preservations, citizen safety, and security. Good Governance has been opted to evaluate the happiness index of the individuals who belong to a specific area by predicting the availability of water. However, different parameters such as cultural preservation, citizen safety, and security can also be utilized to evaluate the level of happiness index. Therefore, the above-discussed parameters such as cultural preservation, citizen safety, and security will be included in the proposed study to enhance productivity and stability concerning the prediction of the happiness index.

Publications

1. Yasir Afaq & Ankush Manocha, (2021). Analysis on change detection techniques for remote sensing applications: A review. "Ecological Informatics", 101310. (Published: SCI/SCIE Indexed with IF 3.142).

2. Yasir Afaq & Ankush Manocha, 2021. "Happiness Index Determination by Analyzing Satellite Images for Urbanization", "Applied Artificial Intelligence " (Published: SCI/SCIE Indexed with Impact Factor 1.580).

3. Yasir Afaq & Ankush Manocha, (2021). Fog-inspired water resource analysis in urban areas from satellite images. "Ecological Informatics", 101385. (Published: SCI/SCIE with IF 3.142).

4. Yasir Afaq & Ankush Manocha, 2021. "Multi-resolution-based Deep Learning approach for Rice Field Monitoring", "Canadian Journal Of Remote Sensing" (Published: SCI/SCIE with IF 2.763).

5. Yasir Afaq & Ankush Manocha. "Landsat Multispectral Images-based Field Monitoring Using Deep Learning", "The Visual Computer" (Under Review: SCI/SCIE with IF 2.601).

6. Ankush Manocha, Yasir Afaq & Munish Bhatia. "Student Irregularity Prediction for Panic Disorder using IoT and Quantum Probability", "Journal of Experimental & Theoretical Artificial Intelligence" (Revision Submitted: SCI/SCIE with 2.340).

7. Yasir Afaq & Ankush Manocha. "Multi-class satellite imagery classification using Deep Learning Approaches" 3^{rd} "International Conference on innovations in Communication computing and Sciences, 2021". (Scopus Indexed).

8. Yasir Afaq & Ankush Manocha. "Natural Disaster Prediction from Sentinel-2 Images using Convolutional Neural Network", i^{st} "International Conference On Futuristic Sustainable Energy & Technology-2021". (Scopus Indexed).

Bibliography

Abdi, Hervé and Lynne J Williams (2010). "Principal component analysis". In: *Wiley interdisciplinary reviews: computational statistics* 2.4, pp. 433–459.

Abuelgasim, Abdelgadir A et al. (1999). "Change detection using adaptive fuzzy neural networks: Environmental damage assessment after the Gulf War". In: *Remote Sensing of Environment* 70.2, pp. 208–223.

Achanta, Radhakrishna et al. (2012). "SLIC superpixels compared to state-of-the-art superpixel methods". In: *IEEE transactions on pattern analysis and machine intelligence* 34.11, pp. 2274–2282.

Afaq, Yasir and Ankush Manocha (2021a). "Analysis on change detection techniques for remote sensing applications: A review". In: *Ecological Informatics*, p. 101310.

— (2021b). "Fog-inspired water resource analysis in urban areas from satellite images". In: *Ecological Informatics*, p. 101385.

Ajadi, Olaniyi A, Franz J Meyer, and Peter W Webley (2016). "Change detection in synthetic aperture radar images using a multiscale-driven approach". In: *Remote Sensing* 8.6, p. 482.

Albert, Adrian, Jasleen Kaur, and Marta C Gonzalez (2017). "Using convolutional networks and satellite imagery to identify patterns in urban environments at a large scale". In: *Proceedings of the 23rd ACM SIGKDD international conference on knowledge discovery and data mining*, pp. 1357–1366.

Alexandratos, Nikos (2009). "World food and agriculture to 2030/50". In: *Highlights and views from MID-2009: Paper for the Expert Meeting on "How to Feed the World in*. Vol. 2050.

Amici, Valerio et al. (2017). "A multi-temporal approach in MaxEnt modelling: A new frontier for land use/land cover change detection". In: *Ecological informatics* 40, pp. 40–49.

Anderson, James R et al. (1977). "Land use and land cover changes. A framework for monitoring". In: *Journal of Research by the Geological Survey* 5, pp. 143–153.

Arabi, Mohammed El Amin, Moussa Sofiane Karoui, and Khelifa Djerriri (2018). "Optical remote sensing change detection through deep siamese network". In: *IGARSS 2018-2018 IEEE International Geoscience and Remote Sensing Symposium*. IEEE, pp. 5041–5044.

Asokan, Anju and J Anitha (2019). "Change detection techniques for remote sensing applications: a survey". In: *Earth Science Informatics* 12.2, pp. 143–160.

— (2020). "Adaptive Cuckoo Search based optimal bilateral filtering for denoising of satellite images". In: *ISA transactions* 100, pp. 308–321.

Badrinarayanan, Vijay, Alex Kendall, and Roberto Cipolla (2017). "Segnet: A deep convolutional encoder-decoder architecture for image segmentation". In: *IEEE transactions on pattern analysis and machine intelligence* 39.12, pp. 2481–2495.

Ball, John E, Derek T Anderson, and Chee Seng Chan Sr (2017). "Comprehensive survey of deep learning in remote sensing: theories, tools, and challenges for the community". In: *Journal of Applied Remote Sensing* 11.4, p. 042609.

Barber, Jarred (2015). "A generalized likelihood ratio test for coherent change detection in polarimetric SAR". In: *IEEE Geoscience and Remote Sensing Letters* 12.9, pp. 1873–1877.

Belgiu, Mariana and Lucian Drăguţ (2016a). "Random forest in remote sensing: A review of applications and future directions". In: *ISPRS journal of photogrammetry and remote sensing* 114, pp. 24–31.

— (2016b). "Random forest in remote sensing: A review of applications and future directions". In: *ISPRS journal of photogrammetry and remote sensing* 114, pp. 24–31.

Benedetti, Alessia, Matto Picchiani, and Fabio Del Frate (2018). "Sentinel-1 and sentinel-2 data fusion for urban change detection". In: *IGARSS 2018-2018 IEEE International Geoscience and Remote Sensing Symposium*. IEEE, pp. 1962–1965.

Bengio, Yoshua, Aaron Courville, and Pascal Vincent (2013). "Representation learning: A review and new perspectives". In: *IEEE transactions on pattern analysis and machine intelligence* 35.8, pp. 1798–1828.

Bengio, Yoshua, Yann LeCun, et al. (2007). "Scaling learning algorithms towards AI". In: *Large-scale kernel machines* 34.5, pp. 1–41.

Bruzzone, Lorenzo and Roberto Cossu (2002). "RBF neural network approach for detecting land-cover transitions". In: *Image and Signal Processing for Remote Sensing VII*. Vol. 4541. International Society for Optics and Photonics, pp. 223–231.

Bu, Shuhui et al. (2016). "Scene parsing using inference embedded deep networks". In: *Pattern Recognition* 59, pp. 188–198.

Cai, Liping et al. (2018). "A multi-feature fusion-based change detection method for remote sensing images". In: *Journal of the Indian Society of Remote Sensing* 46.12, pp. 2015–2022.

Cao, Cong, Suzana Dragićević, and Songnian Li (2019). "Land-use change detection with convolutional neural network methods". In: *Environments* 6.2, p. 25.

Cao, Guo, Licun Zhou, and Yupeng Li (2016). "A new change-detection method in high-resolution remote sensing images based on a conditional random field model". In: *International Journal of Remote Sensing* 37.5, pp. 1173–1189.

Chatfield, Ken et al. (2015). "On-the-fly learning for visual search of large-scale image and video datasets". In: *International journal of multimedia information retrieval* 4.2, pp. 75–93.

Chen, Hongruixuan et al. (2019). "Change detection in multisource VHR images via deep siamese convolutional multiple-layers recurrent neural network". In: *IEEE Transactions on Geoscience and Remote Sensing* 58.4, pp. 2848–2864.

Chen, Liang-Chieh et al. (2018a). "Encoder-decoder with atrous separable convolution for semantic image segmentation". In: *Proceedings of the European conference on computer vision (ECCV)*, pp. 801–818.

Chen, Tianqi and Carlos Guestrin (2016). "Xgboost: A scalable tree boosting system". In: *Proceedings of the 22nd acm sigkdd international conference on knowledge discovery and data mining*, pp. 785–794.

Chen, Yang et al. (2018b). "Extraction of urban water bodies from high-resolution remote-sensing imagery using deep learning". In: *Water* 10.5, p. 585.

Chu, Yan, Guo Cao, and Hassan Hayat (2016). "Change detection of remote sensing image based on deep neural networks". In: *Proceedings of the 2016 2nd International Conference on Artificial Intelligence and Industrial Engineering (AIIE 2016)*. Vol. 133. 1, pp. 262–267.

De, Shaunak et al. (2017). "A novel change detection framework based on deep learning for the analysis of multi-temporal polarimetric SAR images". In: *2017 IEEE International Geoscience and Remote Sensing Symposium (IGARSS)*. IEEE, pp. 5193–5196.

Devapal, Devi, SS Kumar, and Christy Jojy (2017). "A novel approach of despeckling SAR images using nonlocal means filtering". In: *Journal of the Indian Society of Remote Sensing* 45.3, pp. 443–450.

Dewan, Nilansh, Vaibhav Kashyap, and Anup Singh Kushwaha (2019). "A review of pulse coupled neural network". In: *Iioab J* 10, pp. 61–65.

Ding, Jun et al. (2016). "Convolutional neural network with data augmentation for SAR target recognition". In: *IEEE Geoscience and remote sensing letters* 13.3, pp. 364–368.

Dixit, Siddharth, Meghna Chaudhary, and Niteesh Sahni (2020). "Network Learning Approaches to study World Happiness". In: *arXiv preprint arXiv:2007.09181*.

Du, Ningrui, Henk Ottens, and Richard Sliuzas (2010). "Spatial impact of urban expansion on surface water bodies—A case study of Wuhan, China". In: *Landscape and Urban Planning* 94.3-4, pp. 175–185.

Du, Yun et al. (2016). "Water bodies' mapping from Sentinel-2 imagery with modified normalized difference water index at 10-m spatial resolution produced by sharpening the SWIR band". In: *Remote Sensing* 8.4, p. 354.

El Amin, Arabi Mohammed, Qingjie Liu, and Yunhong Wang (2016). "Convolutional neural network features based change detection in satellite images". In: *First International Workshop on Pattern Recognition*. Vol. 10011. International Society for Optics and Photonics, 100110W.

Famiglietti, James S and Matthew Rodell (2013). "Water in the balance". In: *Science* 340.6138, pp. 1300–1301.

Fan, Jianchao, Kai Lin, and Min Han (2019). "A novel joint change detection approach based on weight-clustering sparse autoencoders". In: *IEEE Journal of Selected Topics in Applied Earth Observations and Remote Sensing* 12.2, pp. 685–699.

Fang, Bo et al. (2020). "GAN-based siamese framework for landslide inventory mapping using bi-temporal optical remote sensing images". In: *IEEE Geoscience and Remote Sensing Letters* 18.3, pp. 391–395.

Fang, Weizhen et al. (2019). "Recognizing global reservoirs from Landsat 8 images: A deep learning approach". In: *IEEE journal of selected topics in applied earth observations and remote sensing* 12.9, pp. 3168–3177.

Feng, Lian et al. (2015). "Long-term distribution patterns of chlorophyll-a concentration in China's largest freshwater lake: MERIS full-resolution observations with a practical approach". In: *remote sensing* 7.1, pp. 275–299.

Feng, Wenqing et al. (2018). "A novel change detection approach for multi-temporal high-resolution remote sensing images based on rotation forest and coarse-to-fine uncertainty analyses". In: *Remote Sensing* 10.7, p. 1015.

Feng, Wensen and Yunjin Chen (2017). "Speckle reduction with trained nonlinear diffusion filtering". In: *Journal of Mathematical Imaging and Vision* 58.1, pp. 162–178.

Ferraris, Vinicius et al. (2017). "Detecting changes between optical images of different spatial and spectral resolutions: a fusion-based approach". In: *IEEE Transactions on Geoscience and Remote Sensing* 56.3, pp. 1566–1578.

Feyisa, Gudina L et al. (2014). "Automated Water Extraction Index: A new technique for surface water mapping using Landsat imagery". In: *Remote Sensing of Environment* 140, pp. 23–35.

Fisher, Adrian, Neil Flood, and Tim Danaher (2016). "Comparing Landsat water index methods for automated water classification in eastern Australia". In: *Remote Sensing of Environment* 175, pp. 167–182.

Franklin, Steven E and Philip T Giles (1995). "Radiometric processing of aerial and satellite remote-sensing imagery". In: *Computers & Geosciences* 21.3, pp. 413–423.

Fytsilis, Anastasios L et al. (2016). "A methodology for near real-time change detection between Unmanned Aerial Vehicle and wide area satellite images". In: *ISPRS Journal of Photogrammetry and Remote Sensing* 119, pp. 165–186.

Gandhi, G Meera et al. (2015). "Ndvi: Vegetation change detection using remote sensing and gis–A case study of Vellore District". In: *Procedia computer science* 57, pp. 1199–1210.

Garcia-Garcia, Alberto et al. (2017). "A review on deep learning techniques applied to semantic segmentation". In: *arXiv preprint arXiv:1704.06857*.

Geng, Zhiqiang et al. (2020). "An improved intelligent early warning method based on MWSPCA and its application in complex chemical processes". In: *The Canadian Journal of Chemical Engineering* 98.6, pp. 1307–1318.

Golilarz, Noorbakhsh Amiri, Hui Gao, and Hasan Demirel (2019). "Satellite image de-noising with harris hawks meta heuristic optimization algorithm and improved adaptive generalized gaussian distribution threshold function". In: *Ieee Access* 7, pp. 57459–57468.

Gong, Maoguo, Hailun Yang, and Puzhao Zhang (2017). "Feature learning and change feature classification based on deep learning for ternary change detection in SAR images". In: *ISPRS Journal of Photogrammetry and Remote Sensing* 129, pp. 212–225.

Gong, Maoguo et al. (2015). "Change detection in synthetic aperture radar images based on deep neural networks". In: *IEEE transactions on neural networks and learning systems* 27.1, pp. 125–138.

Gu, Wei, Zhihan Lv, and Ming Hao (2017). "Change detection method for remote sensing images based on an improved Markov random field". In: *Multimedia Tools and Applications* 76.17, pp. 17719–17734.

Gualtieri, J Anthony and Robert F Cromp (1999). "Support vector machines for hyperspectral remote sensing classification". In: *27th AIPR Workshop: Advances in Computer-Assisted Recognition*. Vol. 3584. International Society for Optics and Photonics, pp. 221–232.

Guo, Enqiang et al. (2018). "Learning to measure change: Fully convolutional siamese metric networks for scene change detection". In: *arXiv preprint arXiv:1810.09111*.

Guo, Yanming et al. (2016). "Deep learning for visual understanding: A review". In: *Neurocomputing* 187, pp. 27–48.

Hagag, Ahmed, Xiaopeng Fan, and Fathi E Abd El-Samie (2017). "HyperCast: hyperspectral satellite image broadcasting with band ordering optimization". In: *Journal of Visual Communication and Image Representation* 42, pp. 14–27.

Han, Min and Yang Zhou (2017). "An adaptive unimodal subclass decomposition (AUSD) learning system for land use and land cover classification using high-resolution remote sensing". In: *GIScience & Remote Sensing* 54.1, pp. 20–37.

Han, Pengcheng et al. (2019). "Aerial image change detection using dual regions of interest networks". In: *Neurocomputing* 349, pp. 190–201.

Han, Yongming et al. (2020). "An asymmetric knowledge representation learning in manifold space". In: *Information Sciences* 531, pp. 1–12.

Han, Zhizhong et al. (2016). "Unsupervised 3D local feature learning by circle convolutional restricted Boltzmann machine". In: *IEEE Transactions on Image Processing* 25.11, pp. 5331–5344.

He, Pengfei et al. (2014). "A novel dynamic threshold method for unsupervised change detection from remotely sensed images". In: *Remote sensing letters* 5.4, pp. 396–403.

He, Pengfei et al. (2015). "Advanced Markov random field model based on local uncertainty for unsupervised change detection". In: *Remote Sensing Letters* 6.9, pp. 667–676.

Heryadi, Yaya et al. (2020). "The Effect of Resnet Model as Feature Extractor Network to Performance of DeepLabV3 Model for Semantic Satellite

Image Segmentation". In: *2020 IEEE Asia-Pacific Conference on Geoscience, Electronics and Remote Sensing Technology (AGERS)*. IEEE, pp. 74–77.

Heumann, Benjamin W (2011). "An object-based classification of mangroves using a hybrid decision tree—Support vector machine approach". In: *Remote Sensing* 3.11, pp. 2440–2460.

Hinton, Geoffrey E (2002). "Training products of experts by minimizing contrastive divergence". In: *Neural computation* 14.8, pp. 1771–1800.

Hölbling, Daniel, Barbara Friedl, and Clemens Eisank (2015). "An object-based approach for semi-automated landslide change detection and attribution of changes to landslide classes in northern Taiwan". In: *Earth Science Informatics* 8.2, pp. 327–335.

Hu, Fan et al. (2015). "Transferring deep convolutional neural networks for the scene classification of high-resolution remote sensing imagery". In: *Remote Sensing* 7.11, pp. 14680–14707.

Huang, Chang et al. (2015). "An evaluation of Suomi NPP-VIIRS data for surface water detection". In: *Remote Sensing Letters* 6.2, pp. 155–164.

Huang, Faming et al. (2018a). "Object-oriented change detection and damage assessment using high-resolution remote sensing images, Tangjiao Landslide, Three Gorges Reservoir, China". In: *Environmental earth sciences* 77.5, pp. 1–19.

Huang, Fenghua, Ying Yu, and Tinghao Feng (2019). "Automatic building change image quality assessment in high resolution remote sensing based on deep learning". In: *Journal of Visual Communication and Image Representation* 63, p. 102585.

Huang, Gao et al. (2017). "Densely connected convolutional networks". In: *Proceedings of the IEEE conference on computer vision and pattern recognition*, pp. 4700–4708.

Huang, Jin, Shiyou Wu, and Suo Deng (2016). "Relative income, relative assets, and happiness in urban China". In: *Social Indicators Research* 126.3, pp. 971–985.

Huang, Yongzhen et al. (2013). "Feature coding in image classification: A comprehensive study". In: *IEEE transactions on pattern analysis and machine intelligence* 36.3, pp. 493–506.

Huang, Zhenghua et al. (2018b). "Framelet regularization for uneven intensity correction of color images with illumination and reflectance estimation". In: *Neurocomputing* 314, pp. 154–168.

Huete, Alfredo et al. (2002). "Overview of the radiometric and biophysical performance of the MODIS vegetation indices". In: *Remote sensing of environment* 83.1-2, pp. 195–213.

Huete, Alfredo R (1988). "A soil-adjusted vegetation index (SAVI)". In: *Remote sensing of environment* 25.3, pp. 295–309.

Iino, Shota et al. (2018). "CNN-based generation of high-accuracy urban distribution maps utilising SAR satellite imagery for short-term change monitoring". In: *International journal of image and data fusion* 9.4, pp. 302–318.

Ingram, K, E Knapp, and JW Robinson (1981). "Change detection technique development for improved urbanized area delineation". In: *NASA, Comput. Sci. Corp., Springfield, MD, CSC/TM-81/6087*.

Ioannidou, Anastasia et al. (2017). "Deep learning advances in computer vision with 3d data: A survey". In: *ACM Computing Surveys (CSUR)* 50.2, pp. 1–38.

Isikdogan, Furkan, Alan C Bovik, and Paola Passalacqua (2017). "Surface water mapping by deep learning". In: *IEEE journal of selected topics in applied earth observations and remote sensing* 10.11, pp. 4909–4918.

Jannani, Ayoub, Nawal Sael, and Faouzia Benabbou (2021). "Predicting Quality of Life using Machine Learning: case of World Happiness Index". In: *2021 4th International Symposium on Advanced Electrical and Communication Technologies (ISAECT)*. IEEE, pp. 1–6.

Jesús Rubio, José de (2018). "Discrete time control based in neural networks for pendulums". In: *Applied Soft Computing* 68, pp. 821–832.

Ji, Shunping, Shiqing Wei, and Meng Lu (2019). "A scale robust convolutional neural network for automatic building extraction from aerial and satellite imagery". In: *International journal of remote sensing* 40.9, pp. 3308–3322.

Jiang, Huiwei et al. (2020). "Pga-siamnet: Pyramid feature-based attention-guided siamese network for remote sensing orthoimagery building change detection". In: *Remote Sensing* 12.3, p. 484.

Jianya, Gong et al. (2008). "A review of multi-temporal remote sensing data change detection algorithms". In: *The International Archives of the Photogrammetry, Remote Sensing and Spatial Information Sciences* 37.B7, pp. 757–762.

Jin, Baoxuan et al. (2019). "Object-oriented method combined with deep convolutional neural networks for land-use-type classification of remote sensing images". In: *Journal of the Indian Society of Remote Sensing* 47.6, pp. 951–965.

Jing, Ran, Zhaoning Gong, and Hongliang Guan (2020). "Land Cover Change Detection With VHR Satellite Imagery Based on Multi-Scale SLIC-CNN and SCAE Features". In: *IEEE Access* 8, pp. 228070–228087.

Johnson, Brian A et al. (2017). "Employing crowdsourced geographic data and multi-temporal/multi-sensor satellite imagery to monitor land cover change: A case study in an urbanizing region of the Philippines". In: *Computers, Environment and Urban Systems* 64, pp. 184–193.

Kalinicheva, Ekaterina et al. (2020). "Unsupervised change detection analysis in satellite image time series using deep learning combined with graph-based approaches". In: *IEEE Journal of Selected Topics in Applied Earth Observations and Remote Sensing* 13, pp. 1450–1466.

Kang, Ling et al. (2016). "Extraction and preference ordering of multireservoir water supply rules in dry years". In: *Water* 8.1, p. 28.

Karim, Zainoolabadien and Terence van Zyl (2020). "Deep Learning and Transfer Learning applied to Sentinel-1 DInSAR and Sentinel-2 optical satellite imagery for change detection". In: *2020 International SAUPEC/RobMech/PRASA Conference*. IEEE, pp. 1–7.

Katz, David (2016). "Undermining demand management with supply management: Moral hazard in Israeli water policies". In: *Water* 8.4, p. 159.

Kaur, Beant and Anil Garg (2011). "Mathematical morphological edge detection for remote sensing images". In: *2011 3rd International Conference on Electronics Computer Technology*. Vol. 5. IEEE, pp. 324–327.

Kavzoglu, Taskin and Ismail Colkesen (2013). "An assessment of the effectiveness of a rotation forest ensemble for land-use and land-cover mapping". In: *International journal of remote sensing* 34.12, pp. 4224–4241.

Ke, Guolin et al. (2017). "Lightgbm: A highly efficient gradient boosting decision tree". In: *Advances in neural information processing systems* 30, pp. 3146–3154.

Ke, Ling et al. (2018). "Adaptive change detection with significance test". In: *IEEE Access* 6, pp. 27442–27450.

Kerner, Hannah Rae et al. (2019). "Toward generalized change detection on planetary surfaces with convolutional autoencoders and transfer learning". In: *IEEE Journal of Selected Topics in Applied Earth Observations and Remote Sensing* 12.10, pp. 3900–3918.

Kiratiratanapruk, Kantip et al. (2020). "Development of paddy rice seed classification process using machine learning techniques for automatic grading machine". In: *Journal of Sensors* 2020.

Kleynhans, Waldo, Brian P Salmon, and Jan C Olivier (2015). "Detecting settlement expansion in South Africa using a hyper-temporal SAR change detection approach". In: *International Journal of Applied Earth Observation and Geoinformation* 42, pp. 142–149.

Kontgis, Caitlin, Annemarie Schneider, and Mutlu Ozdogan (2015). "Mapping rice paddy extent and intensification in the Vietnamese Mekong River Delta with dense time stacks of Landsat data". In: *Remote Sensing of Environment* 169, pp. 255–269.

Krizhevsky, Alex, Ilya Sutskever, and Geoffrey E Hinton (2017). "ImageNet classification with deep convolutional neural networks". In: *Communications of the ACM* 60.6, pp. 84–90.

Kumar, Gaurav and Kiran Kumari Singh (2020). "Mapping and monitoring the selected wetlands of Punjab, India, using geospatial techniques". In: *Journal of the Indian Society of Remote Sensing* 48.4, pp. 615–625.

Kussul, Nataliia et al. (2017). "Deep learning classification of land cover and crop types using remote sensing data". In: *IEEE Geoscience and Remote Sensing Letters* 14.5, pp. 778–782.

Ladhar, Satnam Singh (2002). "Status of ecological health of wetlands in Punjab, India". In: *Aquatic Ecosystem Health & Management* 5.4, pp. 457–465.

Lan, Rushi et al. (2019). "Hyperspectral image classification using k-sparse denoising autoencoder and spectral–restricted spatial characteristics". In: *Applied Soft Computing* 74, pp. 693–708.

LeCun, Yann, Yoshua Bengio, and Geoffrey Hinton (2015). "Deep learning". In: *nature* 521.7553, pp. 436–444.

Li, Hao et al. (2016). "A multiobjective fuzzy clustering method for change detection in SAR images". In: *Applied Soft Computing* 46, pp. 767–777.

Li, Linyi et al. (2015). "Super-resolution mapping of wetland inundation from remote sensing imagery based on integration of back-propagation neural network and genetic algorithm". In: *Remote Sensing of Environment* 164, pp. 142–154.

Li, Tong, Junping Zhang, and Ye Zhang (2014). "Classification of hyperspectral image based on deep belief networks". In: *2014 IEEE international conference on image processing (ICIP)*. IEEE, pp. 5132–5136.

Li, Xia and AGO Yeh (1998). "Principal component analysis of stacked multitemporal images for the monitoring of rapid urban expansion in the Pearl River Delta". In: *International Journal of Remote Sensing* 19.8, pp. 1501–1518.

Li, Xia et al. (2010). "Parallel cellular automata for large-scale urban simulation using load-balancing techniques". In: *International Journal of Geographical Information Science* 24.6, pp. 803–820.

Li, Xiaodong et al. (2014). "A spatial–temporal Hopfield neural network approach for super-resolution land cover mapping with multi-temporal different resolution remotely sensed images". In: *ISPRS journal of photogrammetry and remote sensing* 93, pp. 76–87.

Li, Yang, Jin Chen, and Yuhan Rao (2018). "A practical sampling method for assessing accuracy of detected land cover/land use change: Theoretical analysis and simulation experiments". In: *ISPRS Journal of Photogrammetry and Remote Sensing* 144, pp. 379–389.

Liang, Shunlin (2005). *Quantitative remote sensing of land surfaces*. Vol. 30. John Wiley & Sons.

Liu, Ganchao et al. (2019a). "Stacked Fisher autoencoder for SAR change detection". In: *Pattern Recognition* 96, p. 106971.

Liu, Guang et al. (2017a). "Multisource remote sensing imagery fusion scheme based on bidimensional empirical mode decomposition (BEMD) and its application to the extraction of bamboo forest". In: *Remote Sensing* 9.1, p. 19.

Liu, Jia et al. (2016a). "A deep convolutional coupling network for change detection based on heterogeneous optical and radar images". In: *IEEE transactions on neural networks and learning systems* 29.3, pp. 545–559.

— (2016b). "A deep convolutional coupling network for change detection based on heterogeneous optical and radar images". In: *IEEE transactions on neural networks and learning systems* 29.3, pp. 545–559.

Liu, Jia et al. (2016c). "Difference representation learning using stacked restricted Boltzmann machines for change detection in SAR images". In: *Soft Computing* 20.12, pp. 4645–4657.

Liu, Qingshan et al. (2017b). "Learning multiscale deep features for high-resolution satellite image scene classification". In: *IEEE Transactions on Geoscience and Remote Sensing* 56.1, pp. 117–126.

Liu, Ruochen et al. (2019b). "Remote sensing image change detection based on information transmission and attention mechanism". In: *IEEE Access* 7, pp. 156349–156359.

Liu, Sicong et al. (2015). "Sequential spectral change vector analysis for iteratively discovering and detecting multiple changes in hyperspectral images". In: *IEEE transactions on geoscience and remote sensing* 53.8, pp. 4363–4378.

Liu, Yan et al. (2018). "Efficient patch-wise semantic segmentation for large-scale remote sensing images". In: *Sensors* 18.10, p. 3232.

Liu, Zhunga et al. (2017c). "Change detection in heterogenous remote sensing images via homogeneous pixel transformation". In: *IEEE Transactions on Image Processing* 27.4, pp. 1822–1834.

Lu, Yan (2020). "Deep Learning for Remote Sensing Image Processing". PhD thesis. Old Dominion University.

Luo, Hui et al. (2018). "Urban change detection based on Dempster–Shafer theory for multitemporal very high-resolution imagery". In: *Remote Sensing* 10.7, p. 980.

Luo, Xiaoqing and Zhancheng Zhang (2016). "WU XA novelalgorithm ofremotesensingima invariantShearlet transformandregionalselection". In: *AEU-InternationalJournalofElectro* 70.2, pp. 186–197.

Luppino, Luigi T et al. (2019). "Unsupervised image regression for heterogeneous change detection". In: *arXiv preprint arXiv:1909.05948*.

Lv, Pengyuan et al. (2016). "Change detection based on a multifeature probabilistic ensemble conditional random field model for high spatial resolution remote sensing imagery". In: *IEEE Geoscience and Remote Sensing Letters* 13.12, pp. 1965–1969.

Lv, Zhibin et al. (2020). "Escherichia coli DNA N-4-methycytosine site prediction accuracy improved by light gradient boosting machine feature selection technology". In: *Ieee Access* 8, pp. 14851–14859.

Lyu, Haobo, Hui Lu, and Lichao Mou (2016). "Learning a transferable change rule from a recurrent neural network for land cover change detection". In: *Remote Sensing* 8.6, p. 506.

Lyu, Haobo et al. (2018). "Long-term annual mapping of four cities on different continents by applying a deep information learning method to landsat data". In: *Remote Sensing* 10.3, p. 471.

Ma, Caihong et al. (2017). "A content-based remote sensing image change information retrieval model". In: *ISPRS International Journal of Geo-Information* 6.10, p. 310.

Ma, Lei et al. (2019a). "Deep learning in remote sensing applications: A meta-analysis and review". In: *ISPRS journal of photogrammetry and remote sensing* 152, pp. 166–177.

Ma, Wenping et al. (2019b). "Change detection in remote sensing images based on image mapping and a deep capsule network". In: *Remote Sensing* 11.6, p. 626.

Manakos, Ioannis and Samantha Lavender (2014). "Remote Sensing in Support of the Geo-information in Europe". In: *Land Use and Land Cover Mapping in Europe*. Springer, pp. 3–10.

Mansaray, Lamin R et al. (2019a). "Optimising rice mapping in cloud-prone environments by combining quad-source optical with Sentinel-1A microwave satellite imagery". In: *GIScience & Remote Sensing* 56.8, pp. 1333–1354.

— (2019b). "Optimising rice mapping in cloud-prone environments by combining quad-source optical with Sentinel-1A microwave satellite imagery". In: *GIScience & Remote Sensing* 56.8, pp. 1333–1354.

Marinelli, Daniele, Francesca Bovolo, and Lorenzo Bruzzone (2017). "A novel method for unsupervised multiple Change detection in hyperspectral images based on binary spectral change vectors". In: *2017 9th International Workshop on the Analysis of Multitemporal Remote Sensing Images (MultiTemp)*. IEEE, pp. 1–4.

Massarelli, Carmine (2018). "Fast detection of significantly transformed areas due to illegal waste burial with a procedure applicable to landsat images". In: *International journal of remote sensing* 39.3, pp. 754–769.

Masse, Antoine et al. (2018). "A New Optimized Denoising Method applied to the Spot World Heritage Initiative and its Spot 5 Supermode images". In: *IGARSS 2018-2018 IEEE International Geoscience and Remote Sensing Symposium*. IEEE, pp. 4089–4092.

Maulik, Ujjwal and Debasis Chakraborty (2017). "Remote Sensing Image Classification: A survey of support-vector-machine-based advanced techniques". In: *IEEE Geoscience and Remote Sensing Magazine* 5.1, pp. 33–52.

McFeeters, Stuart K (1996). "The use of the Normalized Difference Water Index (NDWI) in the delineation of open water features". In: *International journal of remote sensing* 17.7, pp. 1425–1432.

Meng, Lingkui et al. (2019). "An automatic extraction method for lakes and reservoirs using satellite images". In: *IEEE Access* 7, pp. 62443–62456.

Mittal, Mamta et al. (2019). "Deep learning based enhanced tumor segmentation approach for MR brain images". In: *Applied Soft Computing* 78, pp. 346–354.

Mohamed, Nafisa, Babikir Mobarak, et al. (2016). "Change detection techniques using optical remote sensing: a survey". In: *American Scientific*

Research Journal for Engineering, Technology, and Sciences (ASRJETS) 17.1, pp. 42–51.

Mountrakis, Giorgos, Jungho Im, and Caesar Ogole (2011). "Support vector machines in remote sensing: A review". In: *ISPRS Journal of Photogrammetry and Remote Sensing* 66.3, pp. 247–259.

Nagaraju, A, R Mohandas, et al. (2021). "Multifactor Analysis to Predict Best Crop using Xg-Boost Algorithm". In: *2021 5th International Conference on Trends in Electronics and Informatics (ICOEI)*. IEEE, pp. 155–163.

Nelson, Ross F (1983). "Detecting forest canopy change due to insect activity using Landsat MSS". In: *Photogrammetric Engineering and Remote Sensing* 49.9, pp. 1303–1314.

Nemoto, Keisuke et al. (2017). "Building change detection via a combination of CNNs using only RGB aerial imageries". In: *Remote Sensing Technologies and Applications in Urban Environments II*. Vol. 10431. International Society for Optics and Photonics, 104310J.

Niu, Zijia et al. (2018). "DeepLab-based spatial feature extraction for hyperspectral image classification". In: *IEEE Geoscience and Remote Sensing Letters* 16.2, pp. 251–255.

Norouzi, Mohammad, Mani Ranjbar, and Greg Mori (2009). "Stacks of convolutional restricted boltzmann machines for shift-invariant feature learning". In: *2009 IEEE Conference on Computer Vision and Pattern Recognition*. IEEE, pp. 2735–2742.

Nuarsa, I Wayan, Fumihiko Nishio, and Chiharu Hongo (2011). "Spectral characteristics and mapping of rice plants using multi-temporal Landsat data". In: *Journal of Agricultural Science*.

Ok, Asli Ozdarici, Ozlem Akar, and Oguz Gungor (2012). "Evaluation of random forest method for agricultural crop classification". In: *European Journal of Remote Sensing* 45.1, pp. 421–432.

Oommen, Thomas et al. (2008). "An objective analysis of support vector machine based classification for remote sensing". In: *Mathematical geosciences* 40.4, pp. 409–424.

Ordóñez, Francisco Javier and Daniel Roggen (2016). "Deep convolutional and lstm recurrent neural networks for multimodal wearable activity recognition". In: *Sensors* 16.1, p. 115.

Otukei, John Richard and Thomas Blaschke (2010). "Land cover change assessment using decision trees, support vector machines and maximum likelihood classification algorithms". In: *International Journal of Applied Earth Observation and Geoinformation* 12, S27–S31.

Ozdarici-Ok, A (2015). "Automatic detection and delineation of citrus trees from VHR satellite imagery". In: *International Journal of Remote Sensing* 36.17, pp. 4275–4296.

Pandey, Brij Kishor and Deepak Khare (2017). "Analyzing and modeling of a large river basin dynamics applying integrated cellular automata and Markov model". In: *Environmental Earth Sciences* 76.22, pp. 1–12.

Papageorgiou, Elpiniki I, Athanasios T Markinos, and Theofanis A Gemtos (2011). "Fuzzy cognitive map based approach for predicting yield in cotton crop production as a basis for decision support system in precision agriculture application". In: *Applied Soft Computing* 11.4, pp. 3643–3657.

Pareeth, Sajid et al. (2019). "Mapping agricultural landuse patterns from time series of Landsat 8 using random forest based hierarchial approach". In: *Remote Sensing* 11.5, p. 601.

Park, Seonyoung et al. (2018). "Classification and mapping of paddy rice by combining Landsat and SAR time series data". In: *Remote Sensing* 10.3, p. 447.

Pasanen, Leena and Lasse Holmström (2015). "Bayesian scale space analysis of temporal changes in satellite images". In: *Journal of Applied Statistics* 42.1, pp. 50–70.

Pawar, Maneesh et al. (2021). "Spectral Calibration of VNIR Hyperspectral Imager". In: *ICOL-2019: Proceedings of the International Conference on Optics and Electro-Optics, Dehradun, India*. Springer Singapore, pp. 465–468.

Peng, Daifeng and Haiyan Guan (2019). "Unsupervised change detection method based on saliency analysis and convolutional neural network". In: *Journal of Applied Remote Sensing* 13.2, p. 024512.

Peng, Daifeng, Yongjun Zhang, and Haiyan Guan (2019). "End-to-end change detection for high resolution satellite images using improved UNet++". In: *Remote Sensing* 11.11, p. 1382.

Peng, Daifeng et al. (2020a). "SemiCDNet: A semisupervised convolutional neural network for change detection in high resolution remote-sensing images". In: *IEEE Transactions on Geoscience and Remote Sensing*.

Peng, Lingxi et al. (2020b). "The transnational happiness study with big data technology". In: *ACM Transactions on Asian and Low-Resource Language Information Processing (TALLIP)* 20.1, pp. 1–12.

Perez, Luis and Jason Wang (2017). "The effectiveness of data augmentation in image classification using deep learning". In: *arXiv preprint arXiv:1712.04621*.

Pérez-Benito, Francisco Javier et al. (2019). "A happiness degree predictor using the conceptual data structure for deep learning architectures". In: *Computer methods and programs in biomedicine* 168, pp. 59–68.

Phiri, Darius et al. (2020). "Sentinel-2 data for land cover/use mapping: a review". In: *Remote Sensing* 12.14, p. 2291.

Planinšič, Peter and Dušan Gleich (2018). "Temporal change detection in SAR images using log cumulants and stacked autoencoder". In: *IEEE Geoscience and Remote Sensing Letters* 15.2, pp. 297–301.

Pomente, Andrea, Matteo Picchiani, and Fabio Del Frate (2018). "Sentinel-2 change detection based on deep features". In: *IGARSS 2018-2018 IEEE International Geoscience and Remote Sensing Symposium*. IEEE, pp. 6859–6862.

Pons, X and A Arcalís (2013). "Diccionari Terminològic de Teledetecció o sobre la necesidad de una referencia semántica para el léxico técnico de nuestra disciplina". In: *Revista de teledetección: Revista de la Asociación Española de Teledetección* 40, pp. 145–146.

Pradhan, Ritesh et al. (2017). "Tropical cyclone intensity estimation using a deep convolutional neural network". In: *IEEE Transactions on Image Processing* 27.2, pp. 692–702.

Prendes, Jorge et al. (2014). "A new multivariate statistical model for change detection in images acquired by homogeneous and heterogeneous sensors". In: *IEEE Transactions on Image Processing* 24.3, pp. 799–812.

Puig, Carlos Javier, Glenn Hyman, and Sandra Bolaños (2002). "Digital classification vs visual interpretation: a case study in humid tropical forests of the Peruvian Amazon". In: *International Center for Tropical Agriculture*, pp. 1–5.

Qi, Zhixin et al. (2015). "A three-component method for timely detection of land cover changes using polarimetric SAR images". In: *ISPRS Journal of Photogrammetry and Remote Sensing* 107, pp. 3–21.

Qu, Jiahui et al. (2020). "Anomaly Detection in Hyperspectral Imagery Based on Gaussian Mixture Model". In: *IEEE Transactions on Geoscience and Remote Sensing*.

Rainforth, Tom and Frank Wood (2015). "Canonical correlation forests". In: *arXiv preprint arXiv:1507.05444*.

Raja, RA Alagu et al. (2013). "Wavelet based post classification change detection technique for urban growth monitoring". In: *Journal of the Indian Society of Remote Sensing* 41.1, pp. 35–43.

Rawat, JS and Manish Kumar (2015). "Monitoring land use/cover change using remote sensing and GIS techniques: A case study of Hawalbagh block, district Almora, Uttarakhand, India". In: *The Egyptian Journal of Remote Sensing and Space Science* 18.1, pp. 77–84.

Reich, Simon, Florentin Wörgötter, and Babette Dellen (2018). "A Real-Time Edge-Preserving Denoising Filter." In: *VISIGRAPP (4: VISAPP)*, pp. 85–94.

Ren, Caijun et al. (2020). "Unsupervised change detection in satellite images with generative adversarial network". In: *IEEE Transactions on Geoscience and Remote Sensing*.

Ridd, Merrill K and Jiajun Liu (1998). "A comparison of four algorithms for change detection in an urban environment". In: *Remote sensing of environment* 63.2, pp. 95–100.

Rouse, John Wilson et al. (1974). "Monitoring vegetation systems in the Great Plains with ERTS". In: *NASA special publication* 351.1974, p. 309.

Sadeghi, Vahid, Farshid Farnood Ahmadi, and Hamid Ebadi (2016). "Design and implementation of an expert system for updating thematic maps using satellite imagery (case study: changes of Lake Urmia)". In: *Arabian Journal of Geosciences* 9.4, p. 257.

Saha, Sudipan, Francesca Bovolo, and Lorenzo Bruzzone (2019). "Unsupervised deep change vector analysis for multiple-change detection in VHR images". In: *IEEE Transactions on Geoscience and Remote Sensing* 57.6, pp. 3677–3693.

Sakurada, Ken and Takayuki Okatani (2015). "Change Detection from a Street Image Pair using CNN Features and Superpixel Segmentation." In: *BMVC*. Vol. 61, pp. 1–12.

Samadi, Farnaam, Gholamreza Akbarizadeh, and Hooman Kaabi (2019). "Change detection in SAR images using deep belief network: a new training approach based on morphological images". In: *IET Image Processing* 13.12, pp. 2255–2264.

Sethy, Prabira Kumar et al. (2020). "Nitrogen deficiency prediction of rice crop based on convolutional neural network". In: *Journal of Ambient Intelligence and Humanized Computing* 11.11, pp. 5703–5711.

Seydi, Seyd Teymoor, Mahdi Hasanlou, and Meisam Amani (2020). "A new end-to-end multi-dimensional CNN framework for land cover/land use change detection in multi-source remote sensing datasets". In: *Remote Sensing* 12.12, p. 2010.

Sharma, Atharva et al. (2017). "A patch-based convolutional neural network for remote sensing image classification". In: *Neural Networks* 95, pp. 19–28.

Shendryk, Iurii et al. (2018). "Deep learning-a new approach for multi-label scene classification in planetscope and sentinel-2 imagery". In: *IGARSS 2018-2018 IEEE International Geoscience and Remote Sensing Symposium*. IEEE, pp. 1116–1119.

Shi, Wenzhong et al. (2020a). "Change detection based on artificial intelligence: State-of-the-art and challenges". In: *Remote Sensing* 12.10, p. 1688.

Shi, Wenzhong et al. (2020b). "Landslide recognition by deep convolutional neural network and change detection". In: *IEEE Transactions on Geoscience and Remote Sensing* 59.6, pp. 4654–4672.

Shi, Yanzi et al. (2020c). "Hyperspectral target detection with RoI feature transformation and multiscale spectral attention". In: *IEEE Transactions on Geoscience and Remote Sensing* 59.6, pp. 5071–5084.

Shuster, William D et al. (2005). "Impacts of impervious surface on watershed hydrology: A review". In: *Urban Water Journal* 2.4, pp. 263–275.

Simonyan, Karen and Andrew Zisserman (2014). "Very deep convolutional networks for large-scale image recognition". In: *arXiv preprint arXiv:1409.1556*.

Singh, Akansha and Krishna Kant Singh (2017a). "Satellite image classification using Genetic Algorithm trained radial basis function neural network, application to the detection of flooded areas". In: *Journal of Visual Communication and Image Representation* 42, pp. 173–182.

Singh, Ashbindu (1984). "Tropical forest monitoring using digital Landsat data in Northeastern India." PhD thesis. University of Reading.

Singh, Krishna Kant and Akansha Singh (2017b). "Identification of flooded area from satellite images using Hybrid Kohonen Fuzzy C-Means sigma classifier". In: *The Egyptian Journal of Remote Sensing and Space Science* 20.1, pp. 147–155.

Slavkovikj, Viktor et al. (2015). "Hyperspectral image classification with convolutional neural networks". In: *Proceedings of the 23rd ACM international conference on Multimedia*, pp. 1159–1162.

Soille, Pierre and Martino Pesaresi (2002). "Advances in mathematical morphology applied to geoscience and remote sensing". In: *IEEE Transactions on Geoscience and Remote Sensing* 40.9, pp. 2042–2055.

Solano-Correa, Yady Tatiana, Francesca Bovolo, and Lorenzo Bruzzone (2018). "An approach for unsupervised change detection in multitemporal VHR images acquired by different multispectral sensors". In: *Remote Sensing* 10.4, p. 533.

Song, Ahram et al. (2018). "Change detection in hyperspectral images using recurrent 3D fully convolutional networks". In: *Remote Sensing* 10.11, p. 1827.

Su, Linzhi et al. (2016). "Detecting multiple changes from multi-temporal images by using stacked denosing autoencoder based change vector analysis". In: *2016 International Joint Conference on Neural Networks (IJCNN)*. IEEE, pp. 1269–1276.

Su, Linzhi et al. (2017). "Deep learning and mapping based ternary change detection for information unbalanced images". In: *Pattern Recognition* 66, pp. 213–228.

Subudhi, Badri Narayan et al. (2014). "Spatio-contextual fuzzy clustering with Markov random field model for change detection in remotely sensed images". In: *Optics & Laser Technology* 57, pp. 284–292.

Suresh, Shilpa and Shyam Lal (2017). "Modified differential evolution algorithm for contrast and brightness enhancement of satellite images". In: *Applied soft computing* 61, pp. 622–641.

Thakkar, Amee K et al. (2016). "An effective hybrid classification approach using tasseled cap transformation (TCT) for improving classification of land use/land cover (LU/LC) in semi-arid region: a case study of Morva-Hadaf watershed, Gujarat, India". In: *Arabian Journal of Geosciences* 9.3, p. 180.

Tian, Dayong and Maoguo Gong (2018). "A novel edge-weight based fuzzy clustering method for change detection in SAR images". In: *Information Sciences* 467, pp. 415–430.

Touati, Redha, Max Mignotte, and Mohamed Dahmane (2020). "Anomaly feature learning for unsupervised change detection in heterogeneous images: A deep sparse residual model". In: *IEEE Journal of Selected Topics in Applied Earth Observations and Remote Sensing* 13, pp. 588–600.

Ursani, Ahsan Ahmad et al. (2011). "Fusion of textural and spectral information for tree crop and other agricultural cover mapping with very-high resolution satellite images". In: *IEEE Journal of selected topics in applied earth observations and remote sensing* 5.1, pp. 225–235.

Ustuner, Mustafa and Fusun Balik Sanli (2019). "Polarimetric target decompositions and light gradient boosting machine for crop classification: A comparative evaluation". In: *ISPRS International Journal of Geo-Information* 8.2, p. 97.

Varghese, Ashley et al. (2018). "ChangeNet: A deep learning architecture for visual change detection". In: *Proceedings of the European Conference on Computer Vision (ECCV) Workshops*, pp. 0–0.

Vázquez-Jiménez, René et al. (2017). "Applying the chi-square transformation and automatic secant thresholding to Landsat imagery as unsupervised change detection methods". In: *Journal of Applied Remote Sensing* 11.1, p. 016016.

Venugopal, N (2020). "Automatic semantic segmentation with DeepLab dilated learning network for change detection in remote sensing images". In: *Neural Processing Letters*, pp. 1–23.

Vetrivel, Anand et al. (2018). "Disaster damage detection through synergistic use of deep learning and 3D point cloud features derived from very high resolution oblique aerial images, and multiple-kernel-learning". In: *ISPRS journal of photogrammetry and remote sensing* 140, pp. 45–59.

Vickers, Neil J (2017). "Animal communication: when i'm calling you, will you answer too?" In: *Current biology* 27.14, R713–R715.

Vignesh, T et al. (2016). "A novel multiple unsupervised algorithm for land use/land cover classification". In: *Indian Journal of Science and Technology* 9.42, pp. 1–12.

Wan, Xue et al. (2018). "An illumination-invariant change detection method based on disparity saliency map for multitemporal optical remotely sensed images". In: *IEEE Transactions on Geoscience and Remote Sensing* 57.3, pp. 1311–1324.

Wang, Guojie et al. (2020a). "Water identification from high-resolution remote sensing images based on multidimensional densely connected convolutional neural networks". In: *Remote Sensing* 12.5, p. 795.

Wang, Mingwei et al. (2017). "Remote sensing image classification based on the optimal support vector machine and modified binary coded ant colony optimization algorithm". In: *Information Sciences* 402, pp. 50–68.

Wang, Moyang et al. (2020b). "A deep siamese network with hybrid convolutional feature extraction module for change detection based on multi-sensor remote sensing images". In: *Remote Sensing* 12.2, p. 205.

Wang, Qing et al. (2018a). "Change detection based on Faster R-CNN for high-resolution remote sensing images". In: *Remote sensing letters* 9.10, pp. 923–932.

Wang, Qunming et al. (2014). "Land cover change detection at subpixel resolution with a Hopfield neural network". In: *IEEE Journal of Selected Topics in Applied Earth Observations and Remote Sensing* 8.3, pp. 1339–1352.

Wang, Xiaoyan et al. (2018b). "Snow cover mapping for complex mountainous forested environments based on a multi-index technique". In: *IEEE Journal of Selected Topics in Applied Earth Observations and Remote Sensing* 11.5, pp. 1433–1441.

Wang, Yafei, Feifei Zhao, and Peipei Chen (2017). "A framework of spatiotemporal fuzzy clustering for land-cover change detection using SAR time series". In: *International Journal of Remote Sensing* 38.2, pp. 450–466.

Weinstein, Stephen and Paul Ebert (1971). "Data transmission by frequency-division multiplexing using the discrete Fourier transform". In: *IEEE transactions on Communication Technology* 19.5, pp. 628–634.

Wu, Yanhong et al. (2019a). "Investigating water variation of lakes in Tibetan Plateau using remote sensed data over the past 20 years". In: *IEEE Journal of Selected Topics in Applied Earth Observations and Remote Sensing* 12.7, pp. 2557–2564.

Wu, Yue et al. (2014). "A novel point-matching algorithm based on fast sample consensus for image registration". In: *IEEE Geoscience and Remote Sensing Letters* 12.1, pp. 43–47.

Wu, Yue et al. (2017). "PSOSAC: particle swarm optimization sample consensus algorithm for remote sensing image registration". In: *IEEE Geoscience and Remote Sensing Letters* 15.2, pp. 242–246.

Wu, Yue et al. (2019b). "Multimodal continuous ant colony optimization for multisensor remote sensing image registration with local search". In: *Swarm and Evolutionary Computation* 47, pp. 89–95.

Wuebbles, Donald J et al. (2017). "Climate science special report: Fourth national climate assessment (NCA4), Volume I". In.

Xiao, Xiangming et al. (2006). "Mapping paddy rice agriculture in South and Southeast Asia using multi-temporal MODIS images". In: *Remote sensing of Environment* 100.1, pp. 95–113.

Xie, Cong et al. (2018). "Spatiotemporal change patterns of urban lakes in China's major cities between 1990 and 2015". In: *International Journal of Digital Earth* 11.11, pp. 1085–1102.

Xie, Fuding et al. (2019). "Unsupervised band selection based on artificial bee colony algorithm for hyperspectral image classification". In: *Applied Soft Computing* 75, pp. 428–440.

Xiong, Boli, Jing M Chen, and Gangyao Kuang (2012). "A change detection measure based on a likelihood ratio and statistical properties of SAR intensity images". In: *Remote Sensing Letters* 3.3, pp. 267–275.

Xiong, Zhangxi et al. (2021). "Pan-Sharpening Based on Panchromatic Image Spectral Learning Using WorldView-2". In: *IEEE Geoscience and Remote Sensing Letters*.

Xu, Di et al. (2017). "Detection of decreasing vegetation cover based on empirical orthogonal function and temporal unmixing analysis". In: *Mathematical Problems in Engineering* 2017.

Xu, Hanqiu (2006). "Modification of normalised difference water index (NDWI) to enhance open water features in remotely sensed imagery". In: *International journal of remote sensing* 27.14, pp. 3025–3033.

Yan, Li et al. (2018a). "A novel approach to unsupervised change detection based on hybrid spectral difference". In: *Remote Sensing* 10.6, p. 841.

Yan, Ying et al. (2018b). "Comparison of multiple bioactive constituents in different parts of Eucommia ulmoides based on UFLC-QTRAP-MS/MS combined with PCA". In: *Molecules* 23.3, p. 643.

Yang, Linqing et al. (2017a). "A robust algorithm for estimating surface fractional vegetation cover from landsat data". In: *Remote Sensing* 9.8, p. 857.

Yang, Naisen et al. (2016). "Dropband: a convolutional neural network with data augmentation for scene classification of VHR satellite images". In.

Yang, Xiucheng et al. (2017b). "Mapping of urban surface water bodies from Sentinel-2 MSI imagery at 10 m resolution via NDWI-based image sharpening". In: *Remote Sensing* 9.6, p. 596.

Yang, Yixin et al. (2020). "Hyperspectral anomaly detection through sparse representation with tensor decomposition-based dictionary construction and adaptive weighting". In: *IEEE Access* 8, pp. 72121–72137.

You, Lexin (2021). "Utilizing Machine Learning to Predict Happiness Index". In: *2021 2nd International Conference on E-Commerce and Internet Technology (ECIT)*. IEEE, pp. 233–238.

Yu, Long et al. (2017a). "Convolutional neural networks for water body extraction from Landsat imagery". In: *International Journal of Computational Intelligence and Applications* 16.01, p. 1750001.

Yu, Xingrui et al. (2017b). "Deep learning in remote sensing scene classification: a data augmentation enhanced convolutional neural network framework". In: *GIScience & Remote Sensing* 54.5, pp. 741–758.

Yue, Jun et al. (2015). "Spectral–spatial classification of hyperspectral images using deep convolutional neural networks". In: *Remote Sensing Letters* 6.6, pp. 468–477.

Zanchetta, Anna, Gabriele Bitelli, and Arnon Karnieli (2016). "Monitoring desertification by remote sensing using the Tasselled Cap transform for long-term change detection". In: *Natural hazards* 83.1, pp. 223–237.

Zhan, Yang et al. (2017). "Change detection based on deep siamese convolutional network for optical aerial images". In: *IEEE Geoscience and Remote Sensing Letters* 14.10, pp. 1845–1849.

Zhang, Gang et al. (2020). "Learning synthetic aperture radar image despeckling without clean data". In: *Journal of Applied Remote Sensing* 14.2, p. 026518.

Zhang, Liangpei, Lefei Zhang, and Bo Du (2016). "Deep Learning for Remote Sensing Data: A Technical Tutorial on the State of the Art". In: *IEEE Geoscience and Remote Sensing Magazine* 4.2, pp. 22–40. DOI: 10.1109/MGRS.2016.2540798.

Zhang, Meng et al. (2018a). "Mapping paddy rice using a convolutional neural network (CNN) with Landsat 8 datasets in the Dongting Lake Area, China". In: *Remote Sensing* 10.11, p. 1840.

— (2018b). "Mapping paddy rice using a convolutional neural network (CNN) with Landsat 8 datasets in the Dongting Lake Area, China". In: *Remote Sensing* 10.11, p. 1840.

Zhang, Min and Wenzhong Shi (2020). "A feature difference convolutional neural network-based change detection method". In: *IEEE Transactions on Geoscience and Remote Sensing* 58.10, pp. 7232–7246.

Zhang, Mingyang, Maoguo Gong, and Yongqiang Chan (2018). "Hyperspectral band selection based on multi-objective optimization with high information and low redundancy". In: *Applied Soft Computing* 70, pp. 604–621.

Zhang, Puzhao et al. (2016). "Change detection based on deep feature representation and mapping transformation for multi-spatial-resolution remote sensing images". In: *ISPRS Journal of Photogrammetry and Remote Sensing* 116, pp. 24–41.

Zhang, Weihua and David R Montgomery (1994). "Digital elevation model grid size, landscape representation, and hydrologic simulations". In: *Water resources research* 30.4, pp. 1019–1028.

Zhang, Wuxia and Xiaoqiang Lu (2019). "The spectral-spatial joint learning for change detection in multispectral imagery". In: *Remote Sensing* 11.3, p. 240.

Zhou, Ya'nan et al. (2014). "Multiscale water body extraction in urban environments from satellite images". In: *IEEE Journal of selected topics in applied earth observations and remote sensing* 7.10, pp. 4301–4312.

Zhu, Bin et al. (2018). "Change detection based on the combination of improved SegNet neural network and morphology". In: *2018 IEEE 3rd International Conference on Image, Vision and Computing (ICIVC)*. IEEE, pp. 55–59.

Zhu, Xiao Xiang et al. (2017). "Deep learning in remote sensing: A comprehensive review and list of resources". In: *IEEE Geoscience and Remote Sensing Magazine* 5.4, pp. 8–36.